The Role of Decorin in the Pathogenesis of Primary Open Angle Glaucoma

Dissertation

Zur Erlangung des Doktorgrades der Naturwissenschaften (Dr. rer. nat.)
der Fakultät für Biologie und Vorklinische Medizin
der Universität Regensburg

Durchgeführt am Lehrstuhl für Humananatomie und Embryologie
der Universität Regensburg

vorgelegt von
Magdalena Schneider
aus Straubing

im Jahr 2016

Das Promotionsgesuch wurde eingereicht am:
21.09.2016

Die Arbeit wurde angeleitet von:
Prof. Dr. Rudolf Fuchshofer

Unterschrift:

Meiner Familie

Table of contents

1. Abstract

Primary open angle glaucoma (POAG), one of the leading causes for blindness in the western world, is defined as a progressive optic neuropathy which is characterized by the loss of retinal ganglion cells. Various randomized multicenter studies could show that an elevated intraocular pressure (IOP), which is too high for the health of the eye, is the main risk factor to develop POAG (Collaborative-Normal-Tension-Glaucoma-Study-Group, 1998; Gordon et al., 2002; Johnson et al., 2002; Leske et al., 2003)

Today it is widely acknowledged that the increase in IOP is due to a decreased outflow facility in the trabecular meshwork (TM). The drainage of aqueous humor in the TM is reduced by an increased contractility of TM cells and by an accumulation of extracellular matrix (ECM) in the juxtacanalicular TM (Fuchshofer et al., 2007; Lutjen-Drecoll et al., 2001; Lutjen-Drecoll et al., 1986a; Okka et al., 2004).

The increase in IOP in combination with structural changes of the ECM in the region of the *lamina cribrosa* (LC) lead to a reduced axonal transport of neurotrophic factors to the retina ganglion cells (RGC). The lack of neurotropic factors leads to RGC death which causes the neuropathy of the optic nerve and the optical field defects characteristic for POAG (Guo et al., 2005); Fuchshofer 2011; Zode et al. 2011).

Many studies could show that the growth factors TGFβ and CTGF may play an important part in the pathogenesis of POAG (Fuchshofer *et al*., 2005; Fuchshofer, 2011; Junglas *et al.*, 2012; Junglas *et al.*, 2009; Tamm & Fuchshofer, 2007). Therefore proteins able to inhibit these factors are of high interest as possible therapeutic agents. This work focuses on the small leucine-rich proteoglycan Decorin (DCN). DCN inhibits TGFβ via direct binding or via the up regulation of Fibrillin 1 synthesis (Neill et al., 2012; Yamaguchi, 1990). Possible interactions between DCN, TGFβ and CTGF should be analyzed *in vitro* and *in vivo.* Further it was aim of this study to analyze if DCN is able to inhibit the expression of ECM proteins in cell types involved in the pathogenesis of POAG. Additionally it was investigated if the AKT signaling pathway is involved in the regulation of TGFβ and CTGF via DCN in optic nerve astrocytes. The final aspect of this work was the observation of the effects of a DCN knockout *in vivo* in the eye in mice of mixed background and in mice of a pure CD1 background.

The experiments showed that a treatment with TGFβ and CTGF leads to a decreased synthesis and expression of DCN in various cell types of the eye which play an important part in the development of POAG. On the other hand, a treatment with DCN led to a decreased synthesis of TGFβ-1, TGFβ-2 and CTGF in these cell types. Additionally, the synthesis of ECM proteins Fibronectin and Collagen IV was down regulated after treatments with DCN. We could further show that DCN regulates TGFβ-1, TGFβ-2 and CTGF via the AKT signaling pathway.

Interestingly we were not able to cultivate optic nerve astrocytes of DCN knockout mice, while optic nerves astrocytes of wildtype littermates grow well in culture.

Immunohistochemical staining showed reduced levels of DCN in the TM of glaucomatous eyes in comparison to the TM of healthy donors.

In vivo a lens specific overexpression of CTGF, which leads to the development of POAG (Junglas *et al.*, 2012) resulted in a reduced DCN Expression in the region of the TM, but not in the optic nerve.

The eyes of DCN knockout mice showed a significant increase in IOP and a significantly reduced number of axons, which are typical characteristics of POAG. These might be due to the enhanced expression of TGFβ, CTGF and ECM proteins in the chamber angle, which could be observed on RNA and protein level. Furthermore levels of pAKT were reduced in the TM, the retina and in the glial lamina of DCN knockout mice.

The results show a clear interaction between DCN and TGFβ/CTGF as between DCN and ECM-Proteins *in vitro* and *in vivo*. DCN seems to play an important role in inhibiting processes which can cause POAG. It possibly causes the balance between the necessary and pathogenic expression of TGFβ, CTGF and ECM proteins in the eye.

The results lead to the conclusion that DCN is a highly promising candidate for a therapeutic against POAG. It will be of high interest to observe the effects of DCN treatments or an adenoviral gene transfer of DCN to the eyes of βB1-CTGF and DCN knockout mice. We hypothesize that such treatments will lead to a decrease in IOP and to a reduction of axonal loss.

2. Introduction

Glaucoma is a group of eye diseases which are defined as an optic neuropathy that leads to visual field defects or even to complete blindness. In 2013 glaucoma affected about 64.3 million people worldwide and it is estimated that the number of patients will increase to 111.8 million by 2040. Different forms of glaucoma are classified by the appearance of the iridocorneal angle. With about 44.1 million cases in 2013 primary open angle glaucoma (POAG) is the most common form. (Tham et al., 2014).

In POAG the iridocorneal angle remains open at all times and multiple randomized, prospective multicenter studies have clearly shown that an increased IOP is the main risk factor to develop POAG (Collaborative-Normal-Tension-Glaucoma-Study-Group, 1998; Gordon et al., 2002; Johnson et al., 2002; Leske et al., 2003). An IOP that is too high for the health of optic nerve leads to the death of retinal ganglion cells (RGC). RGC death causes scomtomas or in severe cases complete blindness. Since the molecular reasons causing elevation of IOP and RGC death are poorly understood it is of great interest to identify key players in these processes – proteins or other molecules that might contribute to the pathological changes occuring in the eye in POAG.

2.1 Trabecular meshwork and aqueous humor outflow

IOP is build up by the circulation of aqueous humor (AH). A healthy IOP is ensured by a balance of AH production by the ciliary body and AH drainage through the trabecular meshwork (TM). The TM lies embedded in the iridocorneal angle and is a sponge-like structure which enables the drainage of AH into the episcleral venous system.

The AH, secreted by the ciliary body, is essential for the stability and the form of the eye and nourishes the lens, the cornea and the TM. It flows from the ciliary body in the posterior chamber through the pupil into the anterior chamber were it passes the TM and drains into Schlemm’s canal (SC). Between the TM and SC the outflow resistance is located. If the production and drainage of AH are in balance an IOP of between 11 and 21mm Hg is created. The aqueous humor mainly drains through the trabecular (= conventional) outflow pathway, only small amounts drain via the

uveoscleral (= nonconventional) outflow pathway. In this pathway the AH drains by diffusing through intracellular spaces between ciliary muscle fibers (Bill and Phillips, 1971).

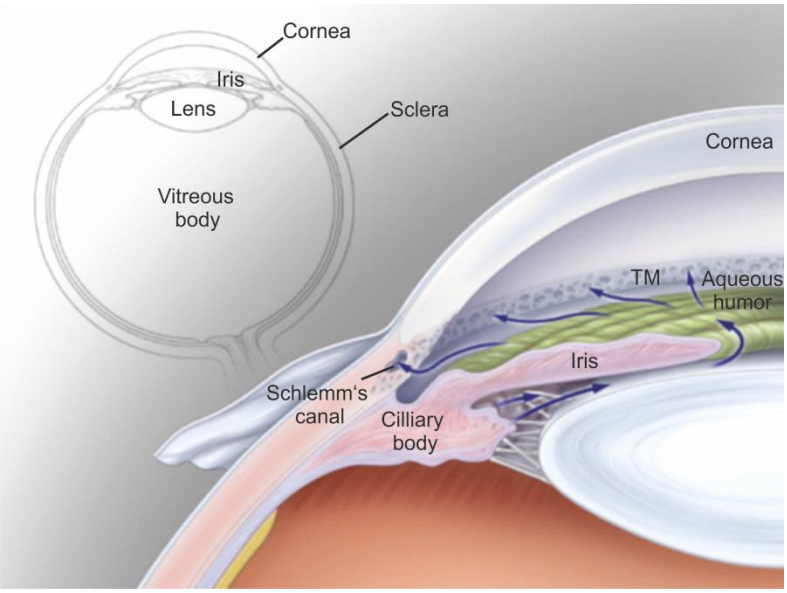

Figure 1: Circulation of aqueous humor. The AH is secreted by the ciliary body and then flows through the pupil from the posterior into the anterior chamber. It then leaves the anterior chamber via the TM and drains in Schlemm's canal which leads into the episcleral venous system (Kwon et al., 2009b).

The TM spans from the scleral spur the Schwalbe's line, representing the separation between corneal endothelium and TM and can be divided into three different parts: the inner uveal meshwork, the corneoscleral meshwork and the juxtacanalicular tissue (JCT) or cribriform meshwork.

The uveal meshwork consists of densely packed bundles of fibers, which terminate on one side in the hyaline substance, forming the Descement's membrane, and are firmly attached to the connective tissue of the iris root and the ciliary muscle on the other side (Speakman, 1959). It consists of about 3 layers of connective tissue beams, the trabecular beams, which are covered by flat confluent TM cells and form irregular intratrabecular fenestrations. These beams can also be found in the corneoscleral meshwork but not in the JCT. The corneoscleral meshwork is formed by 8 to 15 layers of beams covered by TM cells. These beams form intratrabecular spaces giving it a sponge-like structure. The outer beam cells of these regions are highly phagocytic and are seen as a sort of pre-filter, removing debris from the AH.

The intratrabecular spaces become smaller as they extend closer to the SC. The intratrabecular spaces in the uveal- and corneoscleral meshwork are too wide to hinder aqueous humor flow, meaning that in this region almost no outflow resistance is created (Buller et al., 1990; Overby et al., 2009; Rohen and van der Zypen, 1968; Sherwood and Richardson, 1988).

In the region of the JCT the structure is inherently different. The JCT cells form a discontinuous cell layer without pores (Lutjen-Drecoll, 1999; Lutjen-Drecoll et al., 1981; Tamm, 2009). The cells of the JCT are star-shaped and form contacts between the TM beam cells and the endothelial cells of SC. The 2 to 5 amorphous and discontinuous cell layers lie embedded in a loose connective tissue ECM. The ECM in this region consists mainly of proteoglycans, hyaluronan (HA), laminin, Collagen Type IV (Col IV) and Fibronectin (FN) (Tamm, 2009; Tawara et al., 1989; Ueda et al., 2002) and most of these proteins are expressed by the JCT cells (Fuchshofer et al., 2006). Tangentially to the SC endothelial lining lies a network of elastic fibers, the cribriform plexus. These fibers connect with the SC inner wall endothelium via their sheath material or via fine fibrils. Anterior tendons of the ciliary muscle anchor in the cribriform plexus. Thereby ciliary muscle contraction may influence the width of the JCT and its intracellular spaces and so have an effect on aqueous humor outflow (Rohen et al., 1981; Rohen et al., 1984).

The inner wall endothelium of SC forms giant vacuoles, where the basal membrane of the endothelium is discontinuous. In these regions the basal membrane is connected to the JCT. The structure of the TM and experimental flow studies indicate that about 90% of AH outflow resistance is created in the region of the JCT and the inner wall of SC (Bill and Phillips, 1971; Ethier et al., 1986; Overby et al., 2009; Rohen et al., 1981; Tripathi, 1971). AH has to cross the endothelium of SC through micron-sized pores, separated by fairly wide distances (20-30µm). This leads to a non-uniform flow pattern, since AH must “funnel” as it approaches a pore. Hence flow patterns in the JCT have to be non-uniform, too. The non-uniform flow decreases the area effectively available for passage, leading to an increase in the hydraulic resistance of this region (funneling hypothesis) (Johnson et al., 1992; Overby et al., 2009).

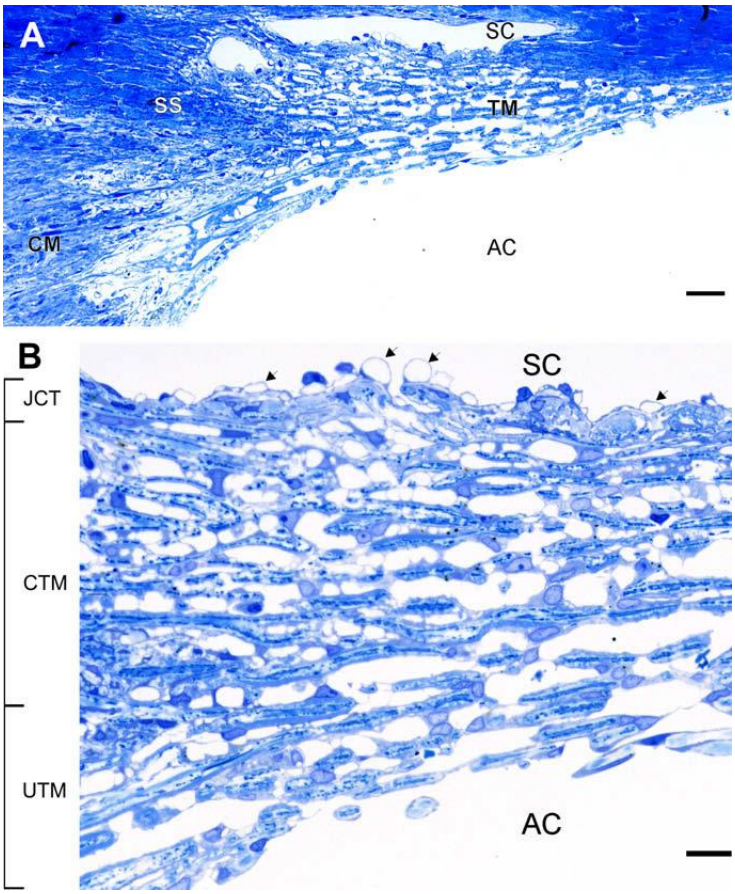

Figure 2: Meridional section through the trabecular meshwork. (B) is a magnification of (A). SC: Schlemm's Canal, TM: Trabecular meshwork, SS: Scleral spur, CM: Ciliary muscle, AC: Anterior chamber, JCT: Juxtacanalicular tissue, CTM: Corneoscleral TM, UTM: Uveal TM; Arrows in (B) point to vacuoles in the inner wall of SC. Scale bars 20 mm (A), 5 mm (B) (Tamm, 2009).

TM cells play a pivotal role in the continuous synthesis of ECM components in the chamber angle. ECM turnover and composition are thought to play a crucial part in the formation of outflow resistance (Acott and Kelley, 2008; Johnson, 2006). This hypothesis is underscored by findings that the turnover of ECM by matrix metalloproteinases (MMPs) is essential for the maintenance of AH outflow (Bradley et al., 2001; Bradley et al., 1998; Keller et al., 2009).

Outflow resistance can also be regulated via changes in the tonus of the actomyosin contractility of TM cells. Thereby the TM can be relaxed or contracted and an increase in TM tone increases outflow resistance (Tian et al., 2000; Wiederholt et al., 2000). Additionally the width of SC and also the contribution of pores formed by SC cells influence outflow facility and heterogeneity (Allingham et al., 1996; Braakman et al., 2015).

Since human TM samples are very rare and can only be analyzed post mortem or in organ culture, animal models are of high interest for glaucoma research. In human TM organ culture there is no possibility to observe the effects of over-expression or knockout of genes of interest in the TM on RGCs and ON axons. In animal models on the other hand, one can observe effects on all tissues involved in POAG and the time course of structural changes. In mice the structure of the TM and SC, as well as the connection between the TM and the inner wall of the SC, is similar to primates, whereas for example the porcine and bovine TM differ from the primate TM. The porcine TM is mostly formed by an angular aqueous plexus (McMenamin and Steptoe, 1991) and cows do not have a lamellate meshwork but a reticular meshwork (Chen et al., 2008). This makes mice the most usable model for outflow regulation and ECM changes in the TM as relevant for glaucoma (Overby et al., 2014a)

2.2 Optic nerve and *lamina cribrosa*

Besides the TM, the region of the optic nerve head (ONH) and the *lamina cribrosa* (LC) undergo the most dramatic changes in POAG. The optic nerve (ON) is formed by the axons of RGCs, which lie in the innermost layer of the retina, and is responsible for the transduction of signals from the retina to the brain. The region, were the RGC axons leave the eye, is called papilla. Since the ON derives from an out-pouching of the diencephalon (optic stalks), it is not a cranial nerve in the narrow sense. That is why it is covered by dura mater, which merges into the sclera.

Astrocytes are the most common form of glial cells in the optic nerve and they are vital for RGC health. In the mid-19th century they were first described as some kind of filling material by Von Virchow in 1846. Today it is known that astrocytes maintain the homeostatic balance of the extracellular environment by absorbing or degrading substances dispensed by neurons. Furthermore, they are an essential part of the blood-retina barrier (Ransom et al., 2003). Astrocytes supply neurons with nutrients by clasping around blood vessels and connecting them to neurons (Bouzier-Sore and Pellerin, 2013) and they can influence neuronal tissue by restructuring the ECM and releasing growth factors, cytokines and other cellular mediators under normal and pathologic conditions (Hernandez, 1992, 2000; Hernandez et al., 1994).

Additionally to the glial fibrillary acid protein (GFAP) positive astrocytes, oligodendrocytes, sheathing the RGC axons and microglia cells can be found in the ON. Astrocytes can be classified into ~11 distinct phenotypes that can be readily distinguished regarding their expression profile and morphology (Abbott et al., 2006). In the human ON three subtypes of astrocytes were identified. Type 2 astrocytes are the dominant subtype in the myelinated postlaminar part of the ON and type 1 astrocytes are the main subtype in the unmyelinated laminar and prelaminar region of the ON (Kobayashi et al., 1997; Ye and Hernandez, 1995).

In humans, where the RGC axons leave the eye, a sieve- like structure formed by many layers of collagen fibers, the LC (see Fig. 3 C) is located. The LC is essential to give the optic nerve head (ONH) a certain amount of elasticity to protect the axons from mechanical stress (Albon et al., 2000). Furthermore, it provides structural and functional support to the axons. The LC is a complex three-dimensional network of flexible connective tissue beams. The connective tissue beams in humans are composed of proteoglycans, laminin, FN, Col I, III, IV, V and VI and elastic fibers (Goldbaum et al., 1989; Morrison et al., 1989a; Morrison et al., 1989b). Besides Astrocytes, mostly GFAP negative, fibroblast like LC cells are present in this region. Together with the astrocytes these cells are involved in the composition of the LC and are responsible for the maintenance of ECM, by synthesizing, for example, Col III and IV, FN and Elastin (EL) (Hernandez et al., 1988).

Type 1 astrocytes and the LC cells form the cribriform plates of the LC. LC cells are located inside the plates of the LC (Hernandez, 1992, 2000; Kobayashi et al., 1997). In the LC and in the prelaminar region the processes of the astrocytes sheath axon bundles, surround blood vessels and link connective tissue surfaces (Anderson, 1969).

In mice, instead of a LC and LC cells, astrocytes form a glial lamina, which takes over the supporting function for axons (Sun et al., 2009).

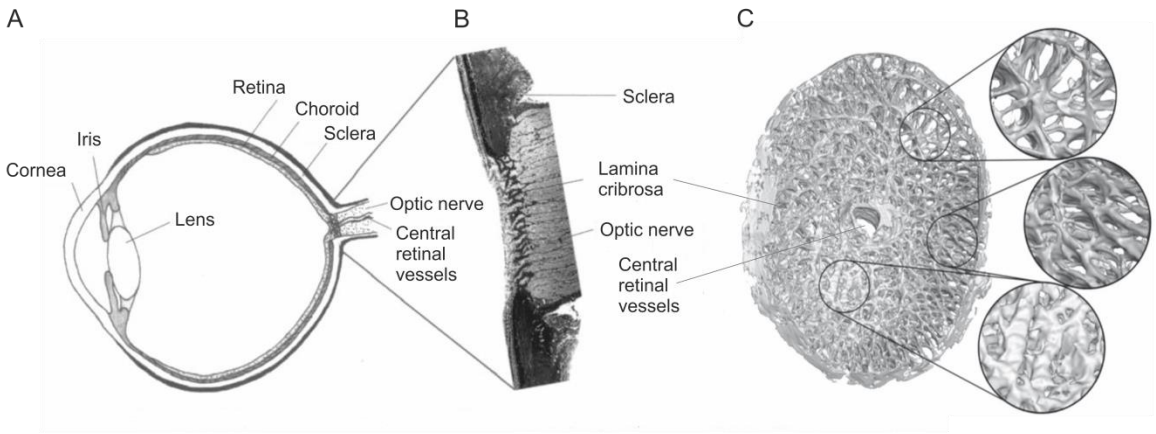

Figure 3: Graphical illustration of the LC. A: Diagram of the anatomy of the eye with the location of the papilla and the ON. B: Histological tangential section through the scleral canal and ONH showing the peripapillary sclera, *Lamina cribrosa*, and retinal ganglion cell axons (Downs et al., 2003), C: 3D reconstruction of the LC, illustrating regional variation in connective tissue density and predominant laminar beam orientation throughout the laminar structure (adapted from Sigal et al., 2010).

2.3 The pathogenesis of primary open angle glaucoma

Like all types of glaucoma, POAG is defined as a progressive optic neuropathy that is characterized by an irreversible loss of RGC axons in the ON. During the progression of POAG the region of the TM and the ONH, especially the LC, undergo drastic changes.

2.3.1 Pathological changes in the trabecular meshwork

Some of the changes occurring in the chamber angle can be observed by electron microscopy. In the JCT of glaucomatous eyes increased amounts of plaque material were observed (Gottanka et al., 1997; Lutjen-Drecoll et al., 1986a, b; Tektas and Lutjen-Drecoll, 2009). From the sheath of these plaques, connecting fibrils extend, which link the SC endothelial cells to JCT cells (Fuchshofer et al., 2006; Hann and Fautsch, 2011). In eyes of glaucomatous donors the sheath of the plaques are thickened and the connecting fibrils show increased amounts of Col IV and other ECM components. In severe cases the fibrils form fibrous plates and it is thought that this could contribute to the blocking of outflow pathways (Lutjen-Drecoll et al., 1981). Further the area occupied by plaques in the JCT correlates with axonal loss in the ON (Gottanka et al., 1997). All in all it is accepted today that the increase in ECM material in the TM leads to a reduction of AH outflow and increases IOP (Tamm and Fuchshofer, 2007).

The second regulatory mechanism of AH outflow, the actomyosin contractility of TM cells also seems to be disturbed in POAG. These changes show in stiffening of the TM in POAG. The glaucomatous TM is approximately 20 times stiffer than the TM of healthy eyes, but it is still unclear whether this is due to an increase in TM cell stiffness or ECM stiffness (Last et al., 2011). Treatments with dexamethason, a corticosteroid that elevates IOP in up to 40% of normotensive eyes and in almost all POAG eyes (Clark et al., 2002; Lewis et al. 1988; (Bollinger et al., 2012), lead to a remarkable stiffening of TM cells and their ECM (Raghunathan et al., 2015). The important role of actomyosin contractility in AH outflow regulation could further be shown in studies using latrunclin. Latrunculin inhibits the formation of actin microfilaments, which results in cellular relaxation, and can therefore increase outflow of AH in the TM and lower IOP (Ko et al., 2016; Okka et al., 2004; Rasmussen et al., 2014).

2.3.2 Pathological changes in the optic nerve head and *lamina cribrosa*

In the ONH region an ECM remodeling process occurs, leading to a stiffening of the peripapillary sclera (Coudrillier et al., 2012), thickening of the connective tissue sheaths around the capillaries (Tektas et al., 2010) and a restructuring of the LC (Pena et al., 1998; Quigley et al., 1991b; Quigley et al., 1983). The elastic fibers of the LC show marked changes as the fibers are no longer organized straightly, but appear curly and seem to be disconnected from the adjacent ECM material (Netland et al., 1995; Pena et al., 1998; Quigley et al., 1991a). The changes of elastic fibers are associated with a restructuring of the collagen network, including qualitative and quantitative changes in the distribution and density of collagen fibers in the laminar beams (Hernandez et al., 1991; Quigley et al., 1991b). Those ECM alterations of the LC may form the biochemical basis for a stiffer and less resilient structure, leading to a decrease in mechanical compliance of the LC in glaucoma (Albon et al., 2000). The structural alterations in conjunction with the increased IOP lead to cupping of the ONH and backward bending of the LC, typical symptoms observed in POAG (Quigley, 2011). Combination of all these factors seems to inhibit antero – and retrograde axonal transport of neurotrophic factors in the region of the LC and depravation of neurotrophic factors induces death of RGCs (Pease et al., 2000; Quigley et al., 2000).

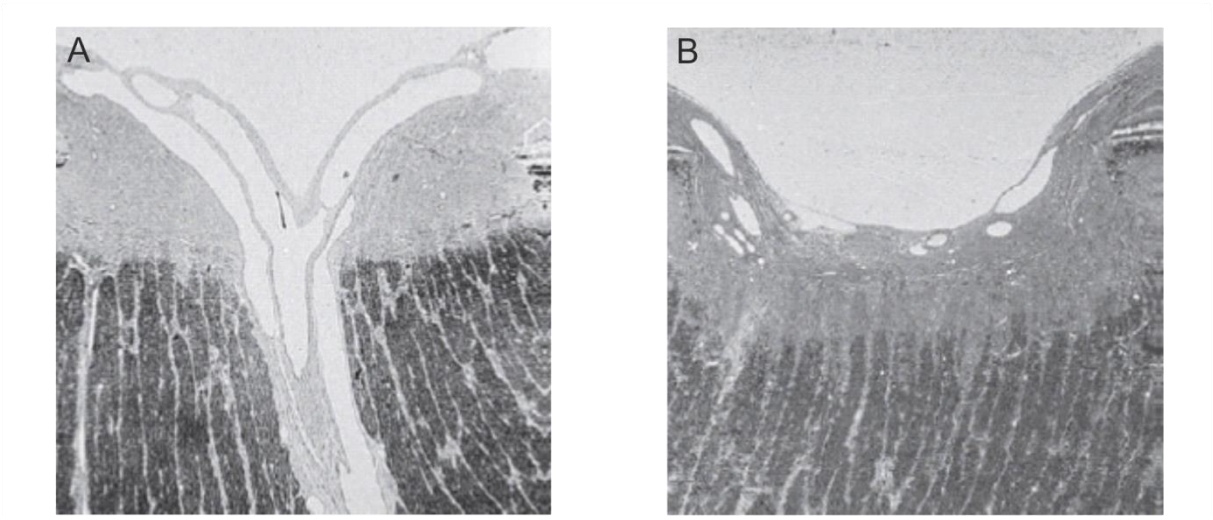

Figure 4: Histological sections of the ONH. A: a typical histological section through a healthy ONH. B: histological section through the ONH of a glaucoma patient. The ONH shows the typical excavation of the ONH (Quigley, 2011).

One question glaucoma research focused on during the last decades is what the source of these increased amounts of ECM material in the ONH and the LC is. Today it is widely acknowledged that mainly astrocytes are responsible for the production of ECM material in the ONH (Hernandez, 1992, 2000; Hernandez et al., 2002). It is suggested that reactivated astrocytes are heavily involved in the restructuring process within the LC. *In situ* hybridization experiments show that astrocytes in glaucomatous ONH express higher levels of collagen type IV than astrocytes of non-affected ONH (Hernandez et al., 1994). Further microarray analysis of cultured human ONH astrocytes from normal and glaucomatous donors could demonstrate that glaucomatous human ONH astrocytes have increased expression levels of different ECM proteins, including laminin, fibulin and collagen type-II, IV and XI, whereas the proteoglycans, like for example aggrecan, were downregulated (Hernandez et al., 2002; Lukas et al., 2008). Under normal conditions astrocytes of the ONH are in a quiescent state, but during the cause of glaucoma they undergo a process of reactivation called astrogliosis. Astrogliosis shows in alterations in astrocyte morphology, like thickening of processes and hypertrophy of the cell body. In human ONH with chronically elevated IOP and moderate or advanced glaucomatous axonal damage astrocytes show these morphological changes and an increased immunoreactivity for GFAP (Hernandez and Pena, 1997; Varela and Hernandez, 1997; Wang et al., 2002).

The molecular reasons for these pathological processes are complex and are only partially elucidated. One molecule that has been in the focus of glaucoma research for many years is the transforming growth factor (TGF-) β. Especially TGF-β2 was found in elevated levels in the aqueous humor of glaucoma patients (Inatani et al., 2001; Ochiai and Ochiai, 2002; Picht et al., 2001; Tripathi et al., 1994b; Yamamoto et al., 2005) and it is known to be involved in the pathogenesis of various fibrotic diseases, like for example in the liver (Baghy et al., 2012; Hellerbrand et al., 1999; Kanzler et al., 1999; Ueberham et al., 2003) or the kidney (Sharma and Ziyadeh, 1994; Yamamoto et al., 1993; Ziyadeh, 1994) but also in the eye (Jester et al., 1997; Karamichos et al., 2010).

2.4 TGF-β and CTGF - key players in primary open angle glaucoma

In eukaryotes three different isoforms, TGF-β1, 2 and 3 are encoded by a distinct gene. In the eye TGF-β2 is the most expressed isoform and it is expressed in multiple eye tissues (Cousins et al., 1991; Jampel et al., 1990; Pasquale et al., 1993; Pena et al., 1999). The major part of the TGF-β is produced by the epithelium of the ciliary body and the lens and then secreted to the AH (Allen et al., 1998; Helbig et al., 1991; Jampel et al., 1990; Pasquale et al., 1993; Schlotzer-Schrehardt and Dorfler, 1993). Nevertheless also TM cells and astrocytes of the optic nerve head are able to express and secrete TGF-β (Pena et al., 1999; Tripathi et al., 1994a).

Members of the TGF-β superfamily act as cytokines and can therefore be involved in various processes in the cell. Depending on cell status and tissue they can for example influence proliferation, differentiation and apoptosis, but are also involved in cell adhesion, embryogenesis, angiogenesis and immune suppression. TGF-β is synthesized as a pro-TGF-β molecule which contains the latency-associated proteins (LAP) and the latent TGF-β binding proteins 1 and 2 (LTBP1/2) connecting the whole complex to the ECM (Nunes et al., 1997). The release of active TGF-β from this complex can take place through proteolytic activity by plasmin, MMP2 and MMP9, through integrins or through the action of thrombospondin (Munger et al., 1997; Munger et al., 1999; Murphy-Ullrich and Poczatek, 2000; Sato and Rifkin, 1989; Yu and Stamenkovic, 2000).

Classical TGF-β signaling starts with binding of TGF-β to TGF-β receptor type II (TGF-β RII) which gets phosphorylated and binds to TGF-β receptor type I (TGF-β RI). Upon binding the TGF-β RI is activated which leads to a phosphorylation of Smad2 and Smad3 (pSmad = small mothers against decapentaplegic). The pSmad2/Smad3 complex dissociates from the receptor and binds Smad4. This complex translocates into the nucleus where it can either activate or inactivate the expression of TGF-β target genes (Derynck and Zhang, 2003).

If present in physiological concentrations in the eye, TGF-β is essentially involved in the immune privilege by oppressing the production of interferon γ (IFN- γ) and interleukin 4 (IL-4), which leads to oppression of the immune system (Ohta et al., 2000a; Ohta et al., 2000b; Streilein, 1999a, b; Taylor et al., 1997).

Pathological levels of TGF-β in the AH, as stated above, are seen as one of the major causes for the pathological changes occurring in the ONH and the TM in POAG (Fuchshofer et al., 2005; Fuchshofer and Tamm, 2009; Fuchshofer et al., 2007; Neumann et al., 2008; Zode et al., 2011). In cultured human TM cells treatment with TGF-β2 leads to an increased expression of various ECM proteins, including FN, Col and Elastin (El). Additionally TGF-β can increase amounts of ECM by inhibiting proteins that degrade ECM components. For example synthesis of plasminogen activator inhibitor-1 (PAI-1) and tissue inhibitor of metalloproteinase-1 (TIMP-1) is elevated after TGF-β2 treatment, leading to a decreased activity of MMP2 (Fuchshofer et al., 2003). Those proteins inhibit proteolytic degradation of ECM components, meaning an elevated activity would lead to an increase in ECM accumulation (Fuchshofer and Tamm, 2009). In ex-vivo perfused anterior eye chambers TGF-β2 leads to a decreased AH outflow rate, most likely by the observed increase of FN, PAI-1 and the accumulation of fibrillary material (Fleenor et al., 2006; Gottanka et al., 2004). Further, adenoviral gene transfer of TGF-β2 causes an elevation of IOP in mice and rats. In mice it could be proven that the AH outflow facility is reduced and the grade of ocular hypertension correlates with TGF-β2 expression level in this mouse model (Shepard et al., 2010).

Regarding the ONH, treatments with TGF-β2 lead to an increased expression and synthesis of EL, Col I, Col IV, Col VI and FN in astrocytes via the canonical Smad signaling pathway (Fuchshofer et al., 2005; Neumann et al., 2008; Zode et al., 2011). *In situ* TGF-β2 levels are elevated in the ONH of glaucoma patients and it was shown that

its source are mostly astrocytes in the prelaminar region (Pena et al., 1999; Zode et al., 2011). Experiments with LC cells provided the same results. In this cell type treatments with TGF-β2 lead to an increased expression and syntheses of ECM components, similar to those observed in the TM (Kirwan et al., 2005; Kirwan et al., 2009; Zode et al., 2011).

TGF-β's downstream mediator CTGF is also strongly involved in the pathogenesis of POAG. It is able to induce restructuring of the ECM, either alone or together with TGF-β, in the TM (Junglas et al., 2009). The 38kDa large protein belongs to the CCN-family (CTGF, cysteine-rich angiogenic protein 61, nephroblastoma overexpression gene and wnt inducible pathway protein 1 – 3) and is therefore also known as CCN2. Members of the CCN family are involved in various cellular processes like adhesion, proliferation, differentiation and survival and also in biological processes like angiogenesis, chondrogenesis, tumorogenesis and wound healing (Brigstock, 2003).

Data on CTGF concentration in the AH of POAG patients is slightly controversial. One study shows that CTGF levels are slightly increased in the AH of POAG patients, while CTGF levels in AH of patients with pseudoexfoliation (PEX) glaucoma are considerably increased(Browne et al., 2011). Another study shows highly elevated levels in the AH of POAG and pseudoexfoliation (PEX) glaucoma patients (Fahmy, 2008). CTGF influences ECM reorganization and the actin cytoskeleton. In the anterior eye segment TM cells and SC cells are able to produce CTGF and this production can be increased in TM cells by treatment with TGF-β1 or via high pressure perfusion (Chudgar et al., 2006). Furthermore SC cells of glaucomatous donors express significantly more CTGF than those of healthy controls (Overby et al., 2014b) and TM cells react to stiffer substrates with an upregulation of CTGF expression (Raghunathan et al., 2013). In recent studies our group could show that actually most effects of TGF-β on TM ECM are mediated by CTGF (Junglas et al., 2009) and that CTGF modulates the biological properties of the actin cytoskeleton increases its contractility (Junglas et al., 2012).

Astrocytes of the ONH do not show accumulation of ECM when treated with TGF-β2 after a knockdown of CTGF. This shows that in this region, too, the fibrotic effects of TGF-β2 depend on the presence of CTGF (Fuchshofer et al., 2005).

In mice a lens-specific overexpression of CTGF leads to glaucomatous changes with elevated IOP and a loss of RGC axons in the optic nerve. This effect is most likely

mediated by the modification of the actin cytoskeleton in the TM. Additionally, levels of FN and smooth muscle actin alpha (α-SMA) are increased in the iridocorneal angle of this mouse model (Junglas et al., 2012). The effects of the CTGF overexpression mimic the pathological changes occurring in human eyes in POAG. That makes these mice an applicable model for POAG and gives us the opportunity to investigate molecular factors involved in the pathogenesis of this disease.

All these findings show the essential role that TGF-β and CTGF are playing in the pathological changes occurring in the TM and the ONH of POAG patients. Since both growth factors are present in a healthy eye and fulfill essential roles there, we hypothesize that endogenous antagonists are necessary to keep the balance between physiological and pathological concentrations of TGF-β and CTGF. Due to that it is of great importance to identify these possible antagonists which might be able to interfere with TGF-β's and CTGF's pathological effects in the eye.

2.5 Decorin – an antagonist of TGF-β and CTGF

DCN is probably the best-studied member of the small leucine-rich proteoglycan (SLRP) family, which includes 18 distinct members in five discrete classes. The protein family is characterized by multiple adjacent domains bearing a leucine-rich repeat (Hocking et al., 1998). Sequences of SLRPs are conserved across multiple species (McEwan et al., 2006; Neill et al., 2012; Schaefer and Iozzo, 2008). The name Decorin is due to its close interaction with collagen fibers that could be seen as "decoration". DCN was initially cloned and named PG40 in 1986 and first seen as a mere structural component of the ECM (Krusius and Ruoslahti, 1986). It was discovered that DCN actually plays essential parts in differentiation, proliferation, spreading and migration and that it is further an important regulator of inflammation (Border et al., 1992; Yamaguchi et al., 1990; Yamaguchi and Ruoslahti, 1988).

DCN is about 90 kDa in size and contains a core protein of about 40 kDa and a single glycosaminoglycan (GAG) side chain of about 50 kDa consisting of either dermatan or chondroitin sulfate. 12 leucine rich repeats (LRRs) are located in the core protein, presenting the typical element of all SLRPs. The protein is divided into four different domains. The first domain contains the signaling peptide and the propeptide, the second

consists of four cysteine residues to which the GAG-sidechain can bind. In the third domain there are the leucine-rich repeats and the fourth domain contains again two cysteine residues, which form a big loop (Iozzo, 1998).

The crystalline structure of DCN is horseshoe-shaped. The concave area is formed by a β-leaflet while the convex area is formed by α-helices. Binding to the collagen triple helix is achieved by the core proteins' inner concave surface (Scott, 1996; Weber et al., 1996). This binding of collagen fibers is essential for a normal organization of the ECM and for the stability of connective tissue. In mice with a homozygous knockout of DCN wound healing is significantly slowed and formation of scare tissue is increased. In comparison to wildtype animals the dermis of DCN knockout ($DCN^{-/-}$) mice is thinner and the expansibility of collagen fibers is reduced (Danielson et al., 1997). Also fibrotic processes are enhanced in $DCN^{-/-}$ mice. For example thioacetamide-induced liver fibrosis is significantly stronger and takes longer to heal than in wildtype mice (Baghy et al., 2011). DCNs' inhibitory effect on cell division could also be demonstrated in $DCN^{-/-}$ mice. In contrast do wildtype mice fibroblast numbers in the periodontal ligament are doubled in $DCN^{-/-}$ mice (Hakkinen et al., 2000).

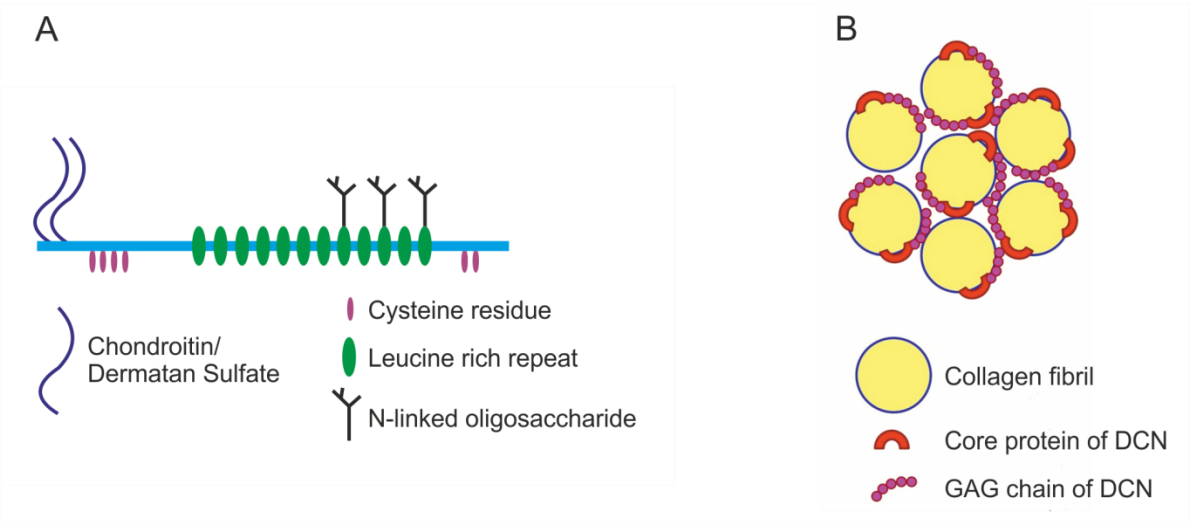

Figure 5: Schematic drawing of DCN structure (A) and binding model to C (B). DCN consists of 12 leucine rich repeats, 6 cysteine residues, a GAG side chain and a variable number of n-linked oligosaccharides (A). Collagen fibrils are assembled into a collagen bundle by the antiparallel complex of the CS/DS hybrid GAG chains of Decorin (B) (Kosho, 2013).

One property that brought DCN in the focus of much research during the last years is its strong involvement in tumor growth. *In vivo* about 30% of $DCN^{-/-}$ mice develop spontaneous intestinal tumors (Bi et al., 2008). Furthermore DCN expression is drastically reduced or completely absent in tumors when compared to expression levels of normal tissue (Bozoky et al., 2014; Liang et al., 2013).

In the eye DCN is present in cornea, retina and TM (Funderburgh et al., 1998; Inatani et al., 1999; Tanihara et al., 1995). Regarding POAG DCN is of special interest since it is able to bind TGF-βs and CTGF and thereby inhibit their profibrotic effects. In 1990 it was demonstrated that Chinese hamster ovary cell growth is inhibited in the presence of DCN and that this is due to the fact that DCN binds TGF-β, which is necessary for growth in this cell type (Yamaguchi et al., 1990). If DCN is bound to the ECM, it may scavenge TGF-βs directly and therefore prevent their interaction with TGF-β RII (Yamaguchi et al., 1990). On the other hand, soluble DCN is able to bind to insulin-like growth receptor I (IGF-IR), an effect that subsequently leads to an upregulation of Fibrillin-1 (FBN1) synthesis via the activation of the pAKT/AKT pathway (Kaartinen and Warburton, 2003; Schonherr et al., 2005). FBN1 is necessary for the control of TGF-β activation, as it controls the assembly and stability of the latent TGF-β complex (Annes et al., 2003). Clearly, the modulation of TGF-β signaling by DCN will indirectly take influence on that of its downstream mediator CTGF, but there is also evidence that DCN is able to bind to CTGF at LRR 10 - 12 and thereby inhibit its effects on ECM expression and synthesis and its capability to induce actin stress fiber formation (Vial et al., 2011).

The regulatory effects of TGF-β on DCN seem to be cell type dependent. In human skin fibroblasts and human chondrocytes TGF-β down-regulate DCN expression (Kahari et al., 1991; Roughley et al., 1994). In murine osteoblasts, on the other hand, TGF-β1 leads to an upregulation of DCN expression (Takeuchi et al., 1993) and the same effect was observed in rat mesangial cells (Border et al., 1990).

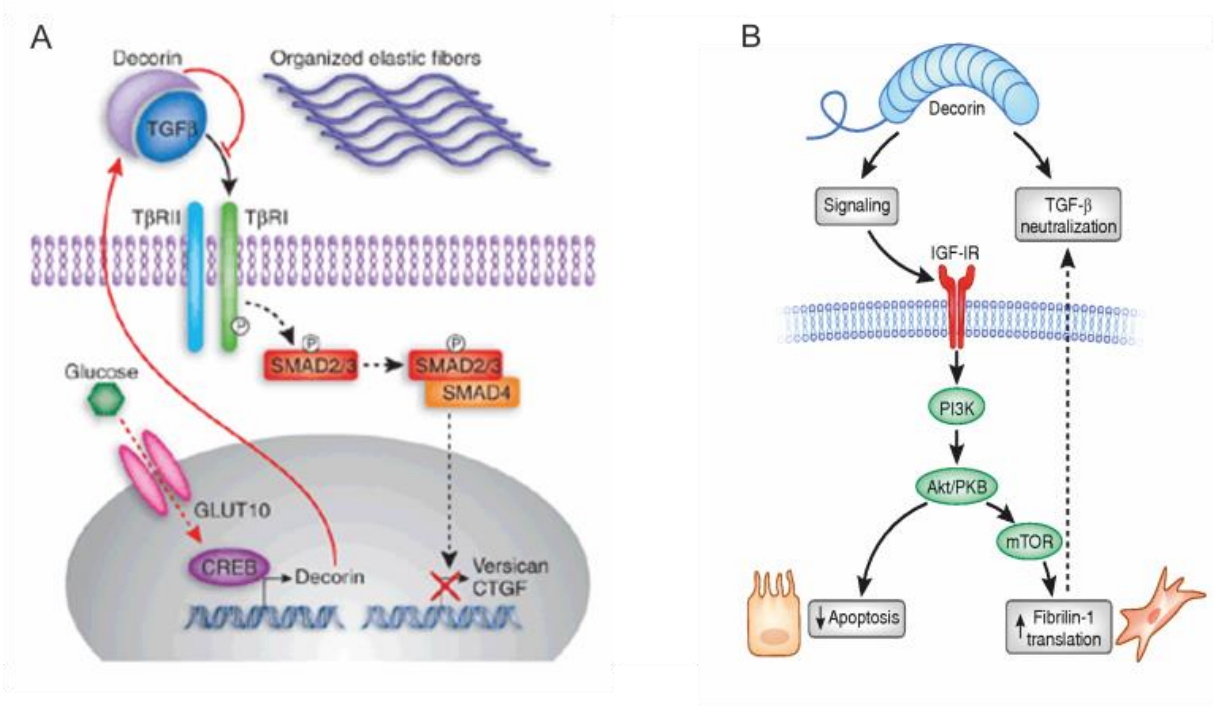

Figure 6: TGF-β inhibition by DCN. Matrix bound DCN (A) binds to directly TGF-β, the canonical TGF-β signaling pathway can't be activated by binding of TGF-β to TGF-β RII. Soluble DCN (B) binds to IGF-IR, Fib 1 translation is upregulated and TGF-β is neutralized (Akhurst, 2006; (Schaefer, 2011).

In the eye, DCN has, up till now, mostly been studied in the context of corneal haze formation, because a mutation in the encoding gene may lead to congenital stromal corneal dystrophy, a condition that is characterized by the presence of corneal opacities which become visible at or shortly after birth (Rodahl et al., 2006). The phenotype may lead to corneal scaring and blindness, a process that is typically associated with and enhanced by increased TGF-β signaling. There is evidence that tissue-specific viral gene transfer of DCN by means of AAV-5 DCN gene therapy inhibits corneal scarring significantly (Mohan et al., 2011) and that this is due to an inhibitory effect of DCN on TGF-β in corneal fibroblasts (Mohan et al., 2010).

More recently, it was shown that SC cells of glaucomatous donors express significantly lower amounts of DCN than SC cells of healthy controls but that DCN is more strongly upregulated by stiffer substrates in glaucomatous SC cells (Overby et al., 2014b). In accordance to this, the ECM deposited of HTM cells treated with dexamethasone is about 4-fold stiffer and contains elevated levels of DCN compared to the ECM of untreated controls (Raghunathan et al., 2015). Till now, it is unclear if DCN serves as a kind of rescue mechanism against too high levels of TGF-β and CTGF in the eye and if

the presence of too little DCN favors the onset of POAG, but in rats with TGF-β induced hypertension intravitreal injections of DCN lowered IOP and reduced RGC loss by reducing ECM accumulation in the TM (Hill et al., 2015). These findings make DCN a highly interesting candidate for lowering IOP and preventing or slowing down the onset and progression of POAG.

2.6 Aims of the study

The aim of this study is to investigate the reciprocal effects of TGF-β2, CTGF and DCN in ocular cell types involved in the pathogenesis of POAG. Further it is of interest to clarify whether DCN is able to reduce the expression and synthesis of ECM components in these cell types.

Since murine ON astrocytes are easier to receive than human ON astrocytes we want to find out if murine ON astrocytes react in the same way to TGF-β2, CTGF and DCN treatments as human ones. Additionally this cell line is used to analyze via which pathway DCN influences TGF-β and CTGF expression.

In vivo, this study focuses on two different mouse models. βB1-CTGF mice are used to investigate the effects of a lens-specific overexpression on DCN expression and synthesis in TM and ON. $DCN^{-/-}$ mice are studied to confirm our hypothesis that a lack of DCN in the eye leads to elevated levels of TGF-β2 and CTGF and thus to elevated IOP and loss of exons.

The following experiments were carried out to achieve these aims:

- Analysis of DCN levels in the chamber angle of eyes of glaucomatous and healthy donors
- Evaluation of reciprocal effects of TGF-β2, CTGF and DCN in human TM cells, human ONH astrocytes and murine ON astrocytes.
- Analysis of FN and Col IV expression and synthesis after DCN treatment in human TM cells and human ONH astrocytes.
- Analysis of the effects of inhibiting the AKT-pathway on DCN ability to regulate TGF-β and CTGF.
- Analysis of DCN levels in the corneo-scleral ring, the ON and the ONH of βB1-CTGF mice.

- Analysis of TGF-β, CTGF, FN and Col IV levels in the corneo-scleral ring and the ON of $DCN^{-/-}$ mice.
- IOP measurements of $DCN^{-/-}$ mice and their wildtype littermates of different ages and in different backgrounds
- Quantification of optic nerve axons of $DCN^{-/-}$ mice and their wildtype littermates of different ages and in different backgrounds

3. Materials and methods

3.1 Materials

3.1.1 Reagents

Designation	Source of supply
0.05 % Trypsin/EDTA	PAA The Cell Culture Company, Pasching, Austria
10 x PCR-Buffer	Qiagen, Hilden, Germany
2-Mercaptoethanol	Roth, Karlsruhe, Germany
2,4,6-Tri(dimethylaminomethyl)phenol (DPM-30)	Roth, Karlsruhe, Germany
2-Dodecenylsuccinic-acid-anhydride (DDSA)	Roth, Karlsruhe, Germany
Acetic acid, glacial	Merck, Darmstadt, Germany
Acetone	Merck, Darmstadt, Germany
Albumin Fraction V (BSA)	Roth, Karlsruhe , Germany
Agarose	Biozym Scientific, Oldendorf, Germany
Ammonium persulfate (APS), 10% (w/v)	Roth, Karlsruhe, Germany
Astrocyte growth supplement (AGS)	Sciencell, Carlsbad, USA
BC Assay Reagent A+B	Interchim, Wörgl, Österreich
BC Assay Reagent 1+2	Roth, Karlsruhe, Germany
Casyton	Roche/Innovatis, Bielefeld, Germany
CDP-Star	Roche, Penzberg, Germany
Chloroform	Roth, Karlsruhe, Germany
Coomassie®Brillant Blue R-250	Sigma-Aldrich, Taufkirchen, Germany
Connective tissue growth factor	Self purification
Connective tissue growth factor	Prospec, Rehovot, Israel
Decorin, human recombinant	R&D Systems, Minneapolis, USA
Decorin, mouse recombinant	R&D Systems, Minneapolis, USA
Desoxynukleosid-Triphosphate (dNTPs)	Qiagen, Hilden, Germany
Dexamethason	Sigma-Aldrich, Taufkirchen, Germany
Dimethylsulfoxid (DMSO)	Roth, Karlsruhe, Germany
DL-Dithiothreitol (DTT)	Sigma-Aldrich, Taufkirchen, Germany
Dulbecco's Modified Eagle Medium (DMEM)	PAA The Cell Culture Company, Pasching, Austria
Dulbecco’s Modified Eagle Medium (DMEM) F12	PAA The Cell Culture Company, Pasching, Austria
Donkey Serum	Abcam, Cambridge, England
EDTA	Roth, Karlsruhe, Germany
Epon	Serva, Heidelberg, Germany
Ethanol 100%	Roth, Karlsruhe, Germany

Ethidiumbromide	Serva, Heidelberg, Germany
Fetal calve serum (FCS)	Biochrom AG, Berlin, Germany
Fluorescein	Qiagen, Hilden, Germany
Fluorescent Mounting Medium	DakoCytomation, Hamburg, Germany
Formaldehyde	Roth, Karlsruhe, Germany
Gelatine	Sigma-Aldrich, Taufkirchen, Germany
Glutaraldehyde, 25% in water	Serva, Heidelberg, Germany
Glycerine	Roth, Karlsruhe, Germany
Glycin	Merck, Darmstadt, Germany
Guanidin HCl	Roth, Karlsruhe, Germany
Hydrochloric acid (37%)	Merck, Darmstadt, Germany
Isoflurane	Baxter, Heidelberg, Germany
Isopropanol	Roth, Karlsruhe, Germany
Ketamine	Wirtschaftsgenossenschaft Deutscher Tierärzte (WDT), Garbsen, Germany
Luminata Forte, Western HRP	Millipore Cooperation, Billerica, USA
Magnesium chloride (25 mM)	Qiagen, Hilden, Germany
Methanol	Merck, Darmstadt, Germany
Milk powder (MM)	Roth, Karlsruhe, Germany
MTT Reagent	Roche, Mannheim, Germany
N,N,N`,N`,-Tetramethylethylendiamine, (TEMED)	Roth, Karlsruhe, Germany
Paraformaldehyde (PFA)	Sigma-Aldrich, Taufkirchen, Germany
PBS	PAA The Cell Culture Company, Pasching, Austria
Penicilllin-Streptomycin	PAA The Cell Culture Company, Pasching, Austria
Phalloidin	Sigma-Aldrich, Taufkirchen, Germany
Phosphatase-Inhibitor-Mix	Sigma-Aldrich, Taufkirchen, Germany
Potassium chloride	Roth, Karlsruhe, Germany
Potassium dihydrogen phosphate	Roth, Karlsruhe, Germany
Protease-Inhibitor-Mix M	Serva Electrophoresis GmbH, Heidelberg, Germany
Proteinase K	Sigma-Aldrich, Taufkirchen, Germany
peqGold TriFastTM (Trizol)	PeqLab, Erlangen, Germany
Roti®-Free Strippingbuffer	Sigma-Aldrich, Taufkirchen, Germany
Rotiphorese® Gel 30 (30 % Acrylamid, 0.8 % Bisacrylamid; 37.5:1)	Sigma-Aldrich, Taufkirchen, Germany
Saccharose	Roth, Karlsruhe, Germany
Sodium chloride	Roth, Karlsruhe, Germany
SDS (Sodium dodecylsulfat)	Roth, Karlsruhe, Germany
Sodium dihydrogen phosphate	Merck, Darmstadt, Germany
Sodium hydroxide	Roth, Karlsruhe, Germany
Sodium phosphate	Roth, Karlsruhe, Germany

SYBR-Green I	Qiagen, Hilden
Tissue-Tek®	Sakura, Zoeterwoude, Netherlands
Transforming Growth Factor 2 (TGFβ2)	R&D Systems, Minneapolis, USA
Triciribine	Selleckchem, Houston, USA
Tris Ultrapure, MB Grade	Usb Coorporation, Cleveland, USA
Tris HCl	Roth, Karlsruhe, Germany
Triton X 100	Roth, Karlsruhe, Germany
Tween 20	Roth, Karlsruhe, Germany
Vectashield Mounting Medium for Fluorescence with DAPI	Vector Laboratories, Burlingame, USA
Water Rotisolv (Rnase-free)	Roth, Karlsruhe, Germany
Xylazine	Serumwerk Bernburg, Bernburg, Germany

Table 1 : **Reagents**

3.1.2 Enzymes and Reagent-Kits

Designation	**Source of supply**
iScript™ cDNA Synthesis Kit	BioRad, Munic, Germany
Hot Star Taq DNA Polymerase	Qiagen, Hilden, Germany
qScript™ cDNA Synthesis Kit	Quanta, Gaithersburg, USA
Taq DNA Polymerase	Self purification

Table 2: Enzymes and reagent kits

3.1.3 Oligonucleotide primers and DNA ladders

Primer	**Species**	**Orientation**	**Sequence 5' to 3'**
DCN 3	*Mus musculus*	forward	ctgaagatgacactggcatcgg
DCN 5	*Mus musculus*	reverse	ccttctggcacaagtctcttgg
DCN PGK	*Mus musculus*	forward	tggatgtggaatgtgtgcgagg
βB1 f	*Mus musculus*	forward	gtgcgggacagaaacctg
βB1 r	*Mus musculus*	reverse	ggaagtgccagctcatcagt
SV40 f	*Mus musculus*	forward	gcgaaggaaccttacttctgtggtg
SV40 r	*Mus musculus*	reverse	gtccttggggtcttctacctttctc

Table 3: Primers for Genotyping PCR

Primer	Species	Orientation	Sequence 5' to 3'	Position
Col IV a2	*Homo sapiens*	forward	acaggacagaaaggagacca	1307 - 1326
Col IV a2	*Homo sapiens*	reverse	ggtgtgatgcctgggaac	1381 - 1400
CTGF	*Homo sapiens*	forward	ctcctgcaggctagagaagc	884 - 903
CTGF	*Homo sapiens*	reverse	gatgcacttttgcccttctt	957 - 977
DCN	*Homo sapiens*	forward	tcgagtggtccagtgttctg	280 - 299
DCN	Homo sapiens	reverse	ccttttggtgttgtgtcca	365 - 384
FN	*Homo sapiens*	forward	ccctgattggaaggaaaaaga	6217-6237
FN	*Homo sapiens*	reverse	atgaagattggggtgtggaa	6265-6284
GNB2L*	*Homo sapiens*	forward	gctactaccccgcagttcc	170 - 188
GNB2L*	*Homo sapiens*	reverse	cagtttccacatgatgatggtc	220 – 241
TGF β 1	*Homo sapiens*	forward	cagccggttgctgaggta	1362 – 1379
TGF β 1	*Homo sapiens*	reverse	aagaagcgggctttggac	1408 – 1425
TGF β 2	*Homo sapiens*	forward	ccaaagggtacaatgccaac	1194 – 1213
TGF β 2	*Homo sapiens*	reverse	cagatgcttctggatttatggtatt	1283 – 1307
CTGF	*Mus musculus*	forward	tgacctggaggaaaacattaaga	948-970
CTGF	*Mus musculus*	reverse	agccctgtatgtcttcacactg	1038-1059
DCN	*Mus musculus*	forward	gagggaactccacttggaca	1039-1058
DCN	*Mus musculus*	reverse	ttgttgttgtgaaggtagacgac	1134-1112
GNB2L*	*Mus musculus*	forward	tctgcaagtacacggtccag	514 – 533
GNB2L*	*Mus musculus*	reverse	gagacgatgataggttgctg	584 – 604

FN	*Mus musculus*	forward	cggagagagtgccctacta	4201 – 4220
FN	*Mus musculus*	reverse	cgatattggtgaatcgcaga	4277 – 4258
GFAP	*Mus musculus*	forward	tcgagatcgccacctacag	1156 – 1174
GFAP	*Mus musculus*	reverse	gtctgtacaggaatggtgatgc	1201 – 1222
RPL32*	*Mus musculus*	forward	gctgccatctgtttacgg	29-47
RPL32*	*Mus musculus*	reverse	tgactggtgcctgatgaact	107-126
TGF β 1	*Mus musculus*	forward	tggagcaacatgtggaactc	1358 – 1377
TGF β 1	*Mus musculus*	reverse	gtcagcagccggttacca	1413 – 1430
TGF β 2	*Mus musculus*	forward	tcttccgcttgcaaaacc	4795 - 4812
TGF β 2	*Mus musculus*	reverse	gtgggagatgttaagtctttgga	4863 - 4885
αSMA	*Mus musculus*	forward	caaccgggagaaaatgacc	667 - 685
αSMA	*Mus musculus*	reverse	cagttgtacgtccagaggcata	752 - 773

Table 4: Primers for Real Time RT PCR; * housekeeper

All primers were purchased from Invitrogen, Karlsruhe, Germany.

3.1.4 Antibodies and molecular weight standards

Protein	**Primary antibody**	**Source of supply**
AKT	Monoclonal rabbit anti human/mouse/rat AKT	Cell Signaling Technology, Cambridge, England
CTGF	Polyclonal goat anti human/rat CTGF	Santa Cruz Biotechnology, Santa Cruz, USA
Collagen-Typ-IV	Polyclonal rabbit anti human Collagen Type IV	RDI, Flanders, NJ, USA
Decorin LF136	Polyclonal rabbit anti human DCN	L. Fisher

Decorin LF113	Polyclonal rabbit anti mouse DCN	L. Fisher
Decorin H80	Polyclonal rabbit anti human/mouse DCN	Santa Cruz Biotechnology, Santa Cruz, USA
Fibronectin	Polyclonal rabbit anti Fibronectin	Dako, Hamburg, Germany
Fibronectin H300	Polyclonal rabbit anti human Fibronectin	Santa Cruz Biotechnology, Santa Cruz, USA
GFAP	Polyclonal chicken-anti-GFAP	Lifespan, Biosciences, Seattle, USA
GFAP	Polyclonal rabbit anti GFAP	Dako, Hamburg, Deutschland
Phospho AKT	Monoclonal rabbit anti human/mouse/rat pAKT	Cell Signaling Technology, Cambridge, England
Phopspho Smad2	Monoclonal rabbit anti human/mouse/rat pSmad2	Cell Signaling Technology, Cambridge, England
Smooth-muscle α-Actin	Monoclonal mouse anti Mouse	Immunotech International (Dianova), Hamburg
Tubulin α	Polyclonal rabbit anti human	Rockland, Pottstown, USA

Table 5: Primary antibodies

Secondary antibody	**Source of supply**
AffiniPure Donkey Anti Rabbit Cy™3 conjugated	Dianova, Hamburg, Germany
AffiniPure Donkey Anti Goat Cy™3 conjugated	Dianova, Hamburg, Germany
Chicken anti Goat IgG, AP conjugated	Santa Cruz Biotechnology, Santa Cruz, USA
Chicken anti Goat IgG, HRP conjugated	Santa Cruz Biotechnology, Santa Cruz, USA
Chicken anti Rabbit IgG, AP conjugated	Santa Cruz Biotechnology, Santa Cruz, USA
Chicken anti Rabbit IgG, HRP conjugated	Santa Cruz Biotechnology, Santa Cruz, USA
Chicken anti Rabbit IgG, AP conjugated	Cell Signaling Technology, Cambridge, England
Chicken anti Rabbit IgG, HRP conjugated	Cell Signaling Technology, Cambridge, England
Rabbit anti GPADH, HRP conjugated	Cell Signaling Technology, Cambridge, England
Streptavidin Alexa Fluor® 488 conjugated	MoBitec Molecular Probes, Goettingen

Table 6: Secondary antibodies

Tables above show all antibodies used for western blotting and immunohistochemistry. In western blot analysis the height of detected bands was determined with a protein molecular weight standard (Fisher BioReagents™ EZ-Run™ Prestained Rec Protein Ladder, Fisher Scientific, Waltham, USA).

3.1.5 Chemical composition of gels, solvents and buffers

Solvent/Buffer	**Composition**
0.1 M Cacodylate Buffer	10.7 g Cacodylate acid in 500 ml dH2O
0.1 M Phosphate Buffer, pH 7.4	100 ml 0.2 M Na_2HPO_4 x $2H_2O$ with 0.2 M NaH_2PO_4 x H_2O, pH 7.4 dilute with dH_2O to 0.1 M
10 x Electrode Buffer	250 mM Tris/HCl 400 mM Glycin 1% (w/v) SDS solved in dH_2O; ad 1 l
Coomassie-Destaining Solution	500 ml Methanol 10 ml Actic acid filled up with ad 1 l
Coomassie-Staining Solution	40 ml Methanol 2 ml Acetic acid 0.2 g Coomassie-Brilliant Blue R-250 filled up with; ad 100 ml
Detection Buffer, pH 9	15.76 g 0.1 M Tris/HCL (pH 6.8) 5.84 g 0.1 M NaCl solved in dH_2O; ad 1 l
Epon Stem A	62 ml Glycidether 100 with 100 ml DDSA
Epon Stem B	100 ml Glycidether 100 with 89 ml NMA
Mowiol with DAPI	2.4 g Mowiol 4-88 6.0 g Glycerin 6.0 ml H_2O dest. 12.0 ml 0.2 M Tris-HCl (pH 8.5) 25.0 ml DABCO per 1.0 ml DAPI (1:10)

PBS, 10x, pH 7.4	80 g NaCl 2 g KCl 4.4 g Na_2HPO_4 2.4 g KH_2PO_4 dH_2O ad 1 l, autoclave
RIPA-Buffer, pH 8	150 NaCl 1 % (v/v) Tergitol 0.5 % (w/v) Deoxycholic acid 0.1 % (w/v) SDS 50 mM Tris
SDS 10 % (w/v)	10 g SDS in dH_2O; ad 100 ml
SDS-PAGE-Running Buffer, 10x	250 mM Tris/HCl 400 mM Glycin 1% (w/v) SDS in dH_2O; ad 1 l
SDS-Sample Buffer, 5x	0.25 M Tris/HCl, pH 6.8 30 % Glycerin 8 % (w/v) SDS 0.02 % (w/v) Bromophenol blue 0.3 M DTT and 10% β-Mercaptoethanol
TBS 10x, pH 7,4	30 g Tris 80 g NaCl 2 g KCl dH_2O ad 1 l, autoclave
TBST 1x	100 ml 10x TBS 0.05% (v/v) Tween 20 dH_2O ad 1 l
Transfer Buffer 10x	5.8 g Tris 2.9 g Glycin 200 ml Methanol 3.7 ml 10% (w/v) SDS in dH_2O, ad 1 l
Tris/HCl, 1.0 M, pH 6.8	121.14 g Tris in dH2O; ad 1 l
Tris/HCl, 1.5 M, pH 8.8	181.71 g Tris in dH_2O, ad 1 l
Washing Buffer for protein isolation	0.3 M Guanidine HCL in 95 % Ethanol

Table 7: Composition of solvents and buffers

3.1.6 Laboratory Equipment

Designation	Source of supply
Axiovert 40 CFL	Zeiss, Göttingen, Germany
BioPhotometer	Eppendorf, Hamburg, Germany
Casy®	Innovatis, Reutlingen, Germany
CFX Connect Real-Time PCR detection system	BioRad, Munic, Germany
Embedder	EM TP Leica, Wetzlar, Germany
FastPrep 24™	MP Biomedicals, Burlingame, USA
Hera Cell 150 Incubator	Heraeus, Hanau, Germany
Hera Safe steril work bench	Heraeus, Hanau, Germany
Inolab pH-Meter	WTW GmbH, Weilheim, Germany
IQ5 Multicolor Real-time PCR Detection System + iCycler	BioRad, Munic, Germany
Julabo SW20 water bath	Julabo Labortechnik GmbH, Seelbach, Germany
Kern PJL 2100-2M analytical balance	Kern & Sohn GmbH, Balingen-Frommern, Germany
LAS 3000 Intelligent Dark Box	Fujifilm, Düsseldorf, Germany
Mastercycler gradient, personal	Eppendorf, Hamburg, Germany
Memmert water bath	Memmert GmbH, Schwabach, Germany
Mettler AE 163 special accuracy scales	Mettler Toledo, Giessen, Germany
Microm HM 500 OM Kryostat	Microm International, Walldorf, Germany
Mikroskop Axio Imager. Z1	Zeiss, Göttingen, Germany
MilliQ Plus PF water purification system	Millipore Corporation, Billerica, USA
Minifold I Dot-Blot System SRC 96 Acryl	Schleicher & Schuell, Dassel, Germany
Model 45-101-i ClassII Electrophoresis System	Peqlab Biotechnologie GmbH, Erlangen, Germany
NanoDrop-1000 Spectrophotometer	Peqlab Biotechnologie GmbH, Erlangen, Germany
Pipetman Pipets	Gilson, Middleton, USA
Polymax 1040 shaker	Heidolph, Kelheim, Germany
PowerShot G5 Digital Camera	Canon, Krefeld, Germany
Research Pipets	Eppendorf, Hamburg, Germany
Semi-Dry Electrophoretic Transfer Cell	Peqlab Biotechnologie GmbH, Erlangen, Germany
Sunrise-Basic ELISA-Reader	Tecan Austria GmbH, Grodig, Austria
Systec V75 Autoclave	Systec GmbH, Wettenburg, Germany
Thermal mixer comfort	Eppendorf, Hamburg, Germany

TonoLab Tonometer	Icare Finnland, Helsinki, Finnland
UV-light screen	Bachhofer Laboratoriumsgeräte, Reutlingen, Germany
Ultracut E-Ultramicrotom	Reichert-Jung, Kirchseeon, Germany
Ultra Thurax	Biolabproducts, Bebensee, Germany
Vortex Genie 2	Scientific Industries Inc., New York, USA
Centrifuges 5415D, 5415R, 5804R, 5810R	Eppendorf, Hamburg, Germany

Table 8: Laboratory equipment

3.1.7 Consumables

Designation	**Source of supply**
„Falcon“ Reaction Tubes 15 ml, 50 ml	Sarstedt, Nürnbrecht, Germany
3MM Blotting ("Whatman") -Paper	Neolab, Heidelberg, Germany
Biosphere Filter Tips	Sarstedt, Nürnbrecht, Germany
CellScraper	Sarstedt, Nürnbrecht, Germany
Culture Slides	BD Falcon, Bedford, USA
Cover slips, 24 x 60mm	Menzel-Gläser, Braunschweig, Germany
Dispomed Syringe, single use	Dispomed Witt oHG, Geinhausen, Germany
EasyFlasks Nunclon™ Δ T25, T75	Nunc, Roskilde, Denmark
Ecoflo Dissecting instruments	Dispomed Witt oHG, Geinhausen, Germany
Glassware	Schott, Roth, VWR, Germany
Liquid Blocker PAP-Pen	SCI Science Services, Munic, Germany
Lysing Matrix D	MP Biomedicals, Burlingame, USA
Microseal®„B“ Film	Biorad, Munic, Germany
Multidishes Nunclon™ Δ 6-well	Nunc, Roskilde, Denmark
Multi-Reactiontubes	Roth, Karlsruhe, Germany
Omnifix syringe, sterile	B. Braun, Wertheim, Germany
Parafilm	Pechiney Plastic Packaging, Chicago, USA
Pasteurpipets	Brand, Wertheim, Germany
PCR Plates, 96 well iCycler IQ	Biorad, Munic, Germany
Personna Razor blades	American Safety Razor Company, Verona,USA
Pipet tips	Sarstedt, Nürnbrecht, Germany
Powderfree Sempercare gloves	Sempermed, Wien, Austria
PVDF-Western Blot Membrane	Roche, Mannheim, Germany
Rotilabo 0,22 µm syringe filter	Roth, Karlsruhe, Germany
Serological pipets	Sarstedt, Nürnbrecht, Germany
Sterican injection cannula	B. Braun, Wertheim, Germany
SuperFrost®Plus object slides	Menzel-Gläser, Braunschweig, Germany

Table 9: Consumables

3.2 Animal models

3.2.1 Animals and animal husbandry

For *in vivo* experiments CD1 wildtype mice, transgenic βB1-CTGF mice in a CD1 background and DCN knockout (DCN $^{-/-}$) mice in a mixed background were used.CD1 mice were offspring of a breeding pair purchased at Charles River, Sulzfeld, Germany, and were bred in the animal facility of Prof. Dr. E. Tamm, institute for human anatomy and embryologie, University of Regensburg. Transgenic βB1-CTGF mice have been generated in our own working group and were kindly provided by Prof. Dr. R. Fuchshofer (Junglas et al., 2012). DCN $^{-/-}$ mice have been generated in the group of Prof. Dr. R. Iozzo at the institute for pathology and cell biology, Thomas Jefferson University, USA (Danielson et al., 1997). These mice were kindly provided by Prof. Dr. L. Schaefer (Pharma Zentrum Frankfurt, Goethe University, Germany).
All animals were kept accordingly to the ARVO Statement for the use of animals in ophthalmic and vision research, at temperatures of 23 ± 2 °C and humidity of 55 ± 5 %, with food and water *ad libitum.* Light-dark circles were set to 12 hours.

3.2.2 βB1-CTGF mice

Transgenic βB1-CTGF mice carry a construct in which murine CTGF cDNA is controlled via the chicken- βB1 promotor. This leads to a lens specific overexpression of CTGF. Additionally a SV40 poly(A) sequence of the SV40 small T-intron is located at the end of the construct. Thereby the polyadenylation signal is transcribed to ensure the stability of CTGF mRNA. To be able to analyze wildtype littermates, a CD1 Wildtype (WT) animal was mated with a transgenic animal. Genotyping of the animals was carried out as described in 3.2.2.1.

Figure 7: βB1 construct of βB1-CTGF mice (Provided by Prof. Dr. R. Fuchshofer, modified)

3.2.3 DCN Knockout ($DCN^{-/-}$) mice

In this mouse line the function of DCN is destroyed by integration of a neomycin resistance cassette under the control of the Pgk promotor. This leads to a systemic knockout of DCN (Danielson *et al.,* 1997). To be able to use wildtype littermates as control groups, heterozygous $DCN^{+/-}$ animals were mated, resulting in homozygous knockout, homozygous wildtype and heterozygous offspring.

3.3 Biomolecular Techniques

3.3.1 Isolation of mouse tail DNA

For genotyping genomic mouse tail DNA was used. Mice were anesthetized with Isoflurane and about 0.5 cm of the tail was cut off, using sterile surgical scissors. The mouse tail was transferred to a 1.5 ml tube and lysed with 200 µl proteinase K lysis buffer for at least 12 h at 55 °C. After this proteinase K was inactivated for 10 min at 95° C. Samples were centrifuged for 10 min at 10000 rpm to sediment insoluble parts. Genotyping PCRs were carried out with specific primers as described in 3.3.2.

3.3.2 Genotyping

Genotypes of the analyzed mice were determined by PCR (polymerase chain reaction) using specific primers (Table 3). Reaction mixes are shown in tables 10, 11 and 13. After amplification of the targeted sequence (Cycler Programs see table 12 and 14) the samples were loaded on agarose gels for electrophoreses.

3.3.2.1 Genotyping of βB1-CTGF mice

Genotyping of βB1-CTGF mice was carried out with specific primers for the βB1- and the SV40 region (Table 3), which are both expressed in transgenic animals only. Reaction mixes for PCRs are shown in table 10 and 11.

βB1 PCR	
H_2O	11.25 µl
Q-Buffer	1.5 µl
βB1 Primer forward 1:10	0.3 µl
βB1 Primer reverse 1:10	0.3 µl
dNTPs (10mM)	0.3 µl
Taq DNA-Polymerase	0.15 µl
DNA	1.2 µl

Table 10: **Reaction mix for βB1 PCR**

SV40 PCR	
H_2O	7.35 µl
Q-Buffer	1.5 µl
5x Glycerol	3 µl
SV40 Primer forward (1:10)	0.3 µl
SV40 Primer reverse (1:10)	0.3 µl
dNTPs (10mM)	0.3 µl
MgCl2 (25mM)	1 µl
Taq DNA-Polymerase	0.25 µl
DNA	1 µl

Table 11: Reaction mix for SV40 PCR

βB1 and SV40 PCR Cycler Programs				
Product	**βB1**		**SV40**	
	360 bp		**300 bp**	
	° C	**Duration**	**° C**	**Duration**
1. Step	96	2 min	94	2 min
2. Step	90	30 sec	94	30 sec
3. Step	65	30 sec	55	30 sec
4. Step	72	20 sec	72	45 sec
5. Step	72	2 min	72	5 min
6. Step	10	∞	10	∞
Cycles (2-5)	35 x		35 x	

Table 12: Thermocycler programs for βB1- and SV40 PCR

3.3.2.2 Genotyping of DCN$^{-/-}$ mice

For genotyping of DCN$^{-/-}$ mice three different primers were used: one forward primer binding specifically in exon 2 (DCN3), one forward primer binding specifically to the pgk neomycin cassette (PGK Neo) and one reverse primer binding specifically to exon 2 (DCN 5). By using all three primers, wildtype-, knockout- and heterozygous animals can

be identified in the same PCR. The PCR results in a 161 bp product for wildtype- and in a 250 bp product for knockout animals. Heterozygous animals show both products.

DCN PCR	
H_2O	22 µl
Q-Buffer	5 µl
DCN 3 (1:10)	1 µl
PGK Neo (1:10)	1 µl
DCN 5 (1:10)	1 µl
dNTPs (10mM)	1 µl
Taq DNA-Polymerase	1 µl
DNA	3 µl

Table 13: Reaction mix for DCN PCR

DCN PCR Cycler Program		
Product	**DCN WT**	**DCN -/-**
	161bp	**250**
	° C	**Duration**
1. Step	95	4 min
2. Step	95	30 sec
3. Step	58	30 sec
4. Step	72	30 sec
5. Step	72	2 min
6. Step	10	∞
Cycles (2-5)	35	

Table 14: Thermocycler programs DCN PCR

3.3.3 Agarose gel electrophoresis

Agarose gel electrophoresis was used to analyze the DNA products of genotyping PCRs. 2 mg of agarose were dissolved in 100 ml TBE Buffer. Afterwards 4 µl of ethidium bromide (EtBr) at a final concentration of 50 ng/ml were added. EtBr intercalates in double stranded DNA and thereby makes the DNA fragments visible under UV light. 10 µl of the PCR product including loading dye were loaded on the agarose gel and then separated for 30 min at 130 V. To determine the size of the PCR product 2 µl of a standard DNA marker were loaded on the gel. DNA fragments were made visible using UV light (302 nm).

3.4 Expression analysis

3.4.1 RNA isolation

RNA from human and murine cells, as well as of mouse tissue was isolated after Chomczynski and Sacchi (Chomczynski and Sacchi, 1987). To decompose the cells and dilute the cell components peqGold TriFast™ Trizol reagent was used (Peqlab Biotechnologie GmbH, Erlangen). This single phase solution is based on phenol and guanidinisothiocyanat, and can be divided into three phases by the addition of chloroform. These phases contain RNA (aqueous phase), DNA (interphase) and proteins (phenol phase).

Samples for Real Time PCR were assimilated using an Ultra Thurax (Biolabproducts, Bebensee, Germany) in 500 µl of pegGold TriFast™ Trizol.

Samples for RNA sequencing were kept in 800µl RNA Later till further use. They were then transferred in 800µl pegGold TriFast™ Trizol in Shredder Tubes (Lysing Matrix D, MP Biomedicals, Burlingame, USA) and shredded for 45 sec and 6 m/s in a FastPrep-24™ instrument (MP Biomedicals, Burlingame USA). Afterwards Shredder Tubes were centrifuged for 2 min at 13000 rpm and the supernatant was transferred into a fresh reaction tube and 200µl pegGold TriFast™ were added.

After 5 min 140 µl per 500 µl pegGold TriFast™ Chloroform were added. After shaking thoroughly samples were incubated on ice for 5 min. Separation of phases was then achieved by centrifugation (20 min, 4 °C, 13200 rpm). The aqueous phase then was transferred carefully, without any components of the inter- or phenol phase, into a new tube and 300 µl of isopropanol were added. For precipitation of the RNA the samples were stored over night at -20 °C. Afterwards samples were centrifuged for 20 min (4 °C, 13200 rpm) to pelletize the RNA. The supernatant was discarded and the RNA pellet was washed twice in 1 ml 75% ethanol for 5 min and then centrifuged for 5 min (4 °C, 7600 rpm). After quantitative removal of the supernatant and drying of the RNA pellet, it was dissolved in 10 µl of RNase-free water. RNA was stored at -80 °C till further use.

3.4.2 RNA quantification

RNA was quantified using a NanoDrop-2000c spectral photometer (Peqlab Biotechnologie GmbH, Erlangen). The optical density of the sample was measured at λ = 260 nm (OD260), which is the absorption peak of nucleic acids (DNA, RNA), and at λ = 280 nm (OD280), which is the absorption peak of proteins against the solvent (H_2O). A OD260 of 1 is consistent with a RNA concentration of 40 µg/ml, therefore the concentration of RNA can be calculated as follows:

$$[\mu g/ml] = OD260 \times 40\ \mu g/ml$$

Purity of RNA can be determined via the OD260 to OD280 ratio. Pure RNA should have a ration between 1.7 and 2.0.

3.4.3 cDNA production

To analyze relative gene expression via real time RT PCR, RNA has to be transcribed to cDNA via reverse transcription. Oligo-dt-chains were used as primer to ensure that mRNA with polyA tail was transcribed. For cDNA synthesis "qScript™ cDNA Synthesis Kit" was used (Qanta Biosciences, Gaithersburg, USA). 200 ng or 500 ng of RNA were diluted in H2O to a volume of 7.5 µl and then 2.0 µl of qScript™ Reaction Mix and 0.5µl of qScript™ reverse Transcriptase were added. For each cDNA synthesis at least 3 negative controls (-RT), containing no reverse transcriptase, were made in addition to the cDNA samples (+RT). –RTs are necessary to estimate possible contamination of RNA. CDNA synthesis was carried out in a Thermocycler (Biorad, Munic, GER) using the following program

Program for cDNA synthesis	
Step 1	Incubation for 5min at 22°C
Step 2	Reverse transcription for 30min at 42°C
Step 3	Inactivation of reverse Transcriptase for 5min at 85°C

Table 15: Program for cDNA synthesis

3.4.4 Procedure of quantitative Real Time RT PCR

Relative gene expression of TGFβ1, TGFβ2, CTGF, FN and Col IV was analyzed in the corneo-scleral ring, in the optic nerve and in the optic nerve head of 8 week old DCN WT and $DCN^{-/-}$ mice. DCN expression was analyzed in the corneo-scleral ring, the optic nerve and the optic nerve head of 8 week old βB1-CTGF mice.

Human trabecular meshwork cells and optic nerve head astrocytes as well as murine optic nerve astrocytes were analyzed regarding their expression of DCN after treatment with either TGFβ2 or CTGF, and regarding their expression of TGFβ1, TGFβ2, CTGF, FN and Col IV after treatment with DCN. Murine optic nerve astrocytes were further analyzed regarding their expression of TGFβ1, TGFβ2, CTGF and DCN after treatments with DCN and the AKT-Signaling inhibitor triciribine.

Real Time PCR was carried out with an iQ5™ Multicolor Real-Time-PCR Detection System with iCycler or with a CFX Connect™ Real-Time PCR detection system (BioRad, Munic, GER). PCR products were detected via SYBR-Green I. Probes can be relatively standardized via the use of housekeeping genes. Used housekeeping genes are listed in Table 3.4. Each cDNA sample (+RT) was analyzed as a triplicate. To exclude possible contamination negative controls (-RT) and non-template controls (NTC) containing RNase free water were included. Each +RT, -RT and NTC was filled up with a Master-Mix (see Table 3.3.7) to a total volume of 10 µl. Samples were pipetted onto a 96-Well-Microtiterplate and 5 µl of Primer-Mix (0.17 µl forward primer, 0.17 µl reverse primer (0.1 M) and 4.66 µl RNase free water) with specific primers for the gene of interest were added.

Master-Mix (one reaction)	
0.3	µl sample (+RT cDNA, -RT cDNA or RNase free water)
2.0	µl 10x PCR Buffer
0.8	µl MgCl2 (25mM)
0.16	µl dNTPs
0.08	µl Taq DNA Polymerase (5 U/µl)
0.25	µl SYBR-Green I (7.4 % (v/v) in DMSO)
0.02	µl Fluorescein
0.17	µl per Primer (1µM)
11.49	µl RNase-free water

Table 16: Master Mix Real Time PCR

Plates were sealed with adhesive foil (Microseal „B“Film, BioRad, Munic, GER) and centrifuged shortly. The Real Time PCR program was carried out as follows:

Step	Temperature	Duration
1	94°C	2min
2 (50x)	94°C 60°C 70°C	20s 10s 20s
3	95°C	1min
4 (81x)	55°C +0.5°C per cycle	6s
5	4°C	∞

Table 17: Program for quantitative Real Time PCR

To analyze relative expression the program CFX Manager 3.1 was used (BioRad, Munic, GER). Via the Ct (Cycle threshold) value, meaning the cycle in which fluorescence is higher than background fluorescence, relative gene expression can be calculated. Therefore lower Ct values represent higher expression levels. Melting curves conduce to check the specificity of the products after the run (Wong and Medrano, 2005). Relative expression of target genes was calculated via the $2^{-\Delta\Delta ct}$ method (Schmittgen and Livak, 2008). Data analysis and graphical representation was carried out using Microsoft® Excel (Microsoft ® Corporation, Redmond, USA).

3.4.5 RNA sequencing

RNA Sequencing of corneo-scleral rings 8 and 12 week old $DCN^{-/-}$- and βB1-CTGF mice and their wildtype litter mates was carried out by M. Kretz and C. Ziegler (University of Regensburg, Germany).

3.5 Biochemical techniques

3.5.1 Protein isolation

3.5.1.1 RIPA-method

Protein from huTM cells as well as human and murine Astrocytes was isolated with RIPA Buffer. Cells were incubated with 300 µl RIPA Buffer + Protease inhibitor (1:100) + Phosphatase inhibitor (1:100) on ice for 5 min. Cells were scraped of the culture dishes and the lysate was transferred into a reaction tube. After 30 min incubation on ice the lysate was centrifuged for 10min and 20000 rpm. The supernatant was transferred into a new reaction tube and kept at -80 °C till further use.

3.5.1.2 peqGold TriFastTM Trizol-method

Protein of human and murine cells and mouse tissue was isolated, after RNA isolation with peqGold TriFast^{TM} Trizol-Reagent, from the inter- and phenol phase. Protein was precipitated with 750 µl Isopropanol per 500 µl peqGold TriFastTM Trizol. Previous steps for homogenization, separation of phases and RNA isolation are described in 3.3.1. Protein was precipitated for 10 min at RT and then pelletized by centrifugation (12000 g, 10 min). Supernatant was discarded and the pellet was washed three times in 1 ml washing buffer (0.3 M guanidinhydrochloride in 95% EtOH) with 20 min incubation at RT and centrifugation for 5 min (7600 g, 4 °C). As a fourth washing step the protein pellet was incubated in 95% ETOH for 20 min. After centrifugation the supernatant was discarded completely and the pellet was dried for 5 min at RT. The pellet was dissolved

in 200 µl SDS + protease inhibitor + phosphatase inhibitor and incubated over night at 50 °C. Insoluble components were sedimented by centrifugation for 10 min (10000 g, 4 °C). The supernatant, containing the protein, was taken off and stored at -80 °C till further use.

3.5.2 SDS-Polyacrylamide-gel electrophoresis

For western blot analysis proteins were separated via gel electrophoresis. Productions of polyacrylamide gels and gel electrophoreses was carried out using the Laemmli method (Laemmli, 1970).

Ingredient	Stacking gel	Running gel		
		6% >130kDa	12 % 35 – 130kDa	15 % < 35kDa
dH_2O	0.68 ml	2.6 ml	1.6 ml	1.1 ml
Rotiphorese® Gel 30	0.17 ml	1.0 ml	2.0 ml	2. 5ml
Tris/HCl, 1 M, pH 6,8	0.1 3ml	-	-	-
Tris/HCl, 1,5 M, pH 8,8	-	1.3 ml	1.3 ml	1.3 ml
10% SDS	0.01 ml	0.05 ml	0.05 ml	0.05 ml
10% APS	0.01 ml	0.05 ml	0.05 ml	0.05 ml
TEMED	0.001 ml	0.004 ml	0.002 ml	0.002 ml

Table 18: Components of SDS gels

For pouring of gels a PeqLab Biotechnology GmbH upper buffer chamber and casting base were used. First the running gel was poured in between two glass slides and covered with 300 µl Isopropanol. After complete polymerization of the running gel, the stacking gel was poured on top of the running gel. A plastic comb was inserted in the liquid stacking gel to create loading wells.

In the stacking gels protein samples can be concentrated due to the difference in pore size, pH and the electrophoretic mobility of ions to the running gel. In the running gels proteins are separated according to size. SDS in the gels ensures denaturation during the electrophoresis. Further proteins SDS ads negative charges to proteins corresponding to their molecular weight. This enables separation according to molecular weight in an electronic field.

Previous to electrophoresis protein samples were denaturated with reducing sample buffer for 5 min in boiling water. Fully polymerized gels were transferred into an

electrophoresis chamber and the tank was filled with 1x running buffer. Samples were loaded in the loading wells and 5 µl of a protein molecular weight marker (Fisher Scientific, Waltham, USA) were loaded in an additional well.
Proteins were separated at 20 mA per gel for 1 h 15 min. The stacking gel was discarded after electrophoresis.

3.5.3 Semidry blotting

Separated proteins were transferred on a polyvinylidene difluoride (PVDF) membrane (Roche, Mannheim, Germany) in a semidry blotting apparatus (Peqlab Biotechnology GmbH, Erlangen, Germany). The PVDF was cut to match the size of the running gel and shortly incubated in Methanol for activation. Afterwards the membrane was equilibrated in transfer buffer. Whatman papers were also soaked in transfer buffer. Blots were assembled as follows:

Semidry Blot:
Cathode (-)
3 layers Whatman paper
Running gel with proteins
PVDF-Membrane
2 layers Whatman paper
Anode (+)

Table 19: Semidry blotting

Blotting was carried out at 14 V, 19 mA per gel for 45 min.

3.5.4 Dot blotting

To analyze levels of secreted DCN in the media of murine astrocytes after treatments with TGFβ-2 or CTGF, medium was taken off the cells and stored at -80 °C till further use. Secreted protein was blotted on PVDF membranes via dot blotting. At first the membrane was activated in methanol and then equilibrated in transfer buffer. One layer of Whatman paper, soaked in transfer buffer was placed on the lower part of the Dot Blotter (Schleicher & Schuell, Dassel, Germany). The PVDF membrane was placed on top of the Whatman paper and the upper part of the Dot Blotter was placed onto the membrane. The Dot Blotter was connected to an aspirator hose to aspirate the medium through the membrane. 100 µl of medium were loaded per dot. After the medium was aspirated completely the membrane was washed in TBST shortly and then incubated in 5% BSA for 1h at RT.

3.5.5 Detection of specific protein bands

To detect proteins of interest PVDF membranes were incubated with specific antibodies after blotting and blocking over night at 4 °C. As loading control α-Tubulin was used.
Antibodies bind specifically to their fitting antigen and this so formed antibody-antigen complex can be bound by a secondary antibody against the host species of the primary antibody. Secondary antibodies are conjugated with horseradish peroxidase (HRP) or alkaline phosphatase (AP). If a HRP- or AP substrate is added to the antibody complex a catalysis reaction takes places in which chemiluminescence is emitted. This emission makes it possible to detect specific proteins.

Primary antibody (dilution)	**Secondary antibody (dilution)**	**Molecular weight**	**Gel**
AKT (rabbit) 1:1000 in 5% BSA	α-rabbit-IgG-HRP (chicken) 1:5000	60 kDa	10%
CTGF (goat) 1:500 in 5% BSA	α-goat-IgG-AP (chicken) 1:2000	37 kDa	12%
Col IV (rabbit) 1:500 in 5% BSA	α-rabbit-IgG-HRP (chicken) 1:5000	170 kDa	6%
DCN (rabbit) LF 113 1:500 in 5% BSA	α-rabbit-IgG-HRP (chicken) 1:5000	40 kDa	12%

DCN (rabbit) H80 1:200 in 5% MM	α-rabbit IgG-AP (chicken) 1:2000	40 kDa	12%
DCN (rabbit) LF 136 1:100 in 5% BSA	α-rabbit-IgG-HRP (chicken) 1:5000	40 kDa	12%
Fibronectin 1:500 in 5% MM	α-rabbit IgG-AP (chicken) 1:2000	262 kDa	6%
GAPDH (rabbit) HRP 1:5000	-	39 kDa	-
pAKT (rabbit) 1:1000 in 5% BSA	α-rabbit-IgG-HRP (chicken) 1:5000	62 kDa	10%
α-Tubulin (rabbit) 1:5000	α-rabbit IgG-AP (chicken) 1:2000	50 kDa	-

Table 20: Dilutions and specifications of primary antibodies

After semidry- or dot blot membranes were incubated in 5% BSA or 5% MM for 1h at RT. Then the membranes were incubated over night at 4 °C with a primary antibody. After three washing steps in TBST (10min each) the secondary antibody was poured on the membrane. 1 h of incubation at RT was followed by three washing steps in TBST (10min each). At all steps the membrane was shaken gently in the solutions. All antibodies were diluted in 1:10 blocking solution in TBST. For detection of HRP conjugated antibodies 800µl Luminata^{TM} Forte (Millipore, Billerica, USA) were dispersed on the membrane and the membrane was covered with foil and incubated in the dark for 5 min. For detection of AP conjugated antibodies the membrane was incubated in detection buffer for 5min at RT and then 800 µl CDP Star (Roche, Penzberg, Germany) diluted 1:100 in detection buffer were used, following the same protocol as for HRP conjugated antibodies. Chemiluminescence signals were detected in a LAS3000 Intelligent Dark Box (Fujifilm, Düsseldorf, Germany). Densitometric analysis was carried out with Aida Advanced Image Data Analyzer Version 4.06 (Raytest, Straubenhardt, Germany).

3.5.6 Coomassie staining

Proteins on the PVDF membranes were made visible with Coomassie staining (Sambrook et al., 1989). Staining was used as an additional loading control.

Membranes were incubated in coomassie staining solution for at least 1 h at RT. Afterwards the staining solution was discarded and the membranes were washed in destaining solution over night at RT. Membranes were dried completely and photographed in a LAS3000 Intelligent Dark Box (Fujifilm, Düsseldorf, Germany). Densitometric analysis was carried out with Aida Advanced Image Data Analyzer Version 4.06 (Raytest, Straubenhardt, Germany).

3.6 Cell culture

3.6.1 Cell lines and culture conditions

Line	Medium	Temperatur/CO_2
human trabecular meshwork cells	DMEM F12 + 5% (v/v) FCS, 100 U/ml Penicillin, 100 µg/ml Streptomycin	37 °C, 5%
human astrocytes	DMEM F12 + 10% (v/v) FCS, 100 U/ml Penicillin, 100 µg/ml Streptomycin	37 °C, 7%
murine astrocytes	DMEM F12 + 10% (v/v) FCS, 100 U/ml Penicillin, 100 µg/ml Streptomycin	37 °C, 7%

Table 21: Culture conditions of used cell lines

3.6.2 General working standards

All treatments and other procedures were carried out under sterile conditions. Glassware was autoclaved prior to use; buffers and solutions were sterile filtered. Used plastic materials were packed sterile. Treatments and passaging as well as production of buffers and solutions were carried out under a sterile working bench (Hera Safe, Heraeus, Hanau, Germany). Cells were cultivated in an incubator (Hera Safe, Heraeus, Hanau, Germany) under sterile conditions with stable temperature, CO_2 concentrations and an atmosphere saturated with water vapor.

3.6.2.1 Passaging of cells

When cells reached confluency, they were detached from the bottom of the culture flask and sown diluted to a new culture flask. For treatments defined numbers of cells were sown in culture wells.

At first culture medium was aspirated of the cells and cells were washed with sterile PBS. Then 1ml of Trypsin was added on the cell layer to detach cells from the culture flask. Cells were incubated with trypsin for about 5 min at 37 °C. Cells were detached from the culture flask by gently knocking on the flask.

Trypsin was inactivated with 5 ml medium containing 10% FCS. To remove all trypsin of the cells, the cell suspension was centrifuged for 5 min at RT and 1000 rpm. The supernatant was discarded and the cell pellet was dissolved in 10 ml medium containing 10% FCS.

To passage cells 1ml of the cell suspension was added to a new culture flask containing an adjusted amount of medium containing 10% FCS.

For treatment cells were counted with a Casy® (Innovatis, Reutlingen, Germany) and the desired number of cells was sown on culture wells.

3.6.3 Isolation of murine optic nerve astrocytes

For the isolation of murine optic nerve astrocytes 10 to 20 day old mice were used. After the mice were sacrificed, both eyes were enucleated using forceps. Till further dissection the eyes were stored shortly in cooled DMEM F12. ON were cut of the globes under a binocular and in a drop of DMEM F12 to prevent cells from drying. The dura was removed by gently sweeping over the optic nerve with forceps while one end of the ON was held in another forceps. On samples were digested in 200 µl Trypsin for 30 min at 37°C. Tissue was then sheared by repeated pipetting and plated on laminin-coated 6 well plates. Cells were grown in DMEM F12 enriched with 10% FCS and 1% AGS. Medium was not changed in the following seven days to allow the cells to attach to the tissue culture plates. After seven days, medium was changed three times a week. A pure astrocyte culture was obtained by shaking the wells for 12 h to remove less adhesive cells. After cells grew to confluence, they were seeded in 25 cm^2 cell culture

flasks. Astrocytes were characterized via GFAP-staining. Only cells from passage 2 to 10 were used for experiments.

3.6.4 *In vitro* experiments

Human TM cells, human astrocytes and murine astrocytes were sown on 6 well plates. When they reached confluency they were serum starved for 24 h. After 24 h medium was changed and proteins or inhibitors were added to the medium. At the end of the treatment medium was aspirated and the cells were washed twice in PBS. Cells were harvested after 30 min to 24 h accordant to the treatment. All treatments were carried out with at least three different charges of cells to ensure proper statistical analysis.

3.6.4.1 Reciprocal effects of TGFβ-2, CTGF and DCN

To analyze reciprocal effects of TGFβ-2 or CTGF and DCN human TM cells, human astrocytes and murine astrocytes were treated with 1 ng TGFβ-2, 50 ng CTGF, 25 ng CTGF or 1 µg DCN for 24 h. Untreated cells served as controls. After 24 h cells were harvested with 500 µl Trifast^{TM} for isolation of RNA and proteins. Medium of treated cells was stored at -80 °C for quantification of secreted DCN, FN and Col IV.
Further human TM cells, human astrocytes and murine astrocytes were sown on glass culture slides. After cells reached about 70% confluency they were serum starved for 24 h and then treated as described above. After 24 h hours cells were washed twice with PBS and fixed in 4% PFA for 10 min. After three washing steps in 0.1 M phosphate buffer (30min each) culture slides were stored at -20 °C till further use.

3.6.4.2 Effects of DCN on AKT signaling

To investigate if DCN influences AKT signaling in murine astrocytes, the cells were treated with 1 µg of DCN for 30 min, 2 h, 3 h and 6 h, untreated cells served as controls. Cells were harvested in 300 µl RIPA buffer and lysates were stored at -80 °C till further use.

3.6.4.3. Inhibition of AKT signaling

To reassess if DCN regulates expression of TGF-β1, TGF-β2 and CTGF via the the AKT signaling pathway (Figure 6) in murine astrocytes cells were treated with 1µg DCN only or in combination with the AKT signaling inhibitor Triciribine in different concentrations (0.5 µM, 1 µM, 5 µM) for 24 h. Cells were harvested in 500 µl Trifast$^{TM.}$

3.7 *In vivo* experiments

3.7.1 Intraocular pressure measurements

IOP was measured using a TonoLab tonometer (Icare, Tuike, Finnland). This tonometer is based on rebound tonometry. This means that the rebound force of the pin from the cornea is measured. The mean of 6 single measurements is taken and displayed in mmHg.

Animals were anesthetized with 6 – 8 mg/kg bodyweight Xylazin and 90 – 120 mg/kg bodyweight Ketamine. First measurements were carried out 5 min after injection to ensure comparable depth of anesthesia.

IOP measurements were either carried out before dissection or every 4 to 8 weeks for one year.

3.7.2 Preparation of anterior eye segments and corneo-scleral rings

Anterior eye segments or corneo-scleral rings of 8 and 12 week old DCN$^{-/-}$ and βB1 CTGF mice and their wildtype littermates were dissected. Mice were killed by exarticulation of the atlanto-occipital joint after IOP measurements.

The anterior eye segment was separated from the bulb by cutting along the *ora serata* and the lens was carefully taken out of the anterior eye segment. The anterior eye segment was transferred into 500 µl pegGold Trifast^{TM} for isolation of RNA and proteins.

To analyze regulation processes in the region of the TM without influences of corneal cells corneo scleral rims which include the TM were dissected. To do so the anterior eye

segment was cut in half after extraction of the lens. As much of the cornea as possible was cut of the corneo-scleral ring carefully.

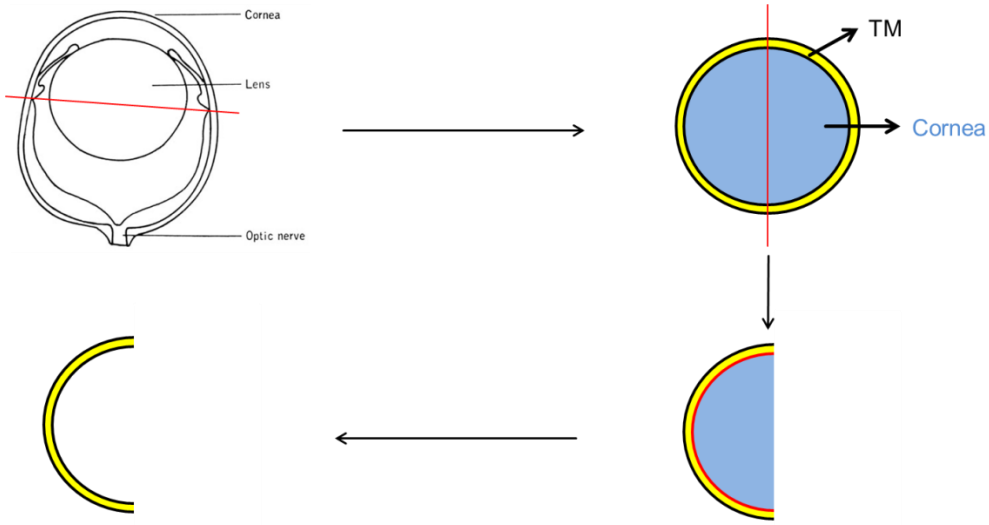

Figure 8: Dissection of the corneo-scleral ring. Red lines indicate cuts. Blue = cornea, yellow = corneo-scleral ring, including TM. Samples were either processed immediately or stored at –80 °C till further use.

3.7.3 Preparation of optic nerves and optic nerve heads

Optic nerves and optic nerve heads of 8 and 12 weeks old DCN$^{-/-}$ and βB1-CTGF mice and their wildtype littermates were dissected.

All muscles and connective tissue were cleaned away from the bulbus around the optic nerve. The optic nerve was cut off directly at the bulbus.

To gain access to the optic nerve head, the anterior eye segment, the lens and the retina were removed. Then the sclera was incised three times all the way down to the optic nerve head, resulting in a four leave clover like shape. The four sclera parts were cut away from the optic nerve head and possibly remaining parts of sclera or retina were cleaned away.

Optic nerves or optic nerve heads of two or three animals of the same genotype were paired in consideration of IOP values to get sufficient amounts of RNA and proteins. Samples were either processed immediately or stored at – 80°C till further use.

3.7.4 Transcardial perfusion

Transcardial perfusion was used to fixate tissue for immunohistochemistry.
Mice were anesthetized with Ketamine and Xylazine as described above. After animals showed no more pain reaction to pinching at the toes they were fixed to the working surface.
An incision through the skin with surgical scissors was made along the thoracic midline and two additional incisions were made from the xiphoid process along the base of the ventral ribcage laterally. The thoracic field was exposed by reflecting the two skin flaps to the sides. The diaphragm was opened gently by raising the xiphoid process with blunt forceps and cutting it carefully with pointed scissors. Afterwards the thoracic musculature and the ribcage were cut on both sides close to the spine and they were fixed cranially with mosquito forceps placed on the xiphoid process. After removing the pericardial sac a perfusion cannula was inserted in the left ventricle right above the *apex cordis* and a small cut was made in the right atrium. Mice were perfused with about 5 ml of PBS till organs, especially the liver turned pale.
Eyes were enucleated with bent forceps and placed in either 4% PFA for 4 h at RT (for immunohistochemistry) or in EM fixation for 24 h at 4 °C. After 1h a small incision was made in the cornea to ensure fixation of all structures of the eye.

3.7.5 Quantification of optic nerve axons

Differences in axon number between $DCN^{-/-}$ animals and wildtype littermates were analyzed using cross sections of optic nerves. The semi thin sections were stained with paraphenylenediamine and then pictures in 100x magnification were taken. The square footage of the optic nerve was measured with Axiovision 3.0.
Axons were counted using Image J (RSB). Axons in five fields (50 x 50 µm each) were counted and then the whole number of axons was calculated using the following formula:

Number of axons = (optic nerve (µm²) / 12500 µm²) · sum of axons in five fields

3.8 Histological techniques

3.8.1 Cryo-embedding and sectioning

After fixing eyes were washed three times in PBS for 30 min. For stabilization of the tissue eyes were incubated in rising concentrations of sucrose in phosphate buffer (10%, 20%, 30%) for about 12 h per step. Eyes were embedded in Tissue-Tek® and stored at – 20 °C till further use. 12 µm sagittal or tangential cryo sections were made with a Microm HM500 OM Cryostat (Microm International, Walldorf, Germany).

3.8.2 Epon-embedding and semi thin sectioning

After fixation in EM fixation eyes were eyes were washed at least 4 times for 30 min in 0.1 M cacodylate buffer. Eyes were additionally fixed in 1% osmimumtetraoxid and eyes were washed again in cocodylate buffer. Eyes were dehydrated in an ascending alcohol series (70%, 80%, 90%, 100%). Epon-embeding was carried out after standardized methods: Ethanol/Acetone 1:1, 100% Acetone, Epon/Aceton 1:2, Epon/Acetone 2:1, 100% Epon; curing for 24 h at 60 °C, curing for 48 h at 90 °C. Epon stem A and Epon stem B were mixed 1:1 for embedding with 2% DMP-30 (Roth, Karlsruhe, Germany). 1 µm sections were made from eyes and optic nerves for light microscopy.

3.8.3 Immunohistochemical staining

Cryo sections were attached to object slides and dried with a hair drier. To dissolve embedding medium slides were washed for 5 min in 0.1 M phosphate buffer or 1x TBS. After shaking of liquids sections were encircled with a fat pen (PapPen) and incubated in blocking solution for 1 h at RT. Afterwards sections were incubated with primary antibodies, dissolved in 1:10 blocking solution, overnight at 4 °C. After three washing steps (5 min in 0.1 M Php buffer / 1x TBS) the fluorescence labeled secondary antibody, diluted in 1:10 blocking solution was added to the sections and incubated for 45 min at RT. After three washing steps sections were stained with 1:10 DAPI in Mowiol and covered with glass slides. Sections were stored in the dark at 4 °C.

Protein	Blocking solution	Primary antibody	Secondary antibody
Collagen-Typ-IV	3% BSA + 0.1% Triton X in 0.1 M Php	Polyclonal Rabbit Anti Human Col-IV, 1:500 in 0.3% BSA + 0.01% Triton X in 0.1 M Php	AffiniPure Donkey Anti Rabbit Cy™3, 1:2000 in 0.3% BSA / 0.1 M Php
Smooth-muscle α- Actin	3% BSA + 0,1% Triton X in 0.1 M Php	Monoclonal Rabbit Anti Mouse SMA, 1:1000 in 0.3% BSA + 0.1% Triton X in 0.1 M Php	Chicken a Rabbit Alexa Fluor® 488 conjugated in 0.3% BSA + 0.01% Triton X in 0.1 M Php
Decorin LF 113	3% BSA in 0.1 M Php	Polyclonal Rabbit Anti Mouse DCN, 1:1000 in 0.3% BSA in 0.1 M Php	AffiniPure Donkey Anti Rabbit Cy™3, 1:2000 in 0.3% BSA / 0.1 M Php
Decorin LF 136	3% BSA in 0.1 M Php	Polyclonal Rabbit Anti Human DCN, 1:100 in 0.3% BSA in 0.1 M Php	AffiniPure Donkey Anti Rabbit Cy™3, 1:2000 in 0.3% BSA / 01 M Php
CTGF	2%BSA, 0,2% CWFG, in 0.1 M Php	Polyclonal Rabbit Anti Human/Mouse CTGF, 1:400 in 0.2% BSA, 0.02% CWFG in 0.1 M Php	AffiniPure Donkey Anti Goat Cy™3, 1:1000 in 0.3% Blotto / 0.1 M Php
Fibronektin	3% BSA + 0.1% Triton X in 0.1 M Php	Polyclonal Rabbit Anti Human FN, 1:500 in 0.3% BSA + 0.01% Triton X in 0.1 M Php	AffiniPure Donkey Anti Rabbit Cy™3, 1:2000 in 0.3% BSA / 0.1 M Php
GFAP	2%BSA, 0.2% CWFG, in 0.1 M Php	Polyclonal Rabbit Anti Mouse GFAP, 1:200 in 0.2% BSA, 0.02% CWFG in 0.1 M Php	Chicken a Rabbit Alexa Fluor® 488 conjugated in 0.3% BSA + 0.01% Triton X in 0.1 M Php
pAKT	2%BSA, 0.2% CWFG, 0.1% Trition X in 1x TBS	Monoclonal rabbit anti mouse/human pAKT, 1:100 in 0.2% BSA, 0,02% CWFG, 0.01% Triton X in 0.1x TBS	AffiniPure Donkey Anti Rabbit Cy™3, 1:2000 in 0.2% BSA, 0,02% CWFG, 0.01% Triton X in 0.1x TBS
pSMAD2	2%BSA, 0.2% CWFG, 0.1% Trition X in 1x TBS	Monoclonal rabbit anti mouse/human pSMAD2, 1:100 in 0.2% BSA, 0,02% CWFG, 0.01% Triton X in 0.1x TBS	AffiniPure Donkey Anti Rabbit Cy™3, 1:2000 in 0.2% BSA, 0,02% CWFG, 0.01% Triton X in 0.1x TBS

Table 22: Antibodies and dilutions for immunohistochemistry and immunocytochemistry

3.8.4. Immunocytochemical staining

Human trabecular meshwork cells, human ONH astrocytes and mouse ON astrocytes were fixe das described above. Cells were stained against DCN, FN, Col Type IV or GFAP as described in 3.7.2.
Cover slips were embedded on glass slides with 1:10 DAPI in Mowiol to make the nucleus visible. Cover slips were stored at 4 °C till further use.

3.8.5. Contrasting of optic nerves

Contrasting of optic nerves was carried out with paraphenylenediamine as follows:
500 mg paraphenylenediamine were dissolved in 50 ml ethanol. The solution was stored for three days in daylight at RT, till the solution turned dark. Semi-thin sections were incubated in the solution for about three min and then washed in ethanol.

3.9 Light and Fluorescence Microscopy

Semi thin sections, immunohistochemical- and immunocytochemical stainings were analysed using an Axio Imager Z1 microscope (Carl Zeiss, Göttingen, Germany).

4. Results

4.1 Expression analysis of the interaction between TGF-β/CTGF and DCN *in vitro*

Negative regulation of TGF-β by DCN has first been reported in hamster ovary cells in 1990 (Yamaguchi et al., 1990) and there is also evidence that DCN is able to inhibit the profibrotic effects of CTGF via direct binding (Vial et al., 2011). The effects of TGF-β on DCN expression and synthesis on the other hand are cell type dependent and there is no data on effects of CTGF on DCN.

In this study we investigate whether TGF-β, CTGF and DCN influence each other's expression and synthesis in human TM cells, human ONH astrocytes and murine ON astrocytes. Expression and synthesis values of the untreated control cells were set to 1 in all analysis.

4.1.1 Human trabecular meshwork cells

TGF-β2 and CTGF contribute to pathologic changes in the outflow tissues in POAG (Fuchshofer and Tamm, 2009, Junglas et al., 2009; Junglas et al., 2012). To analyze the effects of TGF-β2 and CTGF on the expression and synthesis of DCN human TM cells were treated with either 1 ng of TGF-β2 or 25 ng CTGF for 24 h.

Relative quantification of DCN mRNA showed that DCN expression is significantly reduced after 24 h treatment with either 1ng TGF-β2 or 25 ng CTGF (Figure 4.1 A). Treatment with 1 ng of TGF-β2 led to a decrease of DCN mRNA to 0.66 ± 0.13 ($n = 6$, $p = 0.01$) and treatment with 25 ng of CTGF reduced DCN expression to 0.39 ± 0.13 ($n = 5$, $p = 0.0002$). Western blot analyzes of DCN synthesis in human TM cells showed that treatment with 1 ng TGFβ-2 led to a down regulation of DCN synthesis to 0.72 ± 0.02 ($n = 3$, $p = 0.003$) compared to untreated controls after 24 h treatment while CTGF treatment reduced DCN synthesis to 0.45 ± 0.07 ($n = 3$, $p = 0.004$). α-Tubulin was used as a loading control (Figure 9 B and C).

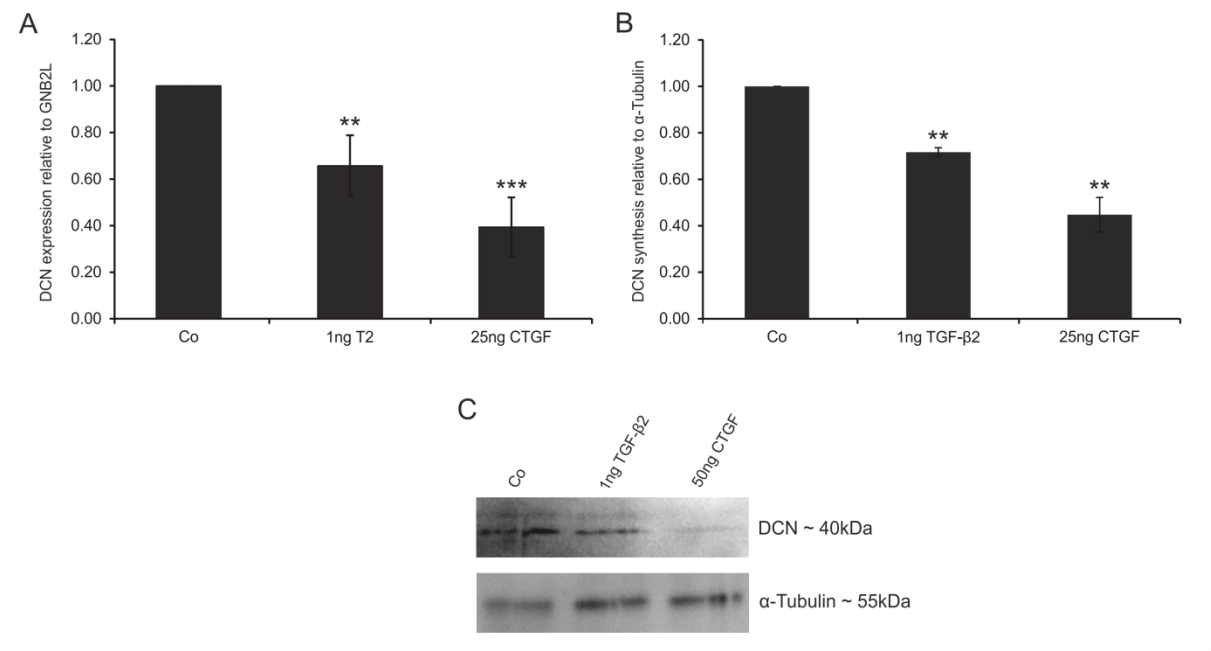

Figure 9: TGF-β2 and CTGF treatment reduces DCN expression and synthesis in human TM cells. DCN expression is reduced significantly to 0.66 ± 0.13 (n = 6, p ≤ 0.01) after treatment with 1 ng TGF-β2 and to 0.39 ± 0.13 (n = 5, p ≤ 0.001) after treatment with 25 ng CTGF. DCN expression was normalized to GNB2L (A). DCN synthesis was reduced to 0.72 ± 0.02 (n = 3, p ≤ 0.01) compared to untreated controls after treatment with 1 ng TGF-β1. Treatment with 25 ng of CTGF led to a reduction of DCN synthesis to 0.45 ± 0.07 (n = 3, p ≤ 0.01). DCN synthesis was normalized to α-Tubulin (B and C).

To analyze the effects of DCN on TGF-β1, TGF-β2 and CTGF expression and synthesis, human TM cells were treated with 1µg of DCN for 24 h. Treatment with 1 µg of DCN led to a significant downregulation of TGF-β1 (0.62 ± 0.1, n = 7, p = 0.004), TGF-β2 (0.75 ± 0.09, n = 7, p = 0.022) and of CTGF mRNA (0.53 ± 0.13, n = 6, p = 0.006); Figure 10, A). GNB2L was used as housekeeping gene. Treatment with 1µg DCN led a slight but significant reduction of CTGF synthesis to 0.79 ± 0.06 (n = 3, p = 0.034) was observed (Figure 10 B and C). α-Tubulin was used as loading control to normalize CTGF synthesis between samples.

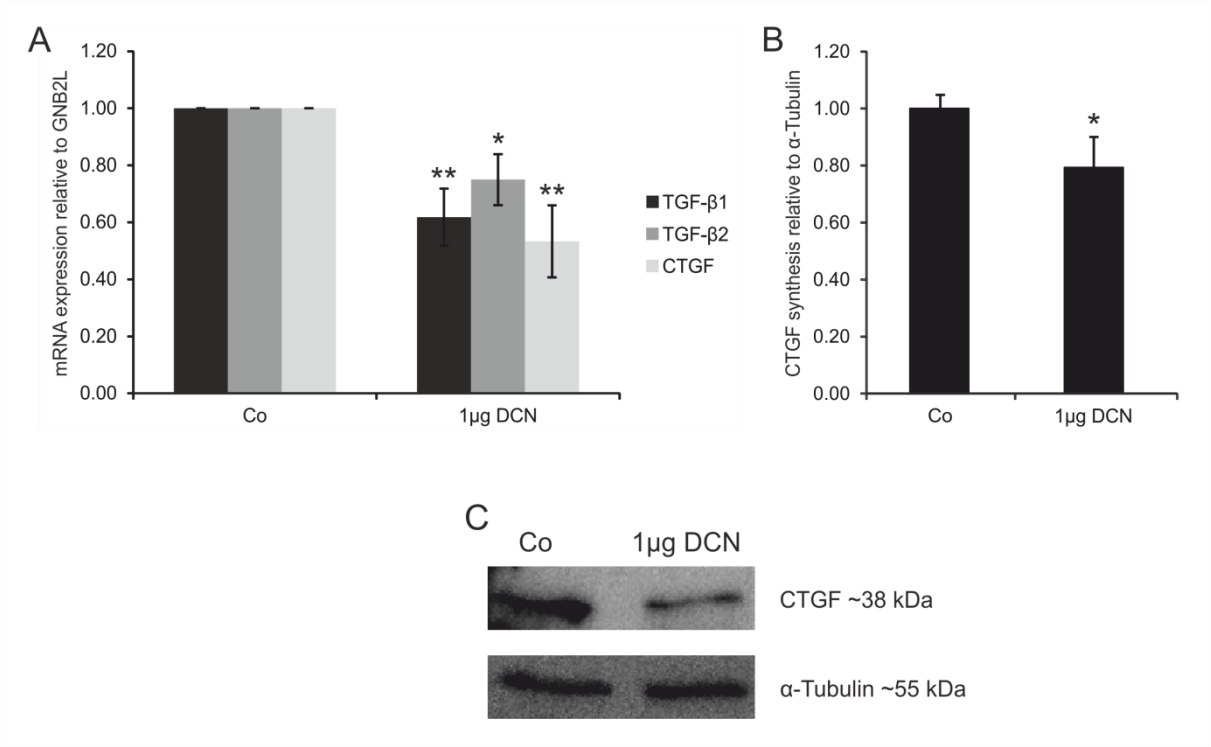

Figure 10: DCN reduces growth factor expression and synthesis in human TM cells. A significant downregulation of TGF-β1 (0.62 ± 0.1, n = 7, p = 0.004), TGF-β2 (0.75 ± 0.09, n = 7, p = 0.022) and of CTGF mRNA (0.53 ± 0.13, n = 6, p = 0.006) was observed (A). Expression was normalized to GNB2L. Treatment with 1 µg of DCN for 24 h led to a significant downregulation of CTGF synthesis to 0.79 ± 0.06 (n = 3, p ≤ 0.05, B). CTGF bands were normalized to α-Tubulin (C).

4.1.2 Human optic nerve head astrocytes

Astrocytes of the ONH react to TGF-β treatments with upregulation of ECM expression (Fuchshofer et al., 2005; Neumann et al., 2008; Zode et al., 2011) and show reactivation in POAG (Hernandez and Pena, 1997; Varela and Hernandez, 1997; Wang et al., 2002. To analyze the effects of TGF-β2 and CTGF on the expression and synthesis of DCN human ONH astrocytes were treated with either 1 ng of TGF-β2 or 50 ng CTGF for 24 h. Vice versa human ONH astrocytes were treated with 1 µg of DCN for 24 h. Real Time RT-PCR against TGF-β1, TGF-β2, CTGF and DCN was carried out, again GNB2L was used as housekeeper.

Relative quantification of DCN mRNA showed that DCN expression was significantly reduced after 24 h treatment with either 1 ng TGF-β2 or 50 ng CTGF (Figure 11 A). Treatment with 1 ng of TGF-β2 led to a decrease of DCN mRNA to 0.56 ± 0.13 (n = 6, p = 0.015) and treatment with 50 ng of CTGF reduces DCN expression

to 0.40 ± 0.09 (n = 5, p = 0.0002). Analysis of DCN synthesis in human ONH astrocytes showed that compared to untreated controls treatment with 1 ng TGFβ-2 leads to a down regulation of DCN synthesis to 0.71 ± 0.11 (n = 4, p = 0.021) while CTGF treatment reduces DCN synthesis to 0.50 ± 0.18 (n = 5, p = 0.009). DCN synthesis was normalized to α-Tubulin (Figure 11 B and C).

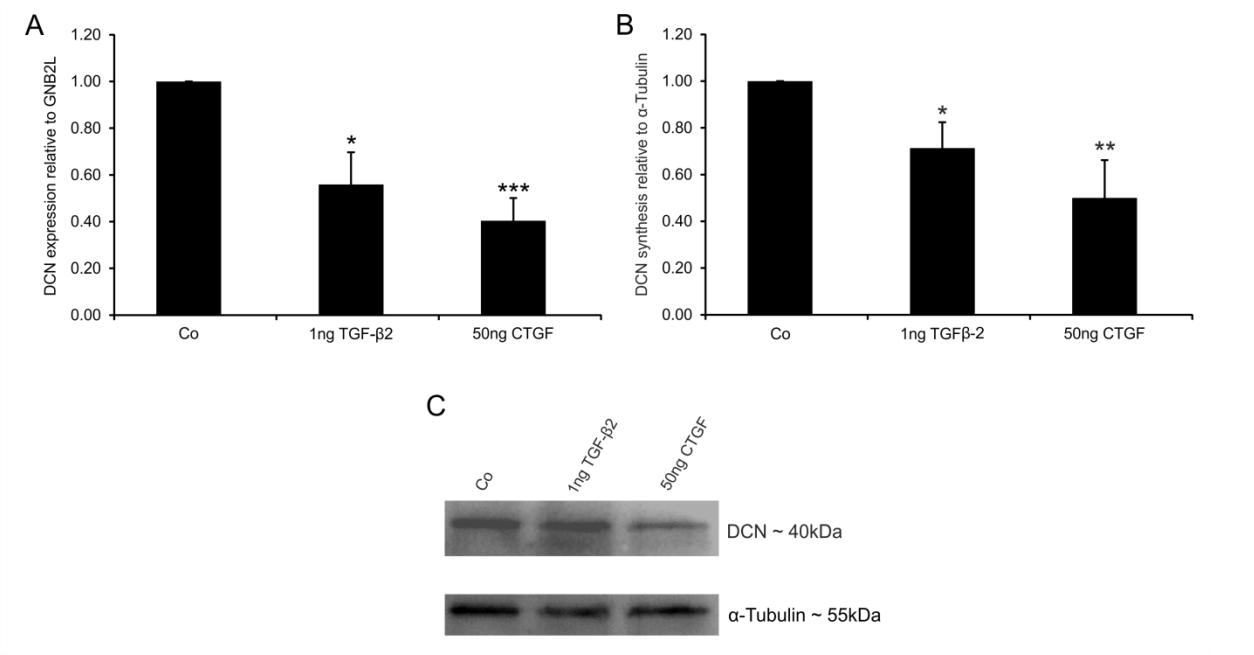

Figure 11: TGF-β2 and CTGF treatment reduces DCN expression and synthesis in human ONH astrocytes. DCN expression is reduced significantly to 0.56 ± 0.13 (n = 6, p ≤ 0.05) after treatment with 1ng TGF-β2 and to 0.40 ± 0.13 (n = 5, p ≤ 0.001) after treatment with 50 ng CTGF. DCN expression was normalized to GNB2L (A). Treatment with 1 ng TGF-β2 reduces DCN synthesis to 0.71 (± 0.11, n = 4, p ≤ 0.05), treatment with 50 ng of CTGF reduces DCN synthesis to 0.50 (± 0.18, n = 5, p ≤ 0.01) in comparison to untreated control cells (B). DCN bands were normalized to α-Tubulin (C).

As previously reported for other cell types, DCN leads to a significant downregulation of TGF-β1 (0.37 ± 0.19, n = 3, p ≤ 0.029) and TGF-β2 (0.27 ± 0.11, n = 5, p ≤ 0.015) and CTGF (0.37 ± 0.16, n = 4, p ≤ 0.011) in human ONH astrocytes compared to untreated controls (Figure 12). GNB2L was used as housekeeping gene to normalize expression.

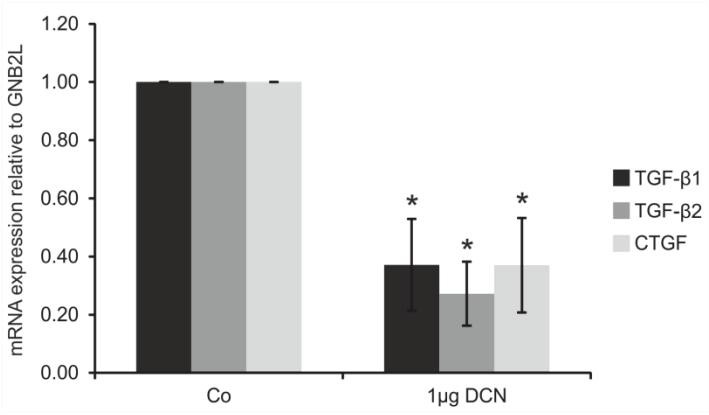

Figure 12: DCN reduces growth factor expression in human ONH astrocytes. After 24 h treatment with 1 µg of DCN expression of TGF-β1 was decreased significantly to 0.37 (± 0.19, n = 3, p ≤ 0.05), TGF-β2 was significantly reduced to 0.27 (± 0.11, n = 5, p ≤ 0.05) and CTGF was significantly reduced to 0.37 (± 0.16, n = 4, p ≤ 0.05). mRNA expression was normalized to GNB2L.

4.1.3 Murine optic nerve astrocytes

Since human ONH astrocytes are only available in very limited amounts our group established a method to isolate and cultivate murine astrocytes of the optic nerve (unpublished data). Due to this this study aimed at analyzing if murine ON astrocytes react in the same way to treatments with TGF-2, CTGF or DCN as human ONH astrocytes do. These experiments will give further insight in how applicable data of mouse models is on humans and it gives us the opportunity to isolate astrocytes of overexpression- or knockout mouse lines.

Murine ON astrocytes were treated the same way as human ONH astrocytes. Expression of all genes was set against GNB2L.

DCN expression was reduced to 0.29 ± 0.12 (n = 4, p = 0.0006) after treatment with 1 ng TGF-β2 and to 0.45 ± 0.09 (n = 4, p = 0.0004) after treatment with 50 ng of CTGF. In human ONH astrocytes CTGF treatment had a stronger negative regulatory effect on DCN expression than TGF-β2 treatment, while the reverse is the case in murine ON astrocytes (Figure 13 A).

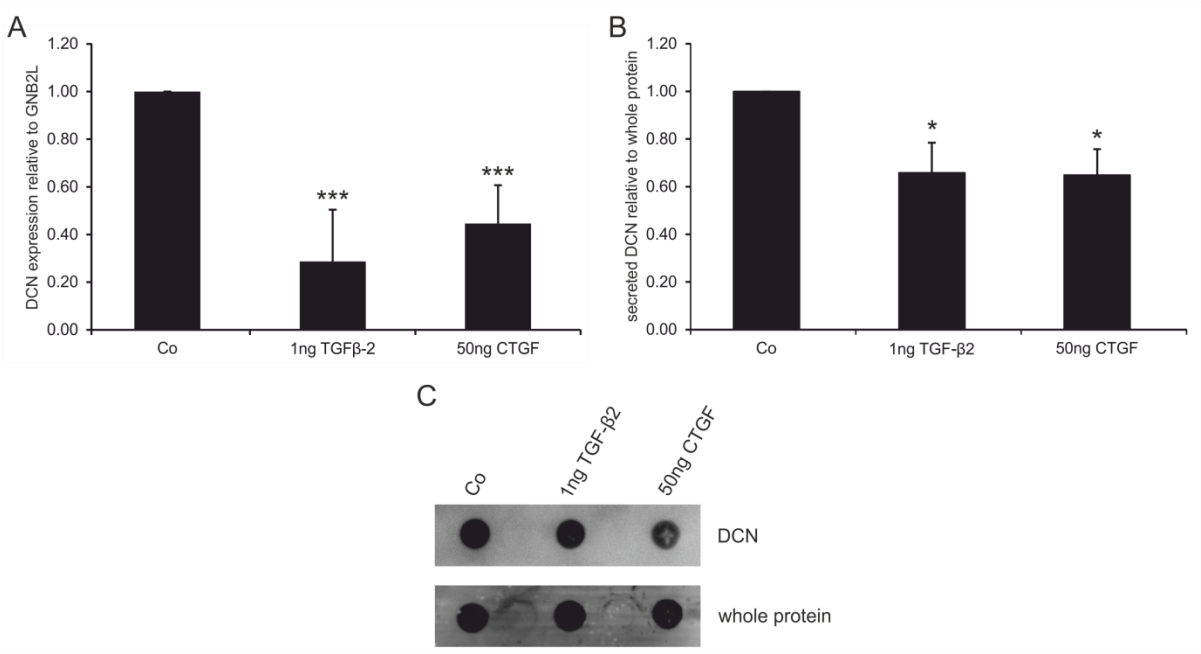

Figure 13: TGF-β2 and CTGF treatment reduces DCN expression and synthesis in murine ON astrocytes. Treatment with 1 ng of TGF-β2 for 24 h reduced DCN expression to 0.29 (± 0.12, n = 4, $p \leq 0.001$, A) while treatment with 50 ng CTGF for 24 h reduced it to 0.45 (± 0.09, n = 4, $p \leq 0.001$, A). Expression was normalized to GNB2L. Amounts of secreted DCN were lowered to 0.66 ± 0.13 (n = 6, $p \leq 0.05$) after TGF-β2 treatment and to 0.65 ± 0.11 (n = 6, $p \leq 0.05$) after CTGF treatment in comparison to secreted DCN in the media of untreated control cells (B). Secreted DCN was normalized to whole secreted protein detected by Sypro Ruby™ (C).

Since it was almost impossible to detect cellular DCN in protein lysate of murine ON astrocytes via western blot, amounts of secreted DCN in the media of treated cells were quantified using dot blot. Amounts of secreted DCN were set of against whole protein content detected with Sypro Ruby™. Amounts of secreted DCN were significantly lowered by treatments with TGF-β2 and CTGF (Figure 13 B and C). A reduction to 0.66 ± 0.13 (n = 6, p = 0.032) was observed after TGF-β2 treatment. A reduction to 0.65 ± 0.11 (n = 6, p = 0.014) was observed after treatment with CTGF.

DCN treatment reduced expression of TGF-β1, TGF-β2 and CTGF significantly in comparison to untreated controls (TGF-β1: 0.56 ± 0.15, n = 6, p = 0.02, TGF-β2: 0.54 ± 0.13, n = 7, p = 0.006, CTGF: 0.59 ± 0.11, n = 7, p = 0.005, Figure 14).

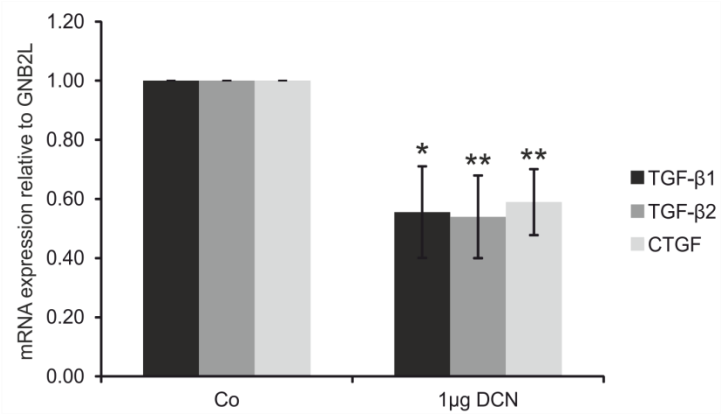

Figure 14: DCN reduces growth factor expression in murine ON astrocytes. TGF-β1 (0.56 ± 0.15, n = 6, p ≤ 0.05), CTGF (0.59 ± 0.11, n = 7, p ≤ 0.01) and TGF-β2 (0.54 ± 0.13, n = 7, p ≤ 0.01) were significantly reduced after DCN treatment. mRNA expression was normalized to GNB2L.

4.2 Decorin reduces extracellular matrix production in human trabecular meshwork cells, human - and mouse optic nerve astrocytes

Since TGF-β2 and CTGF induce the expression and synthesis of ECM components in cell types involved in the pathogenesis of POAG (Fuchshofer et al., 2005; Fuchshofer and Tamm, 2009; Neumann et al., 2008; Zode et al., 2011;) it is of great interest to investigate whether DCN is able to repress ECM production in these cells. To answer this question secreted FN and Col IV in the media of human TM cells were quantified using western blot. Furthermore immunocytochemical staining against FN and Col IV and quantification of mRNA was carried out.

Western Blot analysis revealed that DCN treatment leads to a significant reduction of secretion of FN and Col IV by human TM cells (Figure 15 A and B) when set against whole protein content measured with Sypro Ruby^{TM}. FN was reduced to 0.34 ± 0.13 (n = 3, p ≤ 0.02) and Col IV was reduced to 0.48 ± 0.14 (n = 3, p ≤ 0.04) in comparison to the media of untreated control cells. Immunocytochemical staining confirmed a decrease in FN and Col IV synthesis after DCN treatment (Figure 15 C and D).

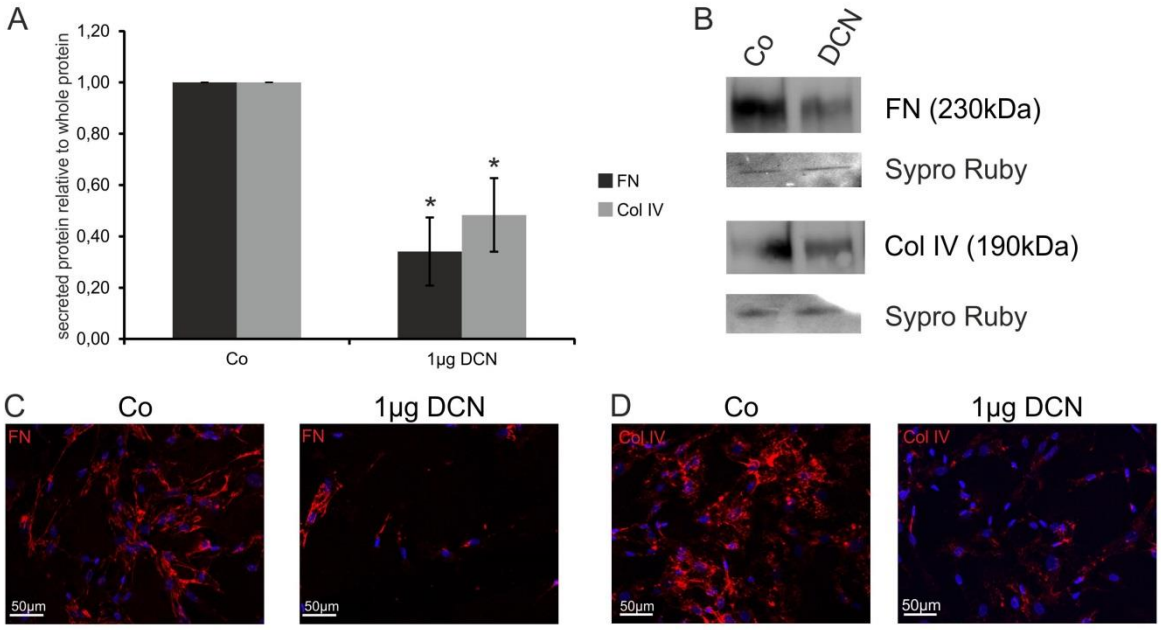

Figure 15: DCN reduces ECM synthesis in human TM cells. A shows densitometry of secreted FN and Col IV relative to whole secreted protein of untreated human TM cells and human TM cells treated with 1 µg of DCN for 24 h. Treatment with DCN significantly reduced secretion of FN (0.34 ± 0.13, n = 3, p ≤ 0.05) and Col IV (0.48 ± 0.14, n = 3, p ≤ 0.05). Signals for FN and Col IV were reduced in media of human TM cells treated with 1 µg of DCN in comparison to untreated controls (B). Immunocytochemical staining against FN and Col IV showed a reduction of FN and Col IV synthesis after DCN treatment (C and D).

Real Time RT PCR yielded the results that mRNA expression of both ECM components was decreased after DCN treatment (Figure 16). FN mRNA is reduced to 0.34 ± 0.23 (n = 4, p = 0.008) and Col IV mRNA is reduced to 0.33 ± 0.11(n = 5, p = 0.005).

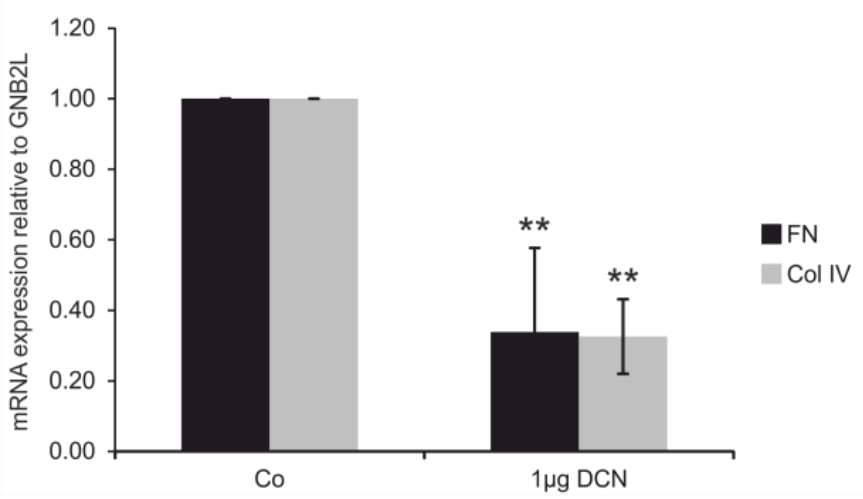

Figure 16: DCN reduces FN and Col IV mRNA in human TM cells. FN mRNA is reduced to 0.34 ± 0.23 (n = 4, p ≤ 0.01) and Col IV mRNA is reduced to 0.33 ± 0.11 (n = 5, p ≤ 0.01) after DCN treatment in comparison to untreated control cells. Expression was normalized to GNB2L.

Immunocytochemical staining against FN and Col IV on human ONH astrocytes treated with 1 µg of DCN showed a reduction of synthesis of both proteins compared to untreated controls (Figure 17 A). Analysis of FN and Col IV mRNA expression after DCN treatment also showed a significant reduction (FN: 0.49 ± 0.25, n = 4, p = 0.049; Col IV: 0.47 ± 0.17, n = 4, p = 0.032, Figure 17 B).

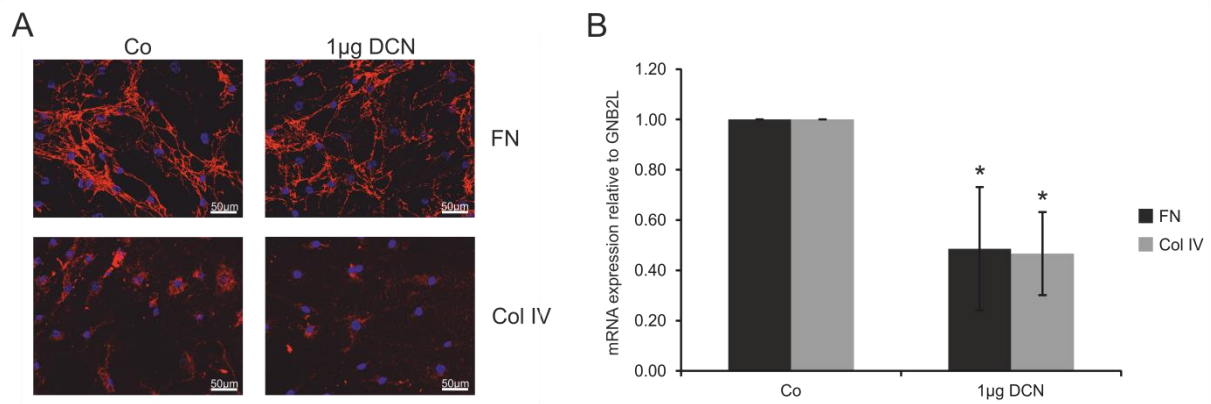

Figure 17: DCN treatment reduces synthesis and expression of FN and Col IV in human ONH astrocytes. Immunocytochemical staining showed a reduction of FN and Col IV synthesis after 24h treatment with 1µg DCN (A). mRNA expression of FN (0.49 ± 0.25, n = 4, p ≤ 0.05) and Col IV (0.47 ± 0.17, n = 4, p ≤ 0.05) are significantly depressed after 24h treatment with 1 µg of DCN. mRNA expression was normalized to GNB2L.

In murine ON astrocytes treatment with 1 µg DCN leads to a significant reduction in FN and Col IV expression (Figure 18). FN expression is reduced to 0.43 ± 0.08 (n = 4, p = 0.0051) and Col IV expression is reduced to 0.25 ± 0.06 (n = 4, p = 0.0001). Expression was normalized to GNB2L.

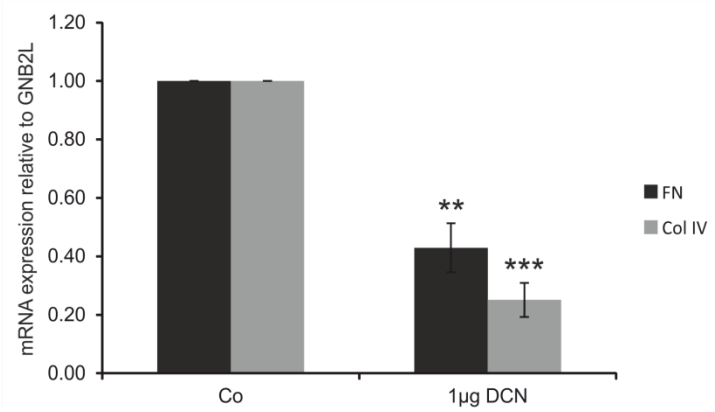

Figure 18: DCN treatment reduces expression of FN and Col IV murine ON astrocytes. FN expression was reduced to 0.43 ± 0.08 (n = 4, p≤ 0.01) and Col IV expression was reduced to 0.25 ± 0.06 (n = 4, p ≤ 0.001). Expression was normalized to GNB2L.

In combination all results show a clear effect of DCN on FN and Col IV. DCN reduces both ECM components significantly in the three analyzed cell types (see Table 23).

After 24 h 1 µg DCN (compared to untreated control)	human TM cells	human ONH astrocytes	murine ON astrocytes
FN mRNA	0.34 ± 0.23	0.49 ± 0.25	0.43 ± 0.08
FN protein	0.34 ± 0.13	-	-
Col IV mRNA	0.33 ± 0.11	0.47 ± 0.17	0.25 ± 0.06
Col IV protein	0.48 ± 0.14	-	-

Table 23: Expression and synthesis of ECM components after DCN treatment in cell types involved in the pathogenesis of POAG. All values are significant.

4.3 DCN activates AKT signaling in murine ON astrocytes

DCN is able to regulate TGF-β activity via two different mechanisms, either via direct binding (Yamaguchi et al., 1990) or via upregulating the synthesis of FBN1 via the pAKT/AKT pathway (Kaartinen and Warburton, 2003; Schonherr et al., 2005). Binding of DCN to IGF-IR leads to phosphorylation of AKT and in the end to an upregulation of FBN1 synthesis. Since the previous experiments showed that all cell types investigated react to DCN, TGF-β or CTGF treatment in the same way and murine ON astrocytes are easiest to obtain, pathway analyses were carried out with murine ON astrocytes only. To investigate whether this pathway is activated by DCN in murine ON astrocytes cells were treated with 1 µg of DCN for 6 h.

After 6 h of treatment with 1 µg of DCN an increase of pAKT in relation to AKT could be observed (Figure 19). The pAKT/AKT ratio of treated cells was 1.36 ± 0.11 (n = 4, p = 0.025) compared to untreated control cells (1 ± 0.07, n = 4), meaning that DCN treatment leads to an activation of the pAKT/AKT pathway in murine ON astrocytes. α-Tubulin was used as loading control to normalize pAKT and AKT.

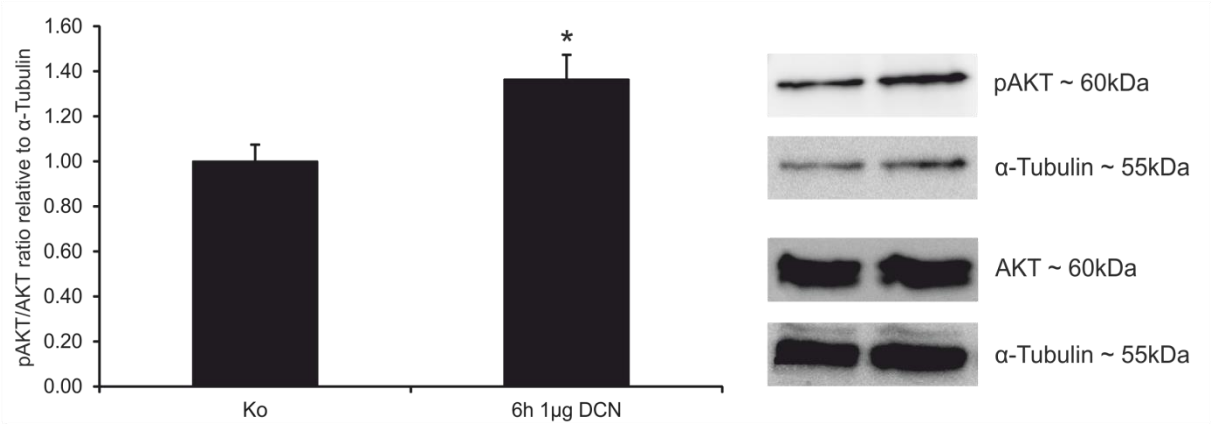

Figure 19: DCN activates AKT signaling in murine ON astrocytes. pAKT/AKT ratio was significantly higher in murine ON astrocytes treated with 1 µg of DCN for 6 h (1.36 ± 0.11, n = 4, p ≤ 0.05) speaking for an activation of the pAKT/AKT signaling pathway in this cell type. pAKT and AKT were normalized to α-Tubulin.

4.4 The negative regulatory effect of DCN on TGF-β1, TGF-β2 and CTGF is mediated via pAKT/AKT signaling in murine ON astrocytes.

To analyze if the negative effects of DCN on expression of TGF-β1, 2 and CTGF are mediated via pAKT/AKT signaling astrocytes were treated with the AKT signaling inhibitor triciribine in combination with DCN. Treatment with DCN resulted in a significant downregulation of all three growth factors (Figure 4.13; CTGF: 0.49 ± 0.13, n = 6, p = 0.007; TGF-β1: 0.41 ± 0.10, n = 5, p = 0.003; TGF-β2: 0.65 ± 0.13, n = 6, p = 0.004) After combined treatment with triciribine and DCN no significant reduction in expression of CTGF, TGF-β1,and TGF-β2 could be observed and expression was significantly higher when compared to cells treated with DCN only (Figure 20; CTGF: 0.81 ± 0.10, n = 5, p = 0.047; TGF-β1: 1.46 ± 0.22, n = 5, p = 0.005; TGF-β2: 1. 57 ± 0.57, n = 5, p = 0.038). Due to these results we conclude that the reduction of growth factor expression by DCN in murine ON astrocytes is mediated via the pAKT/AKT signaling pathway. Expression of all genes was normalized to GNB2L.

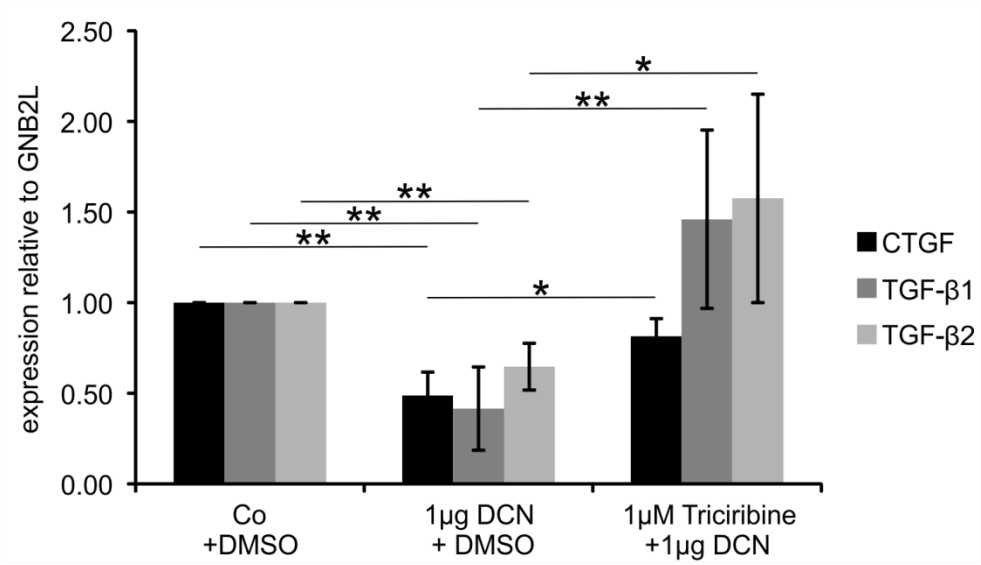

Figure 20: Inhibition of the pAKT/AKT signaling pathway circumvents negative regulation of TGF-β and CTGF by DCN. After treatment with 1 µg of DCN expression of CTGF (0.49 ± 0.13, n = 6, p ≤ 0.01), TGF-β1 (0.41 ± 0.10, n = 5, p ≤ 0.001) and TGF-β2 (0.65 ± 0.13, n = 6, p ≤ 0.001) was significantly lower than in untreated controls. Combined treatment with triciribine and DCN did not lead to changes in expression compared to untreated controls, but expression was significantly higher than in cells treated with DCN only (CTGF: 0.81 ± 0.10, n = 5, p = 0.047; TGF-β1: 1.46 ± 0.22, n = 5, p = 0.005; TGF-β2: 1. 57 ± 0.57, n = 5, p = 0.038). Expression was normalized to GNB2L.

4.5 DCN is reduced in the chamber angle of POAG patients

Previous studies showed that DCN is present in cornea, retina and TM (Funderburgh et al., 1998; Inatani et al., 1999; Tanihara et al., 1995). Anterior eye segments of POAG donors and healthy controls were stained against DCN to analyze whether DCN synthesis is altered in the outflow tissues of POAG patients.

4 sagittal sections of chamber angles of healthy donors and 3 sagittal sections of chamber angles of donors affected by POAG were stained against DCN. In all sections DCN signal was observed in the sclera, the cornea (not shown), the ciliary muscle (CM), the entire TM as well as in the endothelium of SC. Compared to chamber angles of healthy controls DCN signal was considerably weaker in all parts of the chamber angles of POAG donors (Figure 21).

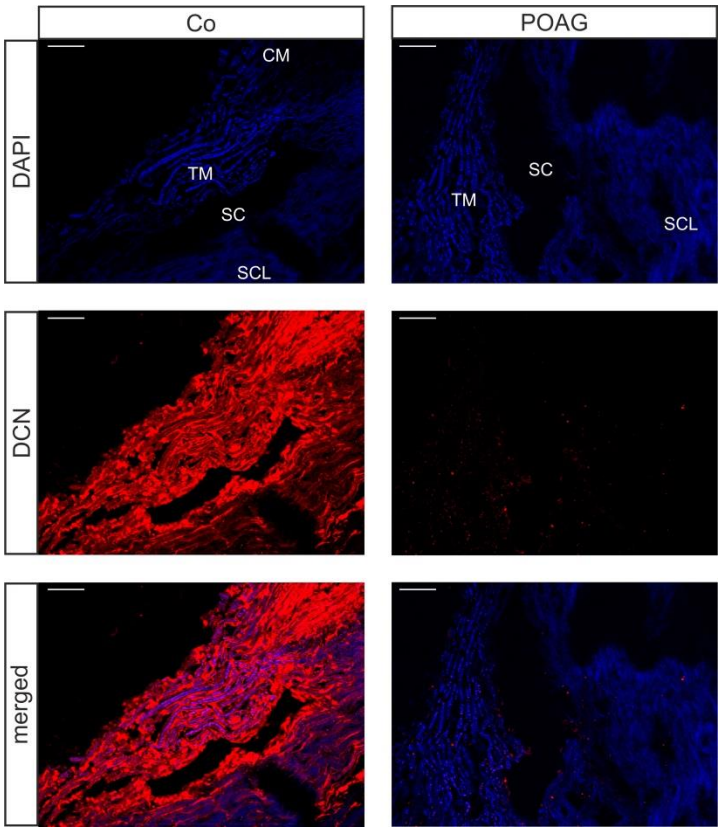

Figure 21: DCN synthesis is reduced in the chamber angle of POAG patients. Staining against DCN revealed that DCN is reduced dramatically in the chamber angle and in the outflow tissue of POAG patients. Blue: DAPI, red: DCN, scale bars: 50 µm.

4.6 The influence of CTGF overexpression on DCN in vivo

4.6.1 Influence of lens-specific overexpression of CTGF on DCN expression and synthesis in the region of the TM

Prior to all experiments animals were genotyped at an age of 21 to 25 days. βB1 (Figure 22 A) and SV40 (Figure 22 B) PCR were carried out. In TG animals SV 40 PCR results in a 360 bp band and βB1 PCR results in a 300 bp band while WT animals show no band when the PCR product is made visible with EtBr. Only animals displaying a band in both PCRs were considered as TG, animals that were positive for only βB1 or SV40 were excluded from analyses.

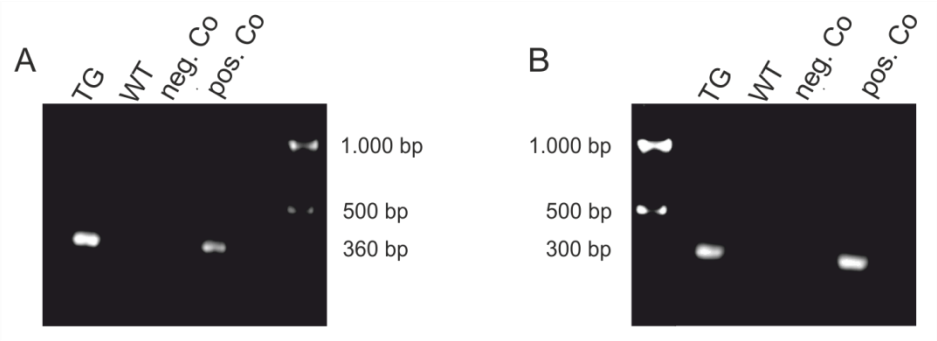

Figure 22: Results of an exemplary βB1 and SV40 PCR. Transgenic animals show a 360 bp band in SV 40 PCR and a 300 bp band in βB1 PCR. Only animals showing bands in both PCRs were considered as TG and used for experiments.

The *in vitro* results showed a reduction of DCN expression and synthesis after treatment with CTGF in TM cells as well as in astrocytes. Due to this we hypothesized that the lens-specific overexpression of CTGF in βB1-CTGF mice will lead to a reduced expression and synthesis of DCN in the region of the TM, the ONH and the ON.

8 week old βB-1 CTGF mice and their wildtype littermates were used for experiments.

Relative quantification of DCN mRNA in the corneo-scleral ring provided first proof of our hypothesis. In comparison to wildtype littermates DCN mRNA was reduced in transgenic animals (WT = 1.00 ± 0.08, n = 9; TG = 0.66 ± 0.09, n = 7, p = 0.02; Figure 23 A).

Western blot signals for DCN were weaker in TG animals in comparison to bands of WT animals (Figure 23 C). Quantification and normalization against α-Tubulin resulted in a significant reduction of DCN synthesis in the corneo-scleral ring of βB1-CTGF mice (WT = 1.00 ± 0.01, n = 5, TG = 0.55 ± 0.17, n = 6, p = 0.04; Figure 23 B).

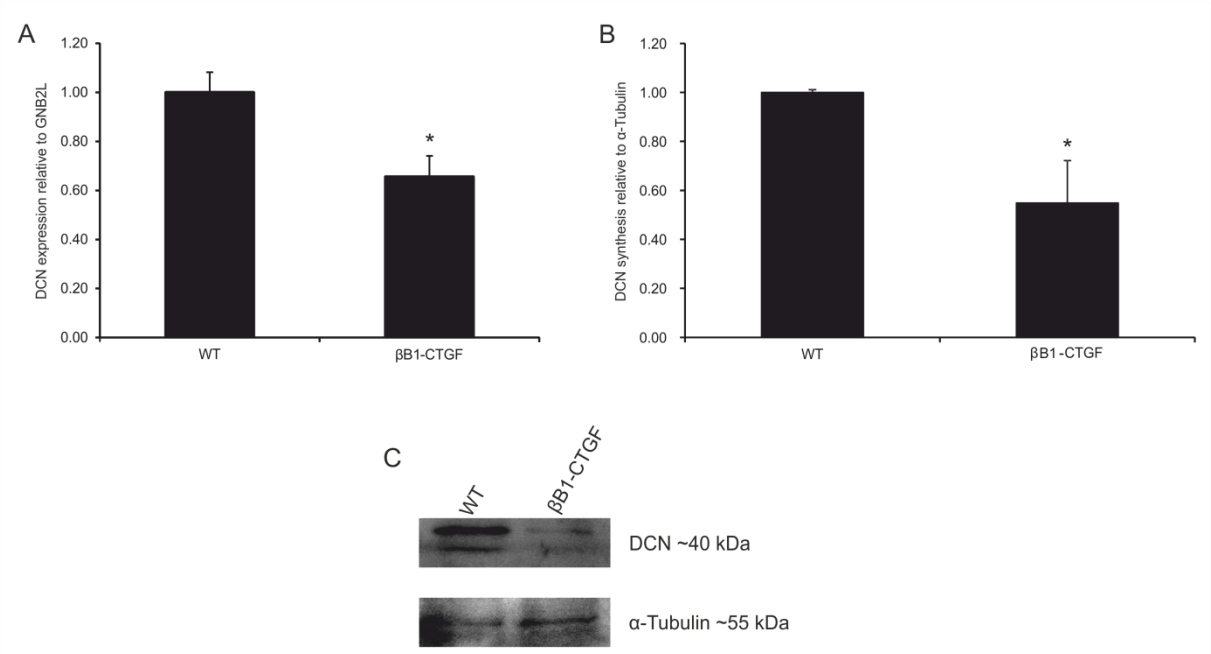

Figure 23: DCN expression and synthesis is reduced in the corneo-scleral rim of βB1-CTGF mice.
A: A lens-specific overexpression of CTGF leads to a significant downregulation of DCN expression in the corneo-scleral ring (WT = 1.00 ± 0.08, n = 9, TG = 0.66 ± 0.09, n = 7, $p \leq 0.05$). C shows a representative western blot for DCN in the corneo-scleral ring of an 8 week old WT animal and its TG littermate. DCN was normalized to α-Tubulin. Quantification of DCN bands yielded a significant reduction of DCN synthesis (B; WT = 1.00 ± 0.01, n = 5, TG = 0.55 ± 0.17, n = 6, $p \leq 0.05$).

Immunohistochemical staining of sagittal sections of 8 week old WT and βB1-CTGF mice eyes against DCN showed a positive signal in the retina (not shown), cornea, ciliary body, iris and the TM. The signal for DCN was weaker in sagittal sections of eyes of βB1-CTGF mice. A weaker signal for DCN could especially be observed in the chamber angle (Figure 24). DCN was reduced in the ciliary body, the cornea, the iris and in the outflow tissues of βB1-CTGF mice.

All results prove our hypothesis that overexpression of CTGF leads to a reduction of DCN expression and synthesis in the anterior eye segment and especially in the region of the TM.

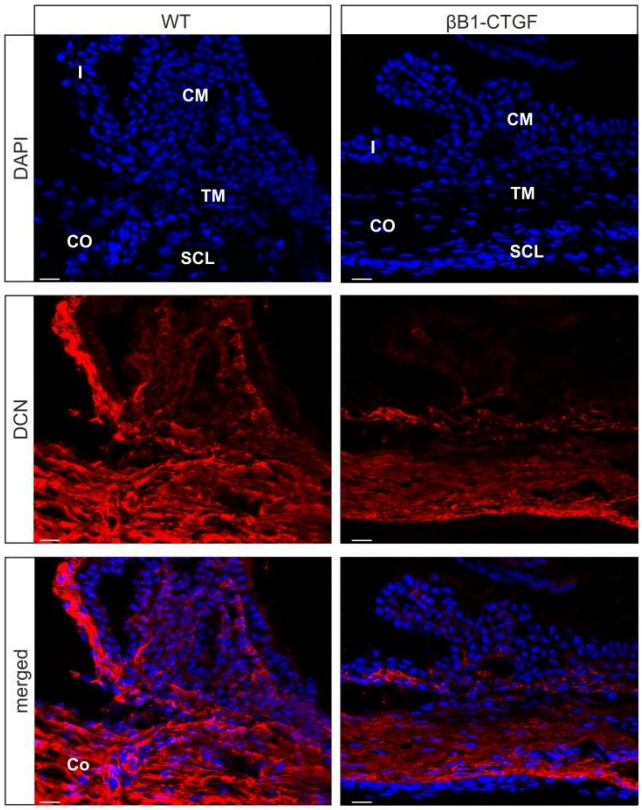

Figure 24: DCN signal is reduced in the region of the TM in βB1-CTGF mice. A positive signal for DCN was observed in the sclera, the retina (not shown), the cornea, the iris, the ciliary muscle and the TM. Signals for DCN were lower in TG animals when compared to their wildtype littermates. SCL = Sclera, CO = Cornea, TM = Trabecular meshwork, CM = Ciliary muscle. Red = DCN, blue = DAPI, scale bars: 20µm.

4.6.2 Influence of lens-specific overexpression of CTGF on DCN in the ON

Intriguingly we could not detect changes in DCN mRNA or protein amounts in the ON of 8 week old βB1-CTGF mice in comparison to WT animals. DCN expression was 1 ± 0.09 in WT mice while it was 0.96 ± 0.13 in βB1-CTGF mice (n = 5, p = 0.84, Figure 25 A). Protein amounts were also not changed in TG animals (WT= 1 ± 0.38, TG = 1.21 ± 0.22, n = 5, p = 0.46, Figure 25 B and C).

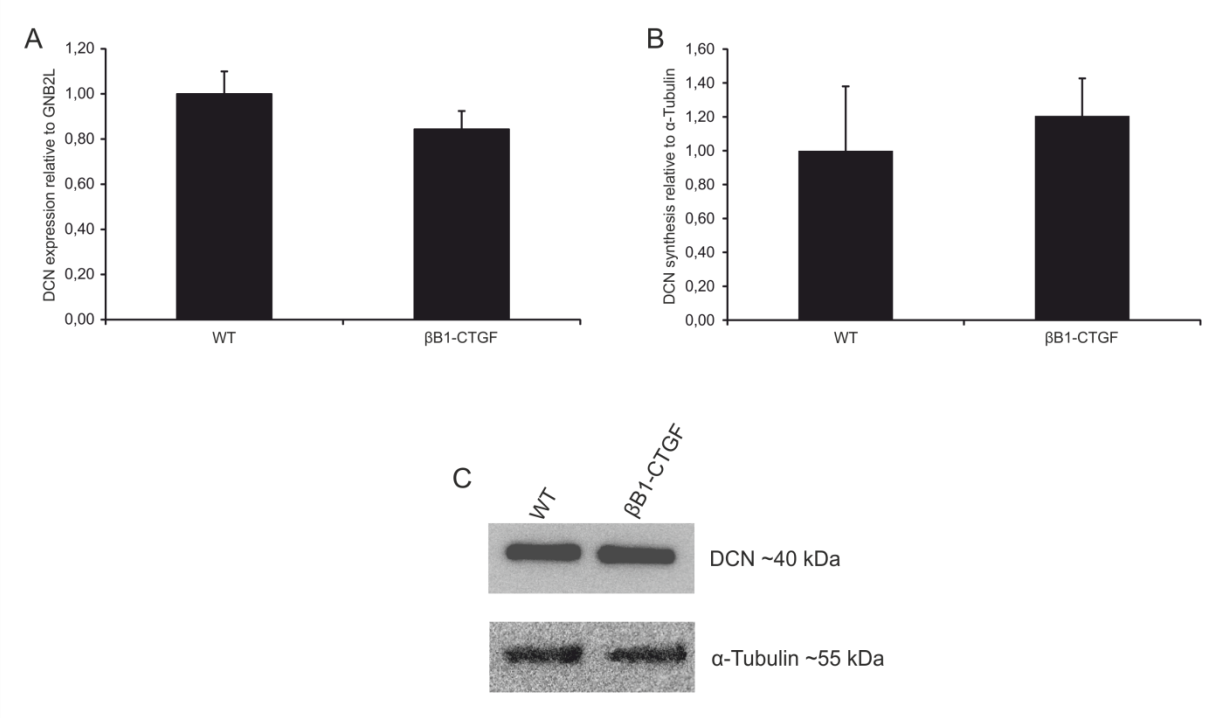

Figure 25: Lens-specific overexpression of CTGF does not influence DCN in the ON. DCN expression was 1 ± 0.09 in WT mice while it was 0.96 ± 0.13 in βB1-CTGF mice (n = 5, p ≥ 005). Protein synthesis was slightly higher in TG animals, but no significant changes could be found (WT= 1 ± 0.38, TG = 1.21 ± 0.22, n = 5, p ≥ 0.05). Expression was normalized to GNB2L, synthesis was normalized to α-Tubulin.

4.7 Decorin deficiency in 129SV/BL Swiss/CD1 mice mimics POAG

4.7.1 Verification of DCN knockout

All animals used for experiments were genotyped at an age of 21 to 25 days. DCN genotyping PCR results in a single 250 bp band in a $DCN^{-/-}$, a single 161 bp band in a wildtype and both bands in a heterozygous ($DCN^{+/-}$) animal (Figure 26).

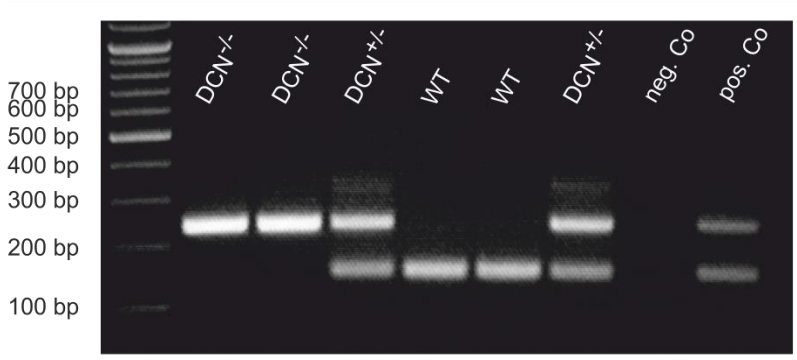

Figure 26: Result of an exemplary DCN genotyping PCR. $DCN^{-/-}$ animals show a single 250 bp band, WT animals a single 161 bp band. Heterozygous animals ($DCN^{+/-}$) show both bands. A heterozygous animal was used as a positive control. H_2O was used in the negative control instead of DNA.

Before first experiments with DCN mice were carried out we verified the knockout of DCN in the eye by western blot. DCN signal was detectable in the anterior eye segment and the retina of WT animals, whereas no signal for DCN was detectable in the anterior eye segment or in the retina of $DCN^{-/-}$ animals by western blot analysis (Figure 27).

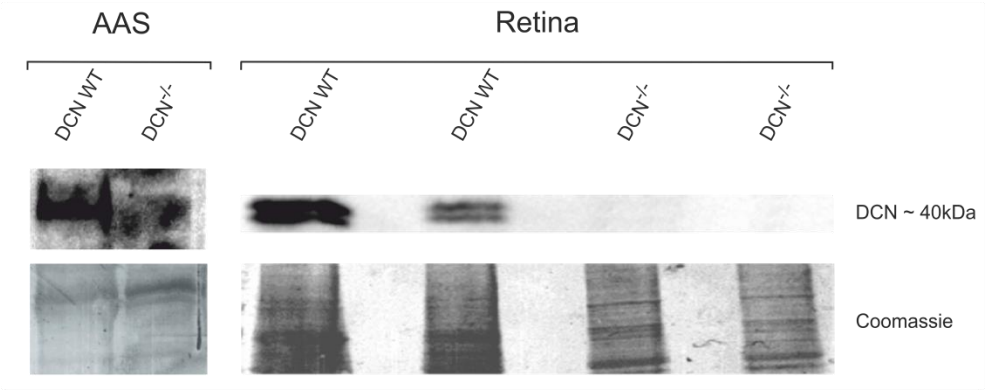

Figure 27: Verification of DCN knockout in the anterior eye segment (AAS) and in the retina. While western blot for DCN showed bands for the AAS and the retina of WT animals no bands could be detected in $DCN^{-/-}$ animals.

4.7.2 Histological analysis of the $DCN^{-/-}$ animals

To ensure that DCN deficiency does not cause developmental changes in eye morphology we analyzed sagittal sections of eyes of $DCN^{-/-}$ and WT mice of different ages by light microscopy.

Regarding the entire eye no visible morphological changes could be seen in the eyes of $DCN^{-/-}$ mice. Cornea, retina, iris, chamber angle and papilla of a 9 month old $DCN^{-/-}$ mouse do not show differences that can be observed by light microscopy

compared to a WT littermate (Figure 28). Both eyes show a normally developed TM and SC. The endothelium of SC looked similar in WT and DCN$^{-/-}$ animals and possessed vacuoles (pictures not shown), indicating that AH outflow is not hindered by severe structural changes.

We could not monitor differences in the chamber angle and the papilla of a 2 month old WT animal and its DCN$^{-/-}$ littermate (Figure 29). The chamber angle is open in both animals and there are no visible differences in structure and organization of the TM. The papilla does not show signs of excavation in the DCN$^{-/-}$ animal. The same observation was made in 6 month old animals (Figure 30). There is no visible blocking of AH outflow in the TM that could cause elevation of IOP, and the papilla is not obviously excavated in the DCN deficient animal.

All in all we conclude that the knockout of DCN in mice does not lead to morphological changes in the eye that can be observed on light microscopy levels. We could not find changes in the region of the TM that would hinder AH outflow and thereby increase IOP and papilla of DCN$^{-/-}$ mice show no obvious signs of excavation at an age of 2, 6 or 9 months.

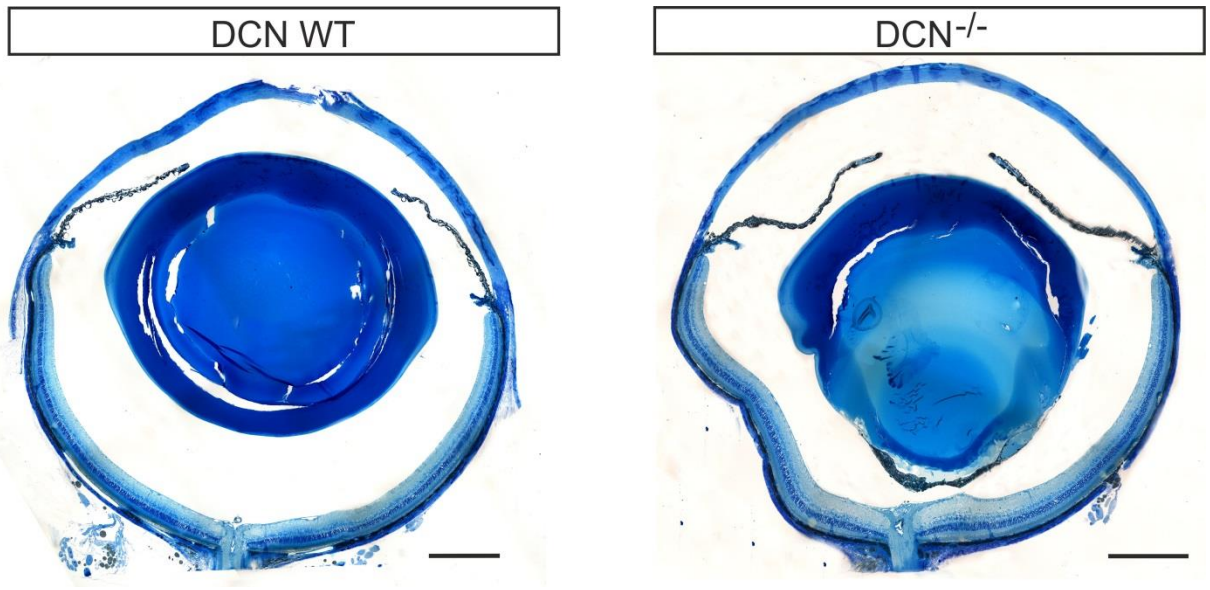

Figure 28: Whole eye of a 9 month old DCN WT mouse and its DCN$^{-/-}$ littermate. No morphological differences could be observed. Scale bars: 500 µm.

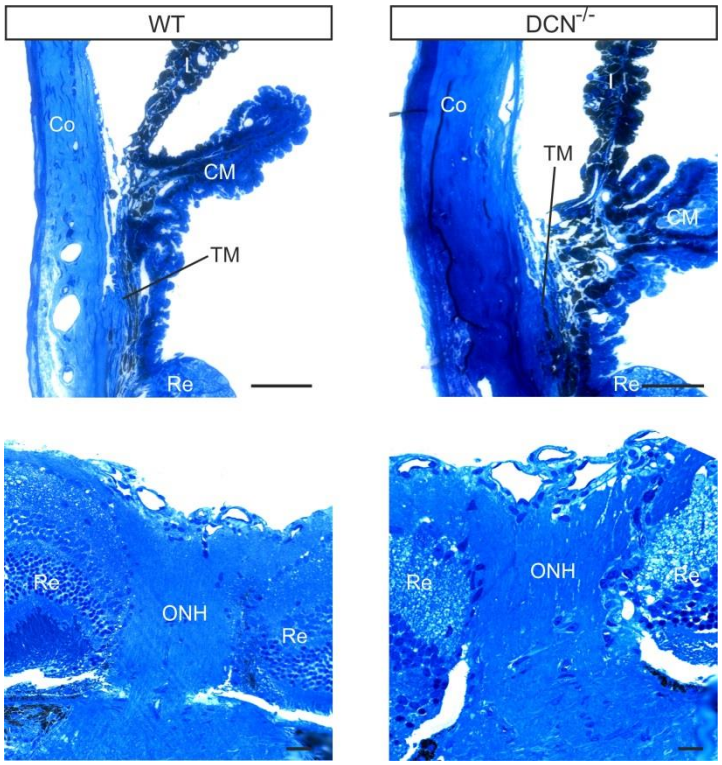

Figure 29: Chamber angle and papilla of a 2 month old DCN WT mouse and its WT littermate. The chamber angle shows no structural changes and the papilla shows no signs of excavation in the DCN$^{-/-}$ mouse. Co: Cornea, I: Iris, CM: Ciliary muscle, TM: Trabecular meshwork, Re: Retina, ONH: Optic nerve head. Scale bars: 50 µm.

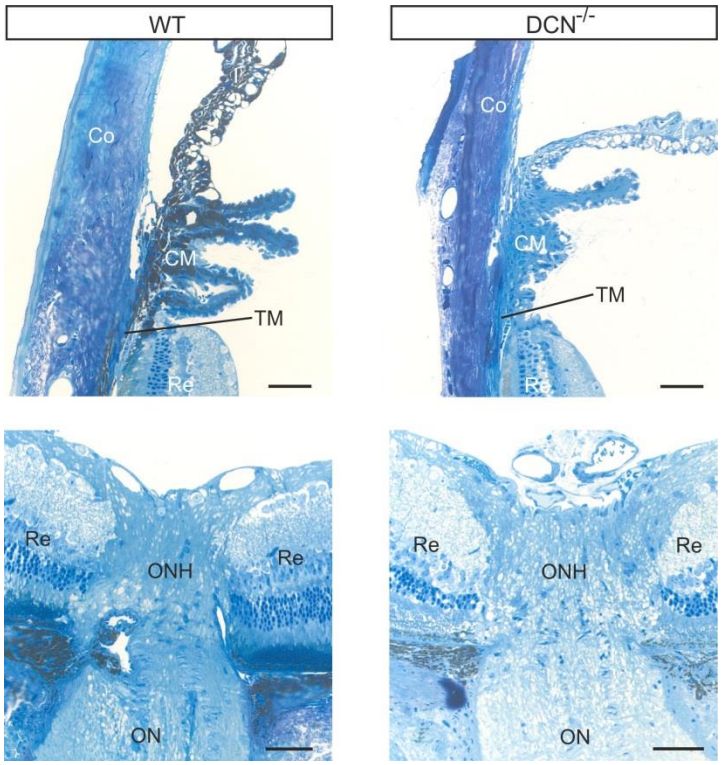

Figure 30: Chamber angle and papilla of a 6 month old DCN WT mouse and its WT littermate. The chamber angle shows no structural changes and the papilla shows no signs of excavation in the DCN$^{-/-}$ mouse. Co: Cornea, I: Iris, CM: Ciliary muscle, TM: Trabecular meshwork, Re: Retina, ONH: Optic nerve head, ON: Optic nerve. Scale bars: 50 µm.

4.7.3 DCN$^{-/-}$ 129SV/BL Swiss/CD1 mice show elevated IOP and loss of optic nerve axons

An elevated IOP is the main risk factor to develop POAG (Collaborative-Normal-Tension-Glaucoma-Study-Group, 1998; Gordon et al., 2002; Johnson et al., 2002; Leske et al., 2003). We hypothesize that DCN deficiency leads to an increase of TGF-β and CTGF and thereby to an increased outflow resistance in the TM. To verify this hypothesis we measured IOP of DCN$^{-/-}$ and wildtype animals every four weeks for one year. Animals were grouped by age into 5 groups (see Figure 31). An increase of IOP over time was observed in WT and in DCN$^{-/-}$ mice, but while over one year an increase of 8.45 mmHg was recorded in DCN$^{-/-}$ mice, increase in IOP was 6.01 mmHg in WT mice. In 1 month old animals there was no difference in IOP between WT and DCN$^{-/-}$ mice, but in all older animals IOP was significantly higher in DCN$^{-/-}$ animals than in WT controls (for exact values see Table 24).

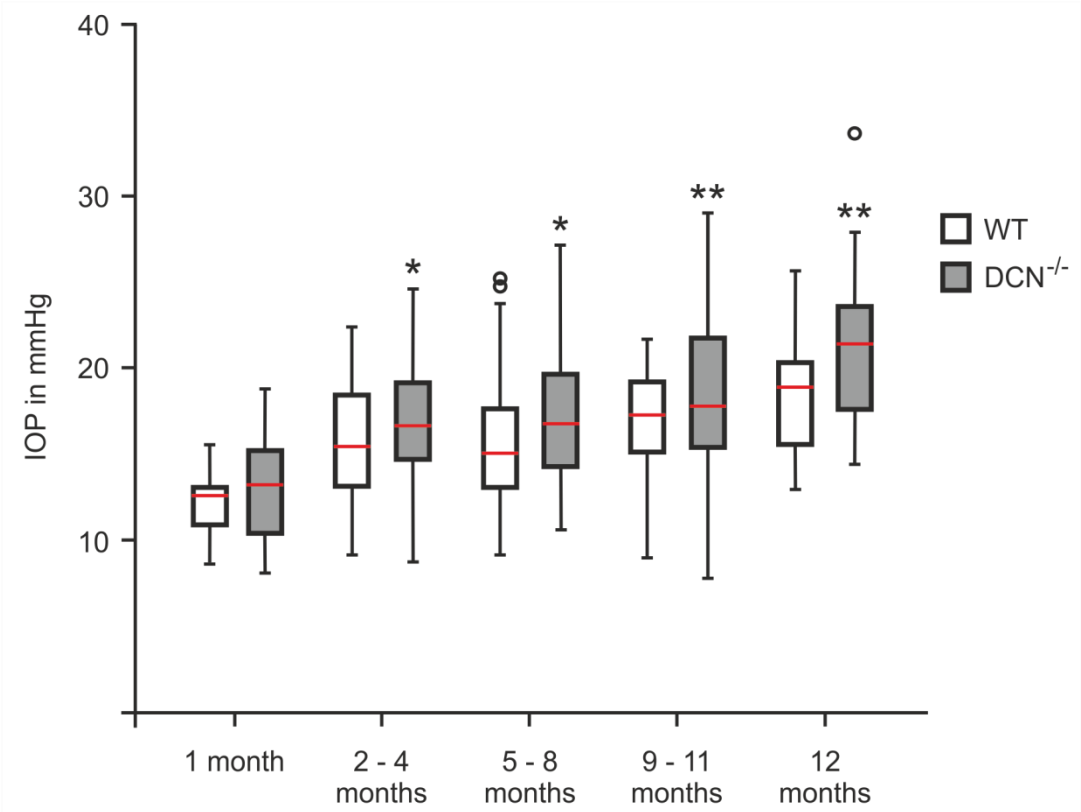

Figure 31: IOP is significantly elevated in DCN$^{-/-}$ mice of different ages. IOP is not elevated in 1 month old DCN$^{-/-}$ mice in comparison to WT animals. In DCN$^{-/-}$ mice of 2 – 4 month, 5 – 8 month, 9 – 11 month and 12 month IOP is significantly higher than in WT controls. Circles represent max. outliers, red lines mark median (* $p \leq 0.05$, ** $p \leq 0.01$).

	1 month	2 – 4 months	5 – 7 months	8 – 10 months	12 months
DCN$^{-/-}$	12.93 ± 2.63	16.74 ± 2.87	17.22 ± 2.76	18.73 ± 4.21	21.38 ± 4.28
WT	12.35 ± 1.80	15.65 ± 3.26	15.65 ± 2.87	16.90 ± 2.63	18.36 ± 3.49
p-Value		0.022	0.011	0.004	0.008
n DCN$^{-/-}$	42	98	94	96	30
n WT	32	82	62	80	26

Table 24: IOP values of DCN$^{-/-}$ and WT mice ± STD.

To analyze if the increased IOP leads to the loss of optic nerve axons, axon numbers of DCN$^{-/-}$ and wildtype mice of 2, 3, 6 and 12 months were counted. Optic nerve sections of DCN$^{-/-}$ mice showed larger areas devoid of axons than cross sections of wildtype littermates (see Figure 32 A). Areas devoid of axons indicate formation of glial scars since dead axons get replaced by ECM material. Quantification of optic nerve axons revealed a significant difference in axon numbers in mice of 3, 6 and 12 months (Figure 32 B). Axon numbers of all age groups and p-values are displayed in table 25.

Intriguingly axons numbers did not decrease with age as expected. Axon numbers in 2 month old WT and DCN$^{-/-}$ mice are not different, but at an age of 3 months DCN$^{-/-}$ have significantly less axons in the optic nerve than WT littermates. Axon numbers only decrease in DCN$^{-/-}$ mice between 2 and 3 months. In WT mice axon numbers were stable at all ages analyzed and in DCN$^{-/-}$ mice older than 3 months.

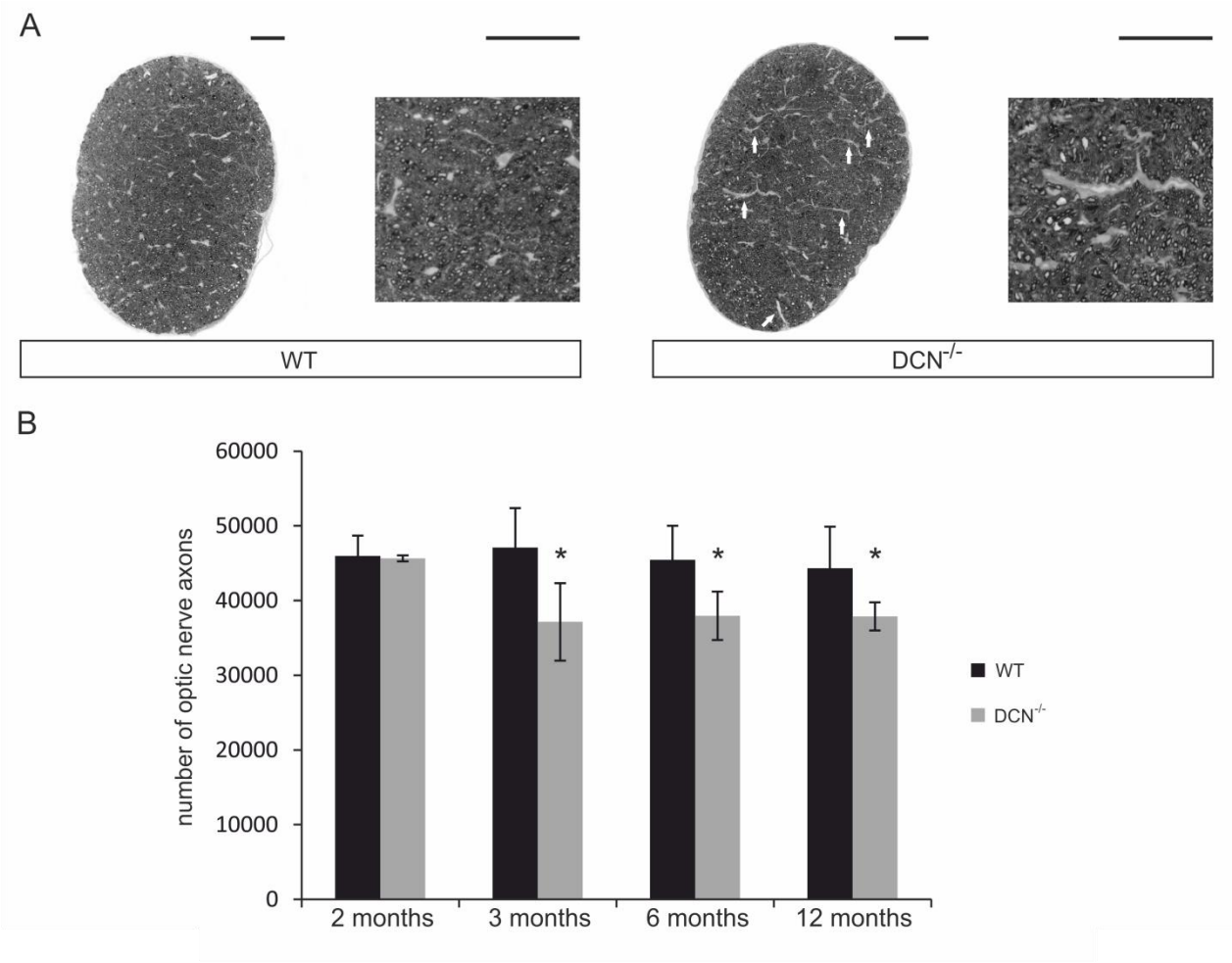

Figure 32: Decorin $^{-/-}$ mice have less optic nerve axons than their wildtype littermates. A: optic nerve cross sections of 12 month old WT and DCN$^{-/-}$ mice. DCN$^{-/-}$ mice show larger areas devoid of axons (right, white arrows). B: Number of optic nerve axons of 2, 3, 6 and 12 month old WT and DCN$^{-/-}$ mice. 3 to 12 month old DCN$^{-/-}$ animals have significantly less axons than WT animals. Means ± STD. Scale bars: 50 µm, * $p \leq 0.05$.

	2 months	3 months	6 months	12 months
DCN$^{-/-}$	45664 ± 400	37156 ± 5183	37970 ± 3232	37886 ±1873
WT	45954 ± 2755	47080 ± 5312	45447 ± 4576	44329 ± 5555
p-Value	0.881	0.022	0.017	0.033
n DCN$^{-/-}$	5	5	5	6
n WT	5	5	5	6

Table 25: Axon number of DCN$^{-/-}$ and WT mice of different ages. Means ± STD.

4.7.4 Expression and synthesis of key players in POAG is altered in the corneo-scleral ring of DCN$^{-/-}$ 129SV/BL Swiss/CD1 mice

4.7.4.1 CTGF

Junglas et al. showed that a lens-specific overexpression of CTGF leads to a glaucomatous phenotype in mice (Junglas et al., 2012) and our *in vivo* and *in vitro* data showed negative reciprocal effects of DCN on CTGF. Therefore we conclude that a lack of DCN should lead to an increased expression and synthesis of CTGF *in vivo*. To test for this hypothesis we analyzed CTGF mRNA and protein in corneo-scleral rings of 8 week old DCN$^{-/-}$ mice and their WT littermates. Real Time RT PCR showed a more than six-fold increase in CTGF expression in the corneo-scleral ring of DCN$^{-/-}$ mice in comparison to WT animals (WT = 1.00 ± 0.19, DCN$^{-/-}$ = 6.55 ± 2.03, n = 6, p = 0.037, figure 33 A). CTGF expression was normalized to RPL32.

Western blot analysis of CTGF synthesis in the corneo-scleral ring showed that CTGF synthesis is significantly higher in the corneo-scleral ring of DCN$^{-/-}$ mice (Figure 33 B and C). CTGF synthesis in the corneo-scleral ring of WT mice was 1 ± 0.46 (n = 5) while CTGF synthesis in DCN$^{-/-}$ mice was 3.27 ± 1.42 (n = 4, p = 0.040). Synthesis of CTGF was normalized to α-Tubulin.

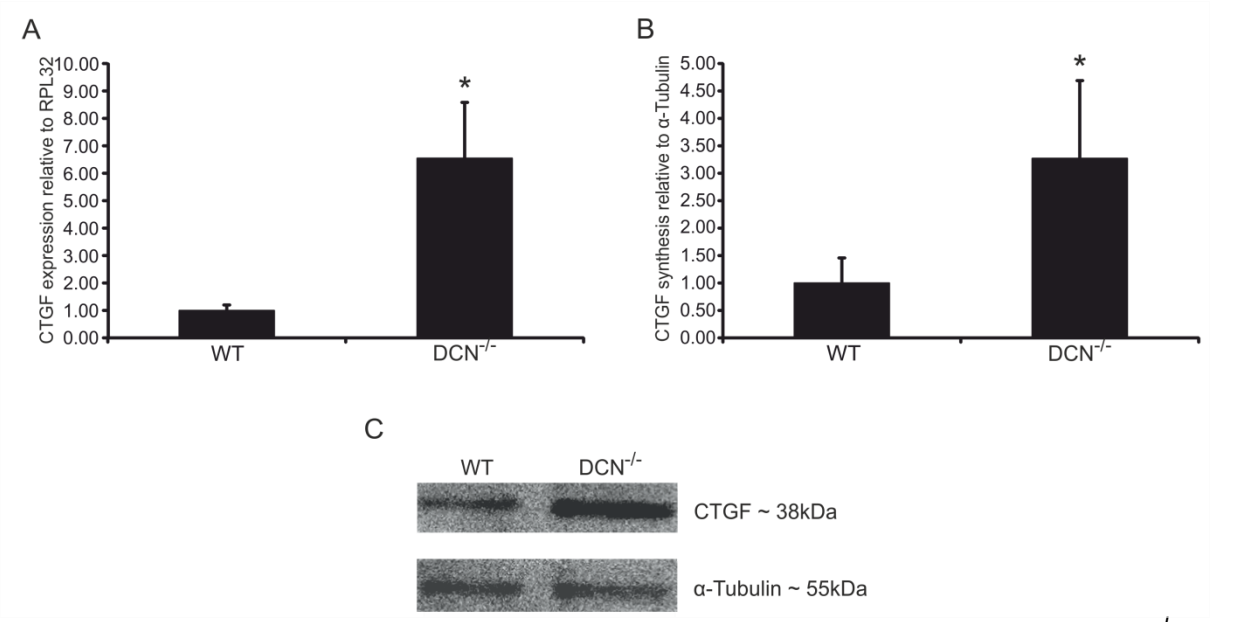

Figure 33:CTGF expression and synthesis is increased in the corneo-scleral ring of DCN$^{-/-}$ mice. Relative Quantification of CTGF mRNA resulted in the observation that CTGF mRNA is significantly elevated in the corneo-scleral ring of DCN$^{-/-}$ mice in comparison to WT animals of the same age (WT = 1.00 ± 0.19, DCN$^{-/-}$ = 6.55 ± 2.03, n = 6, $p \leq 0.05$, A). CTGF expression was normalized to RPL32. B shows densitometry of CTGF signals of corneo-scleral rings of DCN$^{-/-}$ and WT mice normalized to α-Tubulin. CTGF signal in WT mice was 1 ± 0.46 (n = 5) while CTGF signal in DCN$^{-/-}$ mice was 3.27 ± 1.42 (n = 4, $p \leq 0.05$). C shows an exemplary western blot against CTGF and the housekeeper α-Tubulin.

Immunohistochemical staining against CTGF showed elevated synthesis of CTGF in the whole eye of 8 week old DCN$^{-/-}$ mice in comparison to their WT littermates (Figure 34). Staining confirmed the results of Real Time RT PCR and western blot. Signal for CTGF was brighter in the region of the TM in DCN deficient animals. Furthermore a brighter signal for CTGF was observed in retina, sclera, cornea, ciliary body and iris of DCN$^{-/-}$ mice. Negative controls (not shown), testing for unspecific binding of the secondary antibody, showed no signal.

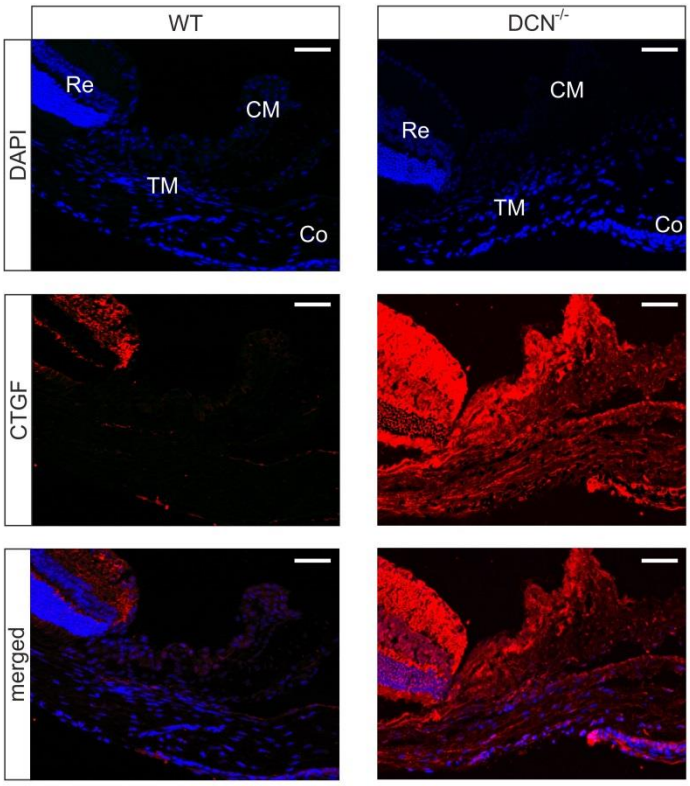

Figure 34: Signal for CTGF is stronger in the anterior eye of DCN$^{-/-}$ mice than in WT animals.
Immunohistochemical staining against CTGF showed higher synthesis of CTGF in the anterior eye of DCN deficient animals. CTGF synthesis seems to be elevated in the Retina (Re), the ciliary muscle (CM), the cornea (Co) and in the region of the trabecular meshwork (TM). Scale bars: 20 µm.

4.7.4.2 TGF-β2

TGF-β2 is also a key player in POAG. For all cell types analyzed this study could show negative reciprocal effects of TGF-β2 and DCN. So we hypothesize that a lack of DCN should increase expression of TGF-β2 in mice. Expression of TGF-β2 was significantly higher in the corneo-scleral ring DCN deficient animals (Figure 35). TGF-β2 mRNA expression is significantly higher in 8 week old DCN$^{-/-}$ mice (4.45 ± 2.15, n = 6) in comparison to WT mice (1 ± 0.58, n = 7, p = 0.044).

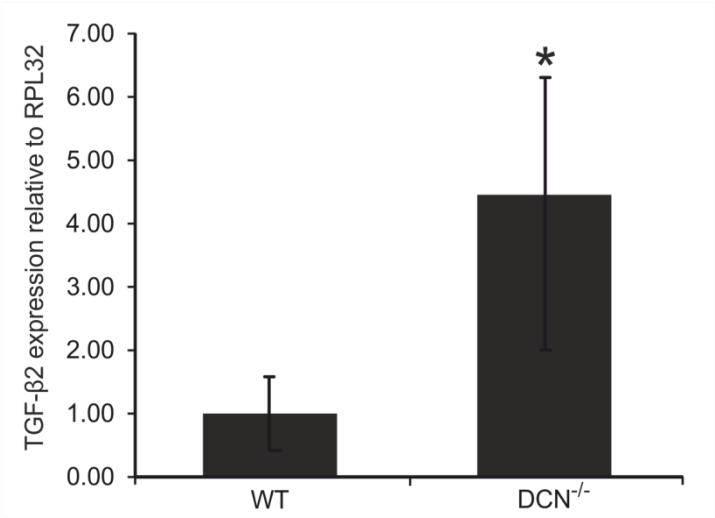

Figure 35: TGF-β2 mRNA expression is elevated in the corneo-scleral ring of DCN$^{-/-}$ mice. TGF-β2 expression was 1 ± 0.58 in WT (n = 7) and 4.45 ± 2.15 in DCN$^{-/-}$ (n = 6, p ≤ 0.05) meaning a significant upregulation of TGF-β2 expression in the corneo-scleral ring of DCN deficient animals.

4.7.4.3 FN and Col IV

It has been described previously that CTGF increases FN and Col IV expression and synthesis in TM cells and astrocytes (Fuchshofer et al., 2005, Junglas et al., 2009) and that βB1-CTGF mice have elevated amounts of FN in the iridocorneal angle (Junglas et al., 2012). Therefore we assumed that the elevation in CTGF expression and synthesis will lead to an increased FN and Col IVexpression and synthesis in the corneo-scleral ring of DCN$^{-/-}$ mice. In order to prove this we analyzed the corneo-scleral rings of 8 week old DCN$^{-/-}$ and WT mice regarding FN and Col IV expression and synthesis.

FN expression is significantly higher in the corneo-scleral ring of DCN$^{-/-}$ mice. FN expression in WT mice was 1 ± 0.13 (n = 9) while FN expression in DCN$^{-/-}$ mice was 3.49 ± 1.50 (n = 6; p = 0.50; Figure 36). Densitometry of western blots against FN in the corneo-scleral rings of WT and DCN$^{-/-}$ mice showed a significant increase in FN synthesis. FN synthesis in WT mice was 1 ± 0.09 (n = 5) while synthesis in DCN$^{-/-}$ mice was 1.82 ± 0.27 (n = 5, p = 0.0419). FN synthesis was normalized to α-Tubulin (Figure 36 B and C).

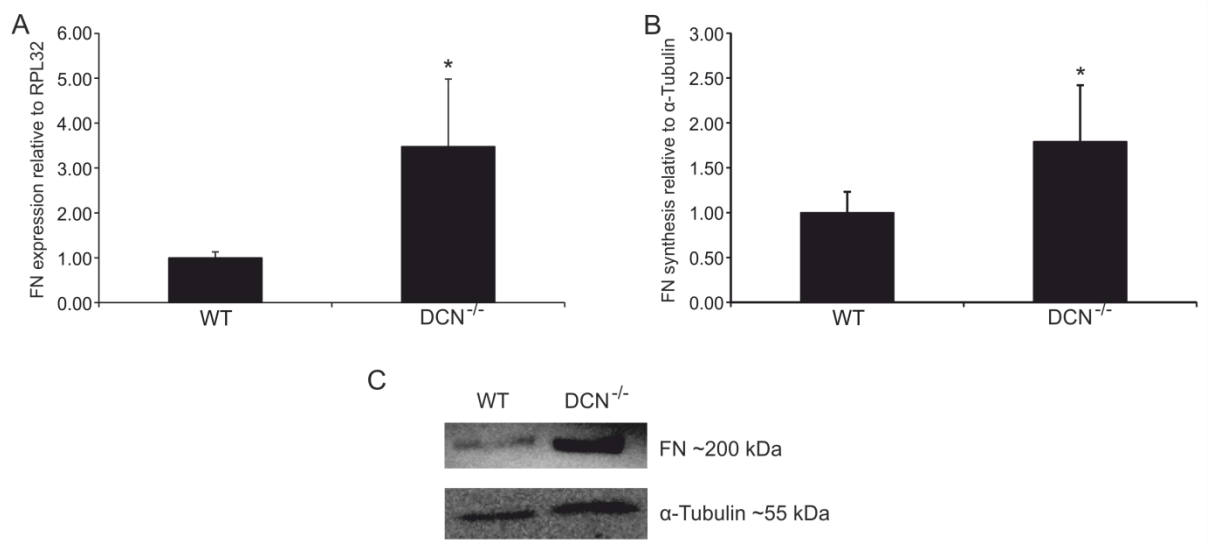

Figure 36: FN expression and synthesis is elevated significantly in the corneo-scleral ring of DCN$^{-/-}$ mice. A: FN expression is significantly higher in the corneo-scleral ring of DCN$^{-/-}$ mice (WT = 1 ± 0.13, DCN$^{-/-}$ = 3.49 ± 1.50 (n = 9, p ≤ 0.05). Expression was normalized to RPL32. B shows densitometry of FN bands after normalization to α-Tubulin. Western blot analysis revealed a significant increase of FN synthesis in DCN$^{-/-}$ animals (1.82 ± 0.27) than in WT littermates (1 ± 0.09; n = 5, p ≤ 0.05).

For further proof of an elevated synthesis of FN sagittal sections of eyes of 8 week old WT and DCN$^{-/-}$ mice were stained against FN. We observed an increase in FN signal in the entire anterior eye segment of DCN$^{-/-}$, but we also noticed that FN synthesis is stronger in the region of the TM and the cornea (Figure 37). Negative controls (not shown), testing for unspecific binding of the secondary antibody, showed no signal.

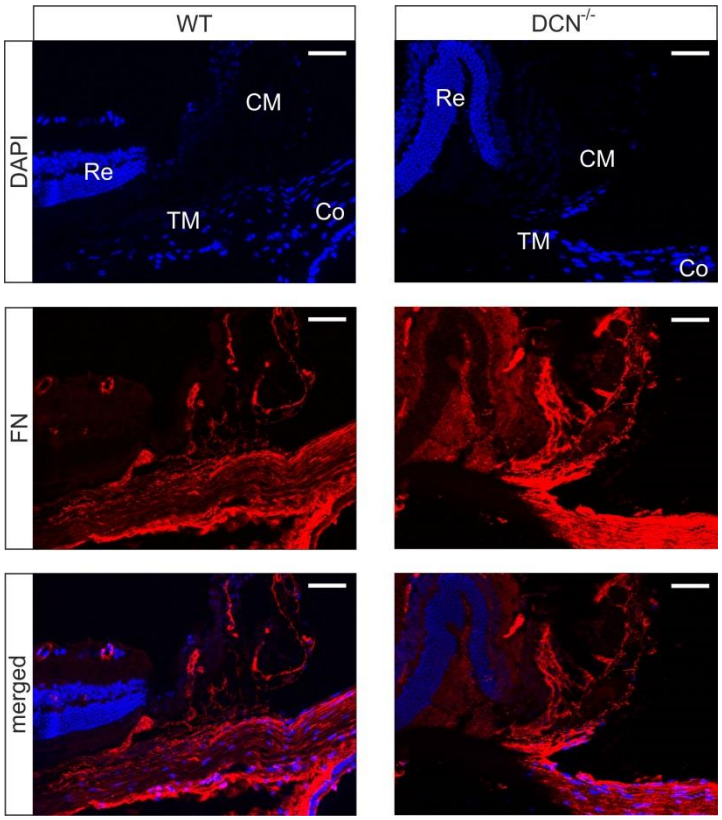

Figure 37: Immunohistochemical staining for FN is stronger in the anterior eye of DCN$^{-/-}$ mice. Signal for FN is stronger especially in the region of the trabecular meshwork (TM) in the anterior eye segments of DCN$^{-/-}$ mice. But FN synthesis seems also to be elevated in the Retina (Re), the ciliary muscle (CM) and the cornea (Co).Blue: DAPI, red: FN. Scale bars: 20 µm.

The knockout of DCN also led to a highly significant upregulation of Col IV expression in the corneo-scleral ring (WT = 1 ± 0.05, DCN$^{-/-}$ = 3.66 ± 0.72, p = 0.01, Figure 38).

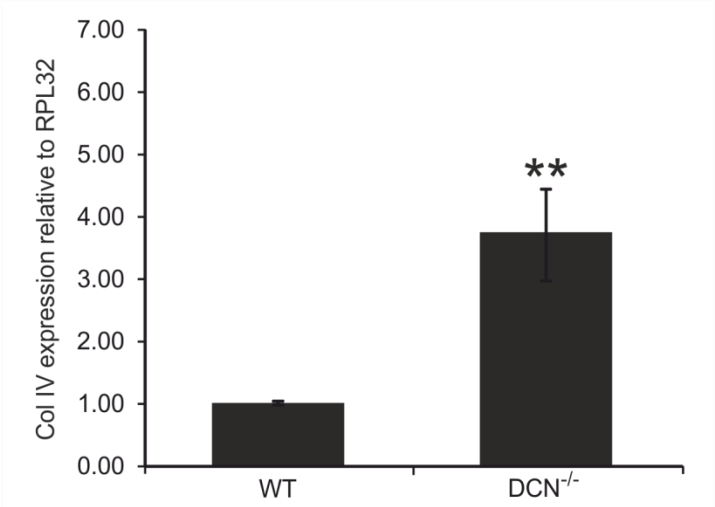

Figure 38: Col IV expression is significantly increased in the corneo-scleral ring of DCN$^{-/-}$ mice. Col IV expression was upregulated significantly in the corneo-scleral ring of DCN deficient animals compared to WT littermates (WT = 1 ± 0.05, DCN$^{-/-}$ = 3.66 ± 0.72, p ≤ 0.01). Expression was normalized to RPL32.

4.7.5 TGF-β and CTGF expression are altered in the optic nerve of DCN$^{-/-}$ 129SV/BL Swiss/CD1 mice

Since the ON also undergoes changes in POAG, which are most likely induced by pathological amounts of TGF-β and CTGF, we analyzed if the complete absence of DCN affects expression of TGF-β1, TGF-β2 and CTGF in the optic nerve.

We could demonstrate that the knockout of DCN leads to a significant increase in expression of all three growth factors in the optic nerve (Figure 39). TGF-β1 was 1 ± 0.15 (n = 9) in WT ON and 1.83 ± 0.23 (n = 10) in DCN$^{-/-}$ ON (p = 0.040). TGF-β2 was 1 ± 0.13 in WT (n = 9) and 1.85 ± 0.20 (n = 10) in DCN$^{-/-}$ (p = 0.036). CTGF was also significantly upregulated in DCN$^{-/-}$ ON (1.84 ± 0.23, n = 7) in comparison to WT mice (1 ± 0.15, n = 7, p = 0.044). Expression was normalized to RPL32.

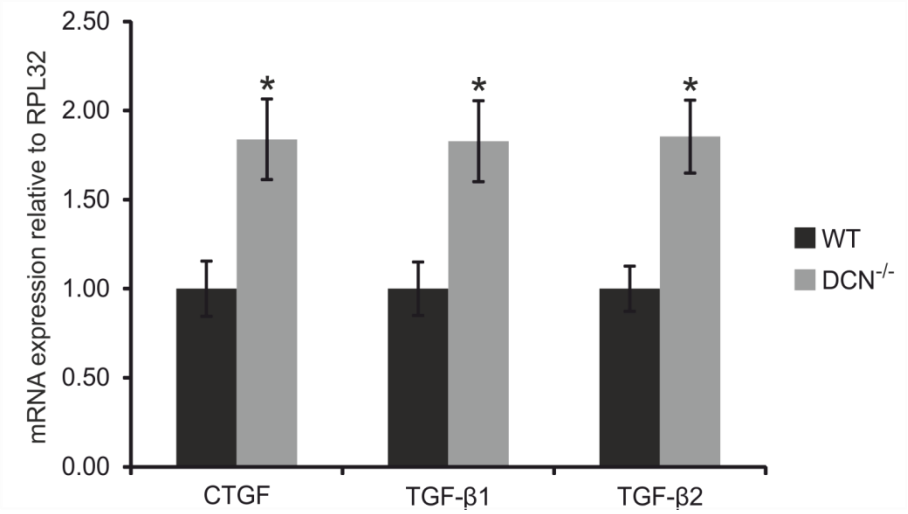

Figure 39: Expression of CTGF, TGF-β1 and TGF-β2 is elevated in the optic nerve of DCN deficient mice. CTGF was increased to 1.84 ± 0.23 in DCN$^{-/-}$ ON (n = 7) in comparison to WT ON (1 ± 0.15, n = 7, p ≤ 0.05). TGF-β1 expression in the ON of DCN$^{-/-}$ mice is significantly increased to 1.83 ± 0.23 (n = 10) compared to WT animals (1 ± 0.15 n = 9, p ≤ 0.05) and TGF-β2 levels are also significantly higher in ON of DCN deficient animals (WT = 1 ± 0.13, n = 9; DCN-/- = 1.85 ± 0.20, n = 10, p ≤ 0.05). Expression of all genes was normalized to RPL32.

To evaluate if the knockout of DCN also leads to elevated synthesis of CTGF in the ON we carried out immunohistochemical staining against CTGF in sagittal sections of eyes of 12 week old DCN WT and DCN$^{-/-}$ animals. Signal for CTGF was higher in the ON of DCN$^{-/-}$ mice compared to their WT littermates (Figure 40). Especially in the region of the ONH we could observe an increase in CTGF signal. Negative controls (not shown), testing for unspecific binding of the secondary antibody, showed no signal.

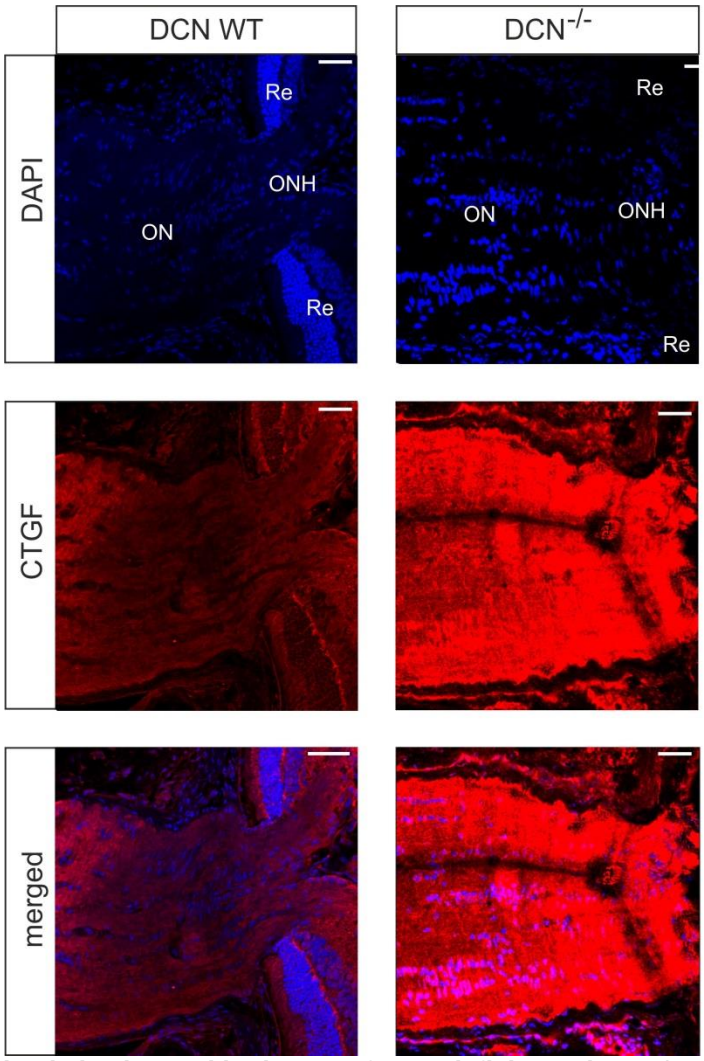

Figure 40: CTGF synthesis is elevated in the ON of DCN deficient mice. Signal for CTGF was stronger in DCN deficient ON, especially in the region of the ONH. Blue: DAPI, red: CTGF. Re: retina, ON: Optic nerve, ONH: optic nerve head, scale bars: 20 µm.

4.7.6 Astrocytes of the laminar region of DCN$^{-/-}$ 129SV/BL Swiss/CD1 mice show signs of reactivation

Reactivation of astrocytes in the region of the LC is one typical observation in the glaucomatous ONH. Reactivation of astrocytes shows in increased amounts of GFAP synthesis and in morphological changes, like thickening of processes and hypertrophy of the cell body (Hernandez and Pena, 1997; Varela and Hernandez, 1997; Wang et al., 2002). To check for signs of astrocyte reactivation on the ONH of DCN deficient mice, we made tangential sections through the glial lamina of 12 week old DCN$^{-/-}$ and WT

mice. Tangential sections were stained against GFAP and nuclei were made visible with DAPI (Figure 41).

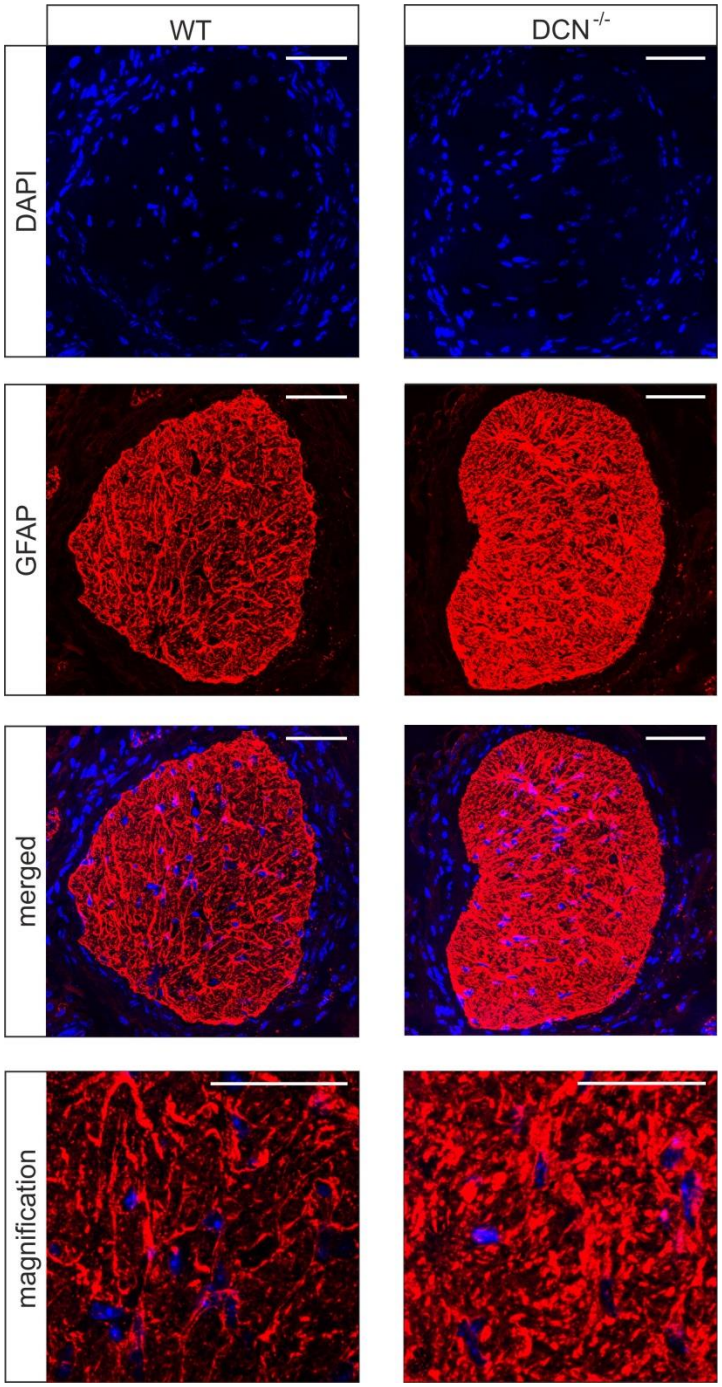

Figure 41: GFAP synthesis and astrocyte morphology is altered in the glial lamina of DCN$^{-/-}$ mice. Signal for GFAP was stronger in the glial lamina of DCN$^{-/-}$ mice. Additionally GFAP negative spaces between astrocytes appear smaller and processes seem thickened. Blue: DAPI, red: GFAP. Scale bars: 100 µm.

Staining against GFAP in the glial lamina indicated reactivation of astrocytes of that region. GFAP signal was increased in the glial lamina of DCN$^{-/-}$ mice in comparison to

WT animals. Accessorily we observed changes in astrocyte morphology. Processes appeared shortened and thickened and areas negative for GFAP, meaning spaces between astrocytes, through which axons can pass, were smaller. Therefore we conclude that a knockout of DCN leads to reactivation of astrocytes in the region of the glial lamina.

4.7.7 Astrocytes of the glial lamina engage in pAKT/AKT signaling

Since staining pattern for pAKT in ON cross sections indicated that astrocytes are a source of pAKT in this region, we carried out double staining against pAKT and GFAP in tangential sections of the glial lamina of 12 week old animals to check for co-localization of the two proteins.

We found a co-localization of pAKT and GFAP in glial lamina (Figure 42), meaning that pAKT/AKT signaling is active in astrocytes of this region.

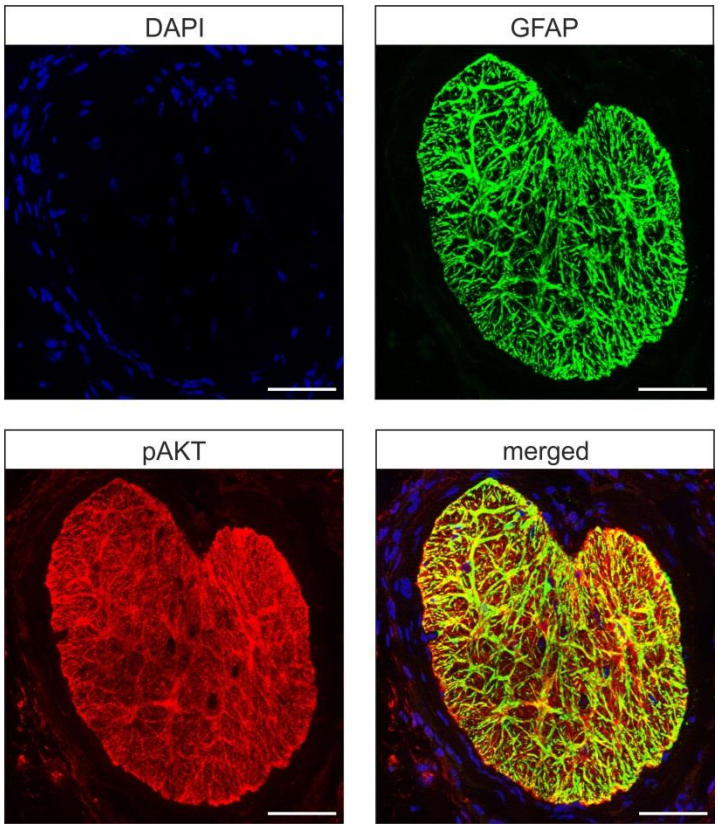

Figure 42: Co-localization of pAKT and GFAP in the glial lamina. Staining against GFAP (green) and pAKT (red) revealed co-localization of both proteins, meaning that pAKT/AKT signaling is active in the glial lamina. Blue: DAPI, scale bars: 50 µm.

4.7.8 pAKT is reduced in the eye of DCN$^{-/-}$ 129SV/BL Swiss/CD1 mice

Since DCN can bind to IGF-IR and thereby activate the pAKT/AKT signaling pathway (Schonherr et al., 2005), the absence of DCN in the eye should lead to a decreased phosphorylation level of AKT. To check if activation of the pAKT/AKT signaling pathway is reduced in the eye of DCN deficient mice we carried out pAKT staining in sagittal and tangential sections of 12 week old WT and DCN$^{-/-}$ mice.

We found that signal for pAKT is reduced in the chamber angle and the TM (Figure 43), the retina (Figure 44) and in the ON (Figure 45) of DCN$^{-/-}$ mice compared to pAKT signal in these regions in WT mice.

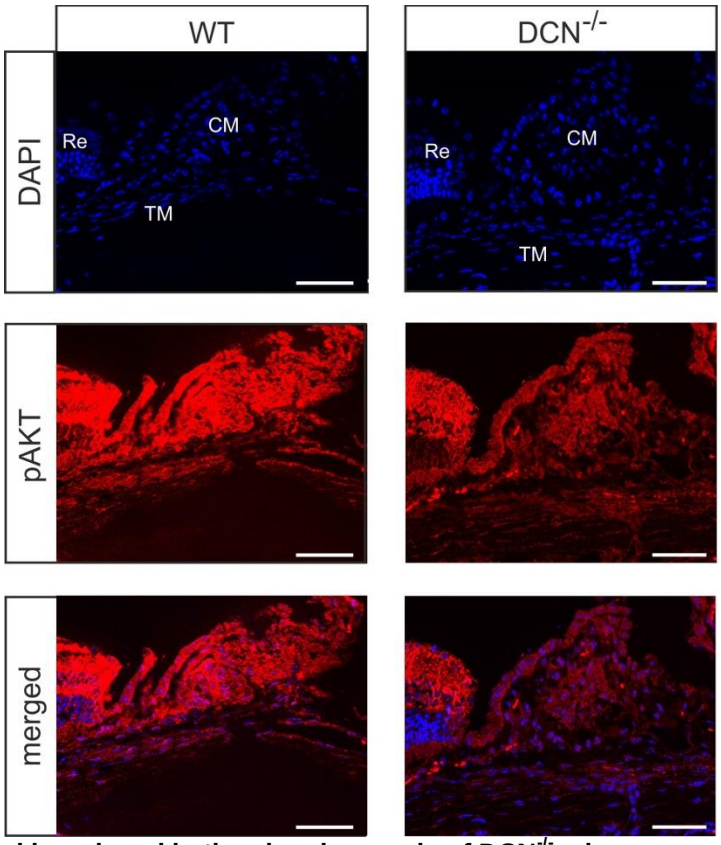

Figure 43: pAKT signal is reduced in the chamber angle of DCN$^{-/-}$ mice compared to WT littermates. Staining intensity in the chamber angle and in the region of the TM was reduced in 12 week old DCN$^{-/-}$ mice. Blue: DAPI, red: pAKT, Re: Retina, TM: Trabecular meshwork, CM: Ciliary muscle, scale bars: 50 µm.

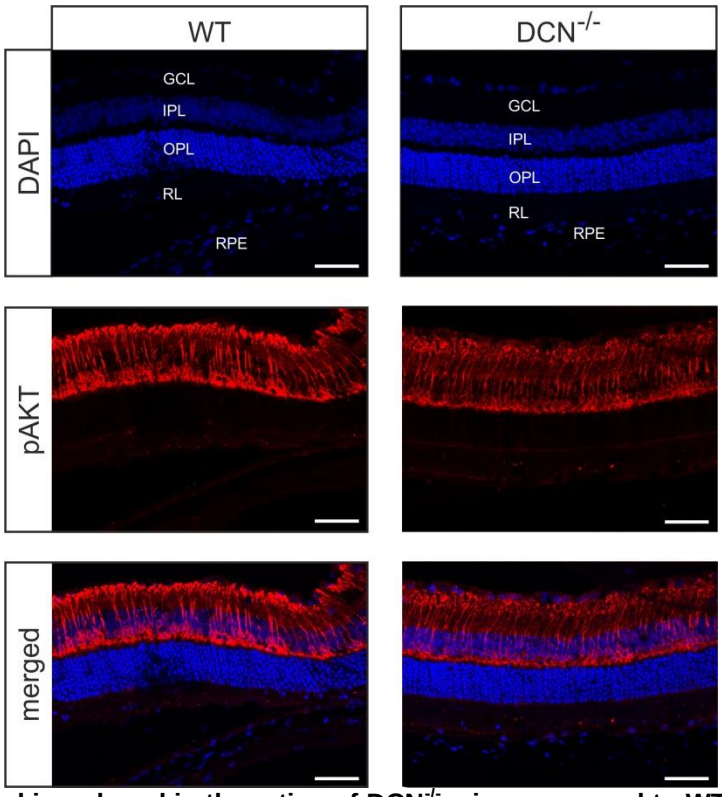

Figure 44: pAKT signal is reduced in the retina of DCN$^{-/-}$ mice compared to WT littermates. Staining intensity in the retina was reduced in 12 week old DCN$^{-/-}$ mice. Distribution of pAKT staining indicates that Mueller cells are the main source of pAKT synthesis. Blue: DAPI, red: pAKT, GCL: Ganglion cell layer, IPL: Inner plexiform layer, OPL: Outer plexiform layer, RL: Receptor layer, RPE: Retinal pigment epithelium, scale bars: 50 µm.

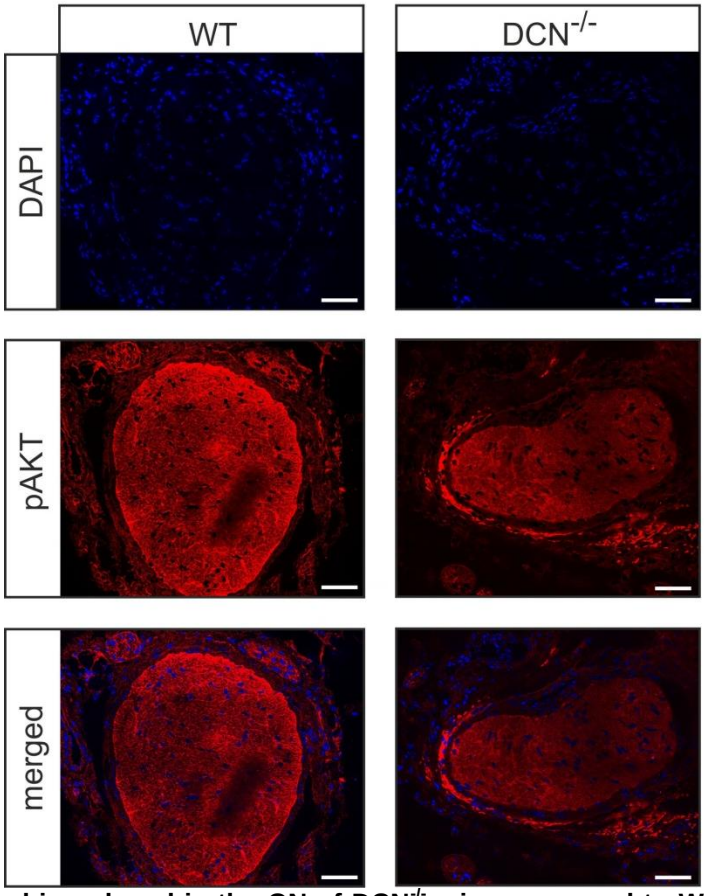

Figure 45: pAKT signal is reduced in the ON of DCN$^{-/-}$ mice compared to WT littermates. Staining intensity in the ON was reduced in 12 week old DCN$^{-/-}$ mice. Distribution of pAKT staining indicates that astrocytes are the main source of pAKT synthesis. Blue: DAPI, red: pAKT, scale bars: 50 µm.

4.7.9 Gene expression in the outflow tissues of DCN deficient 129SV/BL Swiss/CD1 mice

Overall, our *in vitro* data clearly indicate that lack of DCN in TM and ON is associated with an increased activity of TGF-β/CTGF signaling. To obtain more detailed information on the molecular mechanisms that are behind the interactions of DCN with TGF-β/CTGF signaling and might cause high IOP and POAG, we applied deep sequencing technique. RNA was isolated from corneo-scleral rings, including the TM outflow pathways, of DCN$^{-/-}$ mice and their WT littermates at the age of three months. 258 genes were identified that differed in their expression pattern between DCN$^{-/-}$ mice and WT littermates with an expression ratio difference of either greater than 0.5 $\log_2$-fold or less than -1.0 $\log_2$-fold and a p-value of ≤ 0.05. Quite intriguingly, our first screening of the data showed distinct changes in genes and pathways that are known to be involved in

the pathogenesis of POAG. Accordingly, we detected a significant upregulation in the expression of ECM molecules such as collagen type I and IV, alterations in the expression of cytoskeletal genes like tropomyosin, and changes in the expression of members of the Rho, WNT and TGF-β signaling pathways (Table 26). Furthermore multiple genes that have previously been associated with glaucoma were either up- or down regulated in the corneo-scleral ring of $DCN^{-/-}$ mice (Table 27).

GO Term	counts	p-value
cell adhesion	111	7.30E-10
regulation of small GTPase mediated signal transduction	48	1.50E-05
intracellular transport	76	3.60E-05
transmembrane receptor protein tyrosine kinase signaling pathway	41	5.00E-05
cell-cell signaling	54	1.40E-04
extracellular matrix organization	32	3.40E-04
cell-cell adhesion	44	6.10E-04
regulation of Ras protein signal transduction	36	6.30E-04
TGF beta receptor pathway	24	1.80E-03
eye development	31	1.80E-03
protein kinase cascade	42	2.10E-03
camera-type eye development	26	3.80E-03
actin filament-based process	32	5.50E-03
endocytosis	33	8.20E-03
calcium ion transport	23	1.20E-02
negative regulation of apoptosis	39	1.30E-02
monosaccharide metabolic process	32	1.80E-02
regulation of transferase activity	33	1.80E-02
regulation of cell proliferation	76	1.80E-02
negative regulation of cell death	39	1.90E-02
lipid biosynthetic process	44	2.00E-02
regulation of protein kinase activity	31	2.10E-02
cell migration	38	2.20E-02
regulation of apoptosis	77	2.40E-02
MAPKKK cascade	21	2.40E-02
protein complex assembly	36	2.50E-02
Wnt receptor signaling pathway	23	2.70E-02
positive regulation of catalytic activity	40	3.00E-02
regulation of kinase activity	31	3.10E-02
actin cytoskeleton organization	27	3.80E-02
positive regulation of transferase activity	23	3.90E-02
positive regulation of cell communication	30	4.10E-02

Table 26: Significantly enriched gene ontology (GO) terms detected in differentially expressed RNA pattern between 3 month old DCN$^{-/-}$ mice and their wild-type littermates. Only those terms which reported a p-value of ≤ 0.05 and count number ≥ 19 genes were selected for the analysis.

Genes	log2 (fold change)	p- value
branched chain amino acid transaminase 1	-1.92	0.0393
leucine rich repeat and immunoglobin-like domain-containing protein 1	-1,72	0.0175
versican	-1.35	0.0174
fibromodulin	-1.20	0.0122
BCL2 associated X protein	-1.06	0.0246
ras homolog gene family member A	0.55	0.0146
transporter associated with antigen 1	0.61	0.0115
uncoupling protein 2	0.61	0.0156
transporter associated with antigen 2	0.70	0.0423
collagen type IV	0.70	0.0043
EGF receptor	0.71	0.0196
transglutaminase 2	0.78	0.0122
exportin for tRNA	0.86	0.0205
small mother agains decapentaplegic 7	0.95	0.0412
signal transducer and activator of transcription 6	0.95	0.0031
wnt4	1.04	0.0313
C-X-C motif chemokine 10	1.27	0.0370
signal transducer and activator of transcription 1	1.33	0.0010
matrix metalloproteinase-2	1.77	0.0453
tafazzin	1.80	0.0104
tropomyosin 3	1.80	0.0155

Table 27: Alteration of genes associated with glaucoma in the corneo-scleral ring of DCN$^{-/-}$ mice. Various genes that have previously been described in the context of glaucoma are up or down regulated in the corneo-scleral ring of DCN$^{-/-}$ mice. Only genes with a p-value ≤ 0.05 were selected.

4.8 DCN deficient mice in a pure CD1 background show elevated IOP and loss of optic nerve axons

The genetic background of mice strongly influences IOP. Average IOP ranges from 10 to 20 mm/Hg in different mouse strains (Savinova et al., 2001). Moreover CD1 mice are more susceptible to glaucomatous damage than other mice strains (Cone et al., 2010; Cone et al., 2012). Due to that we back-crossed $DCN^{+/-}$ mice of a mixed 129SV/BL Swiss/CD1 background into a pure CD1 background over 8 generations. $DCN^{+/-}$ of the 8^{th} generation were cross-bred to get $DCN^{-/-}$ and WT littermates for experiments. IOP was measured at 12 weeks. Afterwards animals were sacrificed and eyes were used for immunohistochemistry and light microscopy. Total number of ON axons was quantified.

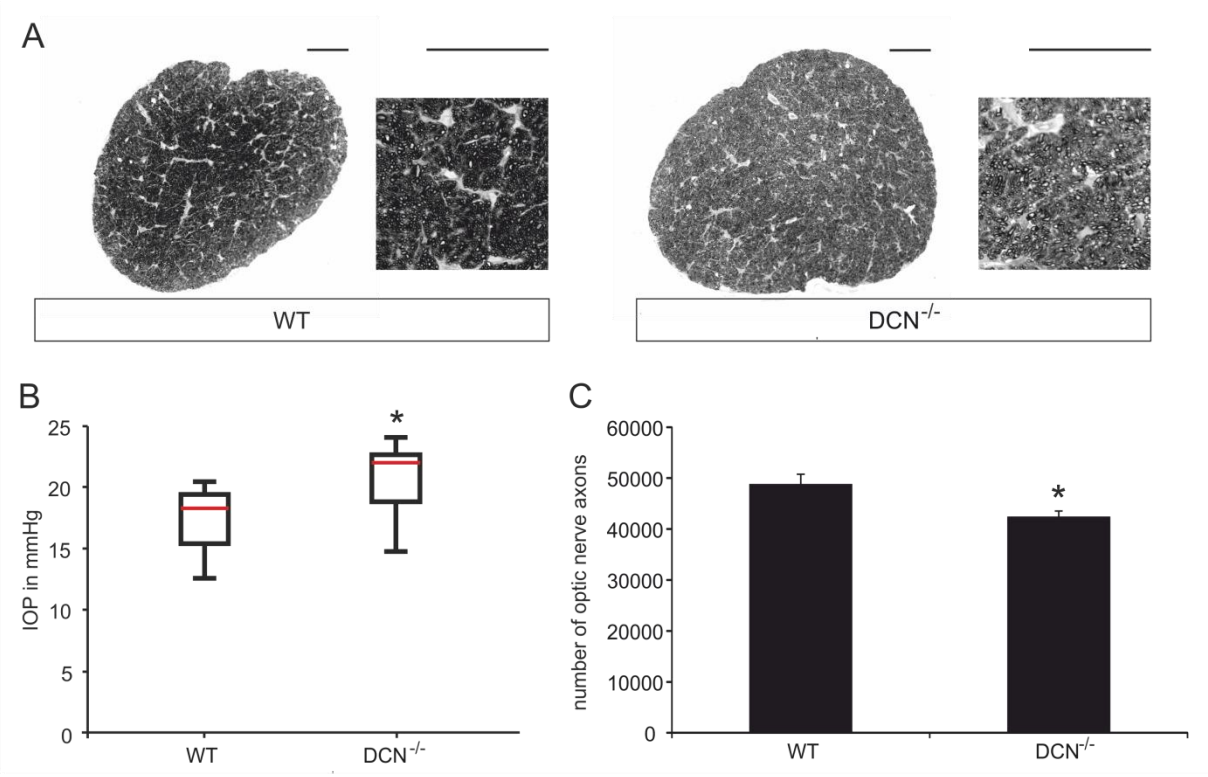

Figure 46: 12 week old $DCN^{-/-}$ mice in a pure CD1 background have a higher IOP and less optic nerve axons than their WT littermates. A shows an exemplary ON cross section of a 12 week old DCN WT and a 12 week old $DCN^{-/-}$ mouse. There are no obvious structural changes in the ON of the DCN deficient animal. IOP values of $DCN^{-/-}$ animals are significantly higher than IOP values of WT mice of the same age (B). Furthermore numbers of ON axons are significantly lower in $DCN^{-/-}$ mice compared to WT littermates (C). Exact numbers are listed in Table 4.5. All values are means ± STD. Scale bars: 50 µm.

	axon numbers	IOP values [mm/Hg]
DCN$^{-/-}$ 12 weeks	42457 ± 1047	20.70 ± 3.33
WT 12 weeks	48852 ± 1907	17.32 ± 2.73
p-Value	0.046	0.031
n DCN$^{-/-}$	3	8
n WT	4	10

Table 28: Axon numbers and IOP of DCN$^{-/-}$ and WT mice in a pure CD1 background. All values are mean ± STD.

IOP was significantly elevated in DCN$^{-/-}$ CD1 mice when collated with IOP in WTlittermates (Figure 46). Optic nerve cross sections of WT CD1 and DCN$^{-/-}$ CD1 mice showed no apparent differences regarding areas devoid of axons (Figure 46 A). Quantification of ON axons showed that with the elevated IOP comes a loss of axons in the ON of DCN$^{-/-}$ mice (Figure 46 C). Exact IOP values and numbers of ON axons are listed in Table 28.

4.9 Comparison of IOP and axons numbers in DCN$^{-/-}$ mice in different backgrounds

We could show that 12 week old CD1 WT mice have a significantly higher IOP than 12 week old SV129/BL Swiss/CD1 mice. IOP of CD1 WT mice was 17.40 ± 2.73 (n = 10) and 14.75 ± 3.42 in 129SV/BL Swiss/CD1 mice (n = 20, p = 0.042). DCN$^{-/-}$ CD1 mice also had a significantly higher IOP than DCN$^{-/-}$ 129SV/BL Swiss/CD1 animals (DCN$^{-/-}$ CD1: 20.07 ± 3.33, n = 8, DCN$^{-/-}$ 129SV/BL Swiss/CD1: 15.91 ± 4.10, n = 34, p = 0.004). While there was no difference in IOP between WT 129SV/BL Swiss/CD1 and DCN$^{-/-}$ 129SV/BL Swiss/CD1 at an age of 12 weeks, DCN$^{-/-}$ CD1 mice had an significantly higher IOP than WT CD1 mice at the same age (p = 0.031, Figure 47).

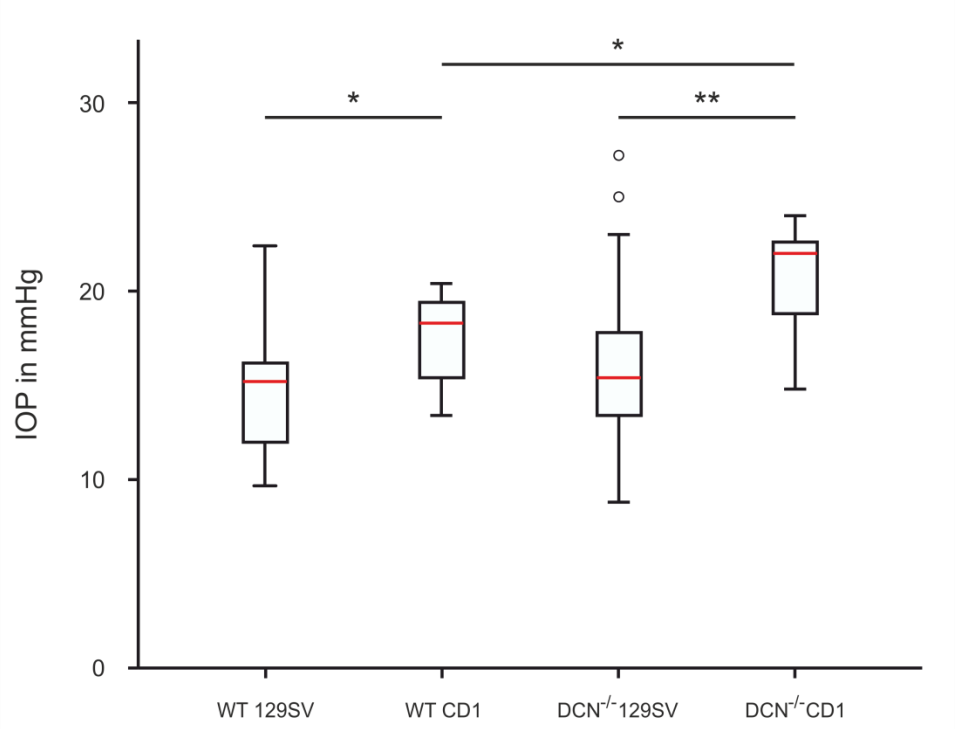

Figure 47: IOP is higher in 12 week old DCN CD1 mice as in 12 week old DCN SV129/BL Swiss/CD1 mice. IOP is significantly higher in 12 week old CD1 mice (17.40 ± 2.73, n = 10) than in 12 week old 129SV/BL Swiss/CD1 (14.75 ± 3.42, n = 20, p ≤ 0.05) mice without genetic modification. Also in $DCN^{-/-}$ CD1 (20.07 ± 3.33, n = 8) animals IOP was significantly higher at an age of 12 weeks than in $DCN^{-/-}$ 129SV/BL Swiss/CD1 mice (15.91 ± 4.10, n = 34, p ≤ 0.05) of the same age. $DCN^{-/-}$ CD1 mice had a significantly higher IOP than WT CD1 mice. 129SV is used as abbreviation for 129SV/BL Swiss/CD1, circles represent max. outliers. All values are mean ± STD.

Axon numbers were not different between CD1 and 129SV/BL Swiss/CD1 mice with or without a knockout of DCN (for exact numbers and p-values see table 29).

	WT CD1	**$DCN^{-/-}$ CD1**	**WT 129SV/BL Swiss/CD1**	**$DCN^{-/-}$ 129SV/BL Swiss/CD1**
Axon numbers	48852 ± 1907	42457 ± 1047	47080 ± 5312	37156 ± 5183
n	4	3	5	5
p-Value			0.602	0.185

Table 29: Axon numbers of 12 week old CD1 and 129SV/BL Swiss/CD1 mice with our without knockout of DCN are not different. All values are mean ± STD.

5. Discussion

5.1 Summary

It was the aim of this study to investigate reciprocal effects of TGF-β2, CTGF and DCN in cell types involved in the pathogenesis of POAG and to analyze the influence of DCN on expression and synthesis of ECM components in these cell types. *In vivo* βB1-CTGF mice with a lens specific overexpression of CTGF were analyzed regarding DCN levels in the region of the TM and the ON. Further this study aims to elucidate the effects of DCN deficiency in mice on morphological structures and molecular factors that are involved in the pathology of POAG.

Treatments with TGF-β2 or CTGF significantly reduced DCN expression and synthesis in all cell types, vice versa DCN treatment reduced expression of TGF-β1, 2 and CTGF in all cell types as well as CTGF synthesis in human TM cells. Besides, DCN treatment reduced expression and synthesis of ECM components and led to an activation of the pAKT/AKT signaling pathway. Inhibition of the pAKT/AKT signaling pathway inhibited the negative regulatory effect of DCN on TGF-β1, 2 and CTGF.

In vivo lens specific overexpression of CTGF results in a downregulation of DCN expression and synthesis in the region of the TM, but does not influence DCN levels in the ON.

DCN deficiency leads to glaucomatous changes in mice. The DCN knockout does not result in developmental changes of chamber angle morphology, but leads to a significantly elevated IOP in DCN deficient animals older than 8 weeks and induces the loss of ON axons in mice older than 12 weeks. RNA sequencing revealed that multiple pathways and genes known to be related to glaucoma are significantly altered in the corneo-scleral ring of 12 week old knockout animals. Furthermore expression and synthesis of growth factors and ECM components are significantly increased in the corneo-scleral ring and in the ON of 8 week old $DCN^{-/-}$ mice compared to WT littermates. Tangential sections of the glial lamina of 12 week old DCN deficient mice showed increased staining intensity for GFAP and changes in astrocyte morphology, indicating that astrocytes of this region undergo reactivation. Activation of the pAKT/AKT pathway was reduced in the TM, the retina and the ON of 12 week old $DCN^{-/-}$ mice.

IOP measurements and quantification of ON axons showed that $DCN^{-/-}$ mice in a pure CD1 background also have elevated IOP and less ON axons than WT littermates.

5.2 Negative reciprocal effects of TGF-β2, CTGF and DCN in cell types involved in the pathogenesis of POAG

TGF-β2 and CTGF have been found in elevated levels in the AH of POAG patients (Inatani et al., 2001; Ochiai and Ochiai, 2002; Picht et al., 2001; Tripathi et al., 1994b; Yamamoto et al., 2005). Moreover, a lens specific overexpression of CTGF leads to glaucomatous changes in mice (Junglas et al., 2012). TGF-β and CTGF can contribute to an accumulation of ECM components in the TM by increasing their expression and by inhibiting proteins that degrade ECM components (Fuchshofer and Tamm, 2009) and thereby cause an elevation of IOP. ONH astrocytes react to treatments with TGF-β2 with an increased expression of ECM components (Fuchshofer et al., 2005; Neumann et al., 2008; Zode et al., 2011) and this upregulation is mediated via CTGF (Fuchshofer et al., 2005). This leads to the assumption that both molecules play an essential part in the pathogenesis of POAG when present in pathological amounts. Since TGF-β2 and CTGF are present in the healthy eye (Tomarev et al., 2003) and TGF-β is essential for the immune privilege of the eye (Streilein, 1999a), there have to be regulators of TGF-β2 and CTGF that are able to create a balance of physiological growth factor levels in the eye. One possible antagonist of TGF-β2 and CTGF could be DCN that is expressed in ocular tissue. DCN is able to bind TGF-β (Yamaguchi et al., 1990) and CTGF (Vial et al., 2011) and can thereby inhibit their biological activity. In 2014 our group could show, in cooperation with D. Overby (Imperial College, London, UK), that SC cells of glaucomatous donors express significantly less DCN than SC cells of healthy donors (Overby et al., 2014b). In this study we could show proof that in POAG patients might be an imbalance between TGF-β2, CTGF and DCN. We could show that the DCN is dramatically reduced in the whole chamber angle, especially in the TM and in the endothelium of SC, in POAG eyes compared to healthy donors.

In vitro reciprocal effects of TGF-β2, CTGF and DCN have not been studied up till now in human TM cells, human ONH astrocytes or murine ON astrocytes. In other cell types the influence of TGF-β on DCN levels was investigated and results indicate that it is cell

type dependent. TGF-β treatment leads to a decreased DCN expression in human skin fibroblasts and human chondrocytes (Kahari et al., 1991; Roughley et al., 1994) while DCN expression is upregulated after TGF-β treatment in murine osteoblasts and rat mesangial cells (Takeuchi et al., 1993). Effects of CTGF on DCN levels have not been studied yet.

In this study we could demonstrate that treatment with TGF-β2 and CTGF leads to a downregulation of DCN expression and synthesis in all investigated cell types. These results led to the assumption that the reduced DCN levels observed in TM and SC endothelium are a result of an increased occurrence of TGF-β2 and CTGF. Decreased expression and synthesis of DCN in the TM could lead to an enhanced activity of TGF-β and CTGF which would result in an increased deposition of ECM material. Lack of DCN could also cause a disorganization of ECM proteins in the TM and in the ONH, since DCN is essential for binding and arranging collagen fibers (Scott, 1996; Weber et al., 1996).

On the other hand TGF-β can be negatively regulated by DCN via direct binding in Chinese hamster ovary cells or via upregulation of FBN1 synthesis in endothelial cells (Schonherr et al., 2005; Yamaguchi et al., 1990). In this study DCN treatment led to a significant downregulation of expression of TGF-β1, 2 and CTGF in all investigated cell types. Negative influence of DCN on the biological activity of CTGF via direct binding has been reported (Vial et al., 2011), but there is no data on the influence of DCN on the expression of CTGF yet.

By reducing the expression and synthesis of TGF-β and CTGF, DCN should be able to lower their profibrotic effects. We could give first proof of this statement by showing reduced deposition of FN and Col IV after DCN treatment. For further proof the effects of DCN on stress fiber formation and the actin cytoskeleton of TM cells should be observed. The fast effect of DCN on the expression of TGF-β and CTGF prompts that DCN binds both growth factors directly in TM cells and ON astrocytes.

Treatment of murine ON astrocytes with DCN led to a significant increase of the pAKT/AKT ratio 6 h after treatment, meaning that the pAKT/AKT signaling pathway is activated by DCN in these cells. Activity of this pathway has previously been reported for human brain derived astrocytes (Garwood et al., 2015), but not in astrocytes of the ON and there is no data of the effect of DCN on pAKT/AKT signaling in astrocytes.

Activation of the pAKT/AKT pathway by DCN leads to an increased synthesis of FBN1 in in rat kidney fibroblasts (Schaefer et al., 2007). FBN1 can actively interfere with TGF-β by preventing the release of active TGF-β from the latent TGF-β complex (Annes et al., 2003; Schonherr et al., 2005). Mutations of FBN1 cause Marfan syndrome (Dietz et al., 1991) and about 2% of Marfan patients are affected by a not categorized type of glaucoma (Faivre et al., 2007). This leads to the assumption that the mutation of FBN1 leads to hyperactivity of TGF-β and could thereby favor the onset of glaucoma. By inhibiting the pAKT/AKT pathway we demonstrated that DCN regulates TGF-β1, 2 and CTGF expression via this pathway in murine ON astrocytes. The study does not completely answer the question whether the effect on CTGF is a direct one or mediated by the down regulation of TGF-β or an altered activity of TGF-β due to changes in synthesis of FBN1. Since we could observe an inhibitory effect on DCNs regulation of TGF-β and CTGF by triciribine after 24 h, it is very likely that DCN directly regulates TGF-β and CTGF via AKT signaling. There is evidence that phosphorylated AKT can bind to Smad3 and inhibit its phosphorylation, resulting in an inhibition of TGF-β signaling (Conery et al., 2004).

All results clearly indicate that TGF-β, CTGF and DCN negatively regulate each other, in cell types involved in POAG. The results harden our hypothesis that a balance between TGF-β, CTGF and DCN is essential to prevent the onset and progression of POAG.

5.3 DCN regulates ECM expression and synthesis in human TM cells and astrocytes

Increased expression and synthesis of ECM components in the TM play an essential part in POAG and can contribute to an increase of IOP (Gottanka et al., 1997; Lutjen-Drecoll et al., 1981; Tamm and Fuchshofer, 2007). Multiple studies demonstrated that TGF-β and CTGF induce expression and synthesis of ECM components in various cell types including human TM cells (Ignotz and Massague, 1986; Junglas et al., 2009; Varga et al., 1987). In human corneal fibroblasts transfection with DCN inhibited the profibrotic effect of TGF-β1 (Mohan et al., 2010). Due to that we hypothesized that DCN acts as an antagonist of the profibrotic effect mediated by TGF-β and CTGF in cell types involved in the pathogenesis of POAG. Treatment of human TM cells, human ONH

astrocytes and murine ON astrocytes with DCN resulted in a decreased expression and synthesis of FN and Col IV. In accordance to our results Hill et al. published that DCN can reduce TGF-β2 induced IOP elevation through fibrolysis in the TM via upregulation of MMP2 and MMP9 and downregulation of TIMP2, indicating that DCN is able to reverse established fibrosis in the TM (Hill et al., 2015). Due to its ability to regulate MMP-2, -9 and TIMP2 the absence of DCN should result in an imbalance of ECM production and degradation. DCN deficiency leads to an upregulation of TIMP2 in fetal membranes (Wu et al., 2014), but there is no data on MMP regulation in $DCN^{-/-}$ mice yet. Upregulation of TIMP2 induces accumulation of ECM material and a negative effect of DCN deficiency on the expression of MMPs would cause reduced outflow facility in the TM. Due to that expression and synthesis of MMPs and TIMP2 should be analyzed in the TM of $DCN^{-/-}$ mice. Our RNA sequencing data already gave a first lead that MMP2 expression is affected by the absence of DCN in the TM, but intriguingly MMP2 expression was increased in $DCN^{-/-}$ mice. In addition it would be of interest to analyze the effects of DCN treatment on SMA expression in human TM cells, since SMA is induced in the TM by CTGF and can contribute to an elevation of IOP by increasing TM cell actomyosin contractility (Junglas et al., 2012; Junglas et al., 2009).

The results of this thesis strongly indicate that DCN could contribute to a reduction of ECM material in the TM and to a lowering of IOP. Thereby it could prevent the onset or the progression of POAG. It could also reduce fibrosis of the ONH by decreasing deposition of ECM material by astrocytes and so reduce RGC death. The effect of DCN on LC cells has not been studied up till now.

5.4 An imbalance between CTGF and DCN favors the onset of POAG

In this study we demonstrated that in the chamber angle of donors affected by POAG DCN protein was dramatically reduced in all regions of the TM and in the endothelium of SC, but we did not investigate whether this reduction of DCN is due to elevated levels of CTGF or TGF-β. Further proof of an imbalance between TGF-β2, CTGF and DCN was published recently. It was shown that SC cells of glaucomatous donors express significantly more TGF-β and CTGF while they express significantly less DCN than SC cells of healthy donors (Overby et al., 2014). This hints that a sensitive balance between

DCN, TGF-β2 and CTGF is essential to prevent the onset of POAG. Disturbance of this balance in favor of TGF-β2 and CTGF could strongly promote the onset and pathogenesis of POAG. For that reason it would be of great interest to analyze models and experimental setups that combine, for example, an overexpression of CTGF and a lack of DCN or to check if the profibrotic effects of CTGF and TGF-β can be reversed by adding DCN to the system.

In mice a lens-specific overexpression of CTGF causes increased IOP and RGC death by elevating ECM synthesis in the TM and altering the actin cytoskeleton of TM cells. This makes βB1-CTGF mice an acknowledged model for POAG (Junglas et al., 2012). Since we could demonstrate a negative regulatory effect of CTGF on expression and synthesis in TM cells and astrocytes we concluded that an overexpression of CTGF *in vivo* should alter expression and synthesis of DCN.

This is the first study to elucidate the influence of CTGF on DCN expression and synthesis in different tissues of the eye *in vivo*. DCN expression and synthesis was significantly reduced in the corneo-scleral ring of βB1-CTGF mice compared to WT littermates. This shows that CTGF has a negative effect on the expression and synthesis of its antagonist DCN which could lead to a potentiation of CTGF expression and synthesis. That CTGF is capable of auto induction has been reported in human TM cells before (Junglas et al., 2009).

Regarding the ON we could not detect DCN mRNA or protein in ONH samples but in samples containing the whole ON. DCN mRNA and protein were not altered in the ON of βB1-CTGF mice compared to WT littermates. Most likely the endogenous CTGF secreted by the lens does not reach the ON and therefore does not influence expression or synthesis of DCN.

Since we observed reduced amounts of DCN protein in the chamber angle of donors affected by POAG we posed ourselves the question whether a knockout of DCN in vivo will lead to glaucomatous changes in the TM and in the ONH and if these would induce an elevation of IOP and a loss ON axons. To answer these questions we analyzed DCN deficient mice and their wildtype littermates of different ages with focus on IOP, axon numbers, gene expression and protein synthesis in the relevant tissues.

An increased IOP is the major risk factor to develop POAG (Collaborative-Normal-Tension-Glaucoma-Study-Group, 1998; Gordon et al., 2002; Johnson et al., 2002; Leske et al., 2003) and the loss of axons in the optic nerve is the main characteristic of this optic neuropathy. So it was one main goal of this study to analyze the IOP of $DCN^{-/-}$ mice and WT mice of different ages and to quantify optic nerve axons. Thus we wanted to ascertain if $DCN^{-/-}$ mice might be a new and useful animal model for POAG. To exclude that structural changes in the chamber angle and the TM, that do not take place in POAG patients, lead to blocking of AH outflow and thereby increase IOP, we examined sagital sections of eyes of $DCN^{-/-}$ and WT mice of different ages. No structural changes were observable by light microscopy. Chamber angles of all animals were open and no synechia or pigment dispersion were obeserved that could block AH outflow and thereby increase IOP. SC was developed normally in $DCN^{-/-}$ mice so that AH is able to drain via the conventional outflow pathway.There were no noticable changes in cornea, retina, lens, papilla or optic nerve, leading to the conclusion that a knockout of DCN does not negatively affect eye development.

In other glaucoma models, elevation of IOP is often caused by structural changes that block AH outflow. In DBA2J mice AH outflow is reduced due to iris atrophy and the associated formation of synechias, making these mice a good model for secondary angle-closure glaucoma (John et al., 1998). Mice with an embryonal conditional knockout of angiopoetin (ANGPT) 1 and 2 do not develop a SC, leading to an early and extreme increase of IOP. These mice show a protruding bulbus at 21 days and IOP is increased up to 4 fold at an age of 10 weeks (Thomson et al., 2014) making these mice a usable model for lowering IOP but not for POAG, since POAG is age associated and is characterized by a more slowely increase of IOP.

Beside genetic based glaucoma models, an increased IOP can be induced by mechanically blocking the AH outflow, e.g. via injection of latex microspheres or polysteren beads (Sappington et al., 2010; Weber and Zelenak, 2001) and ON crush to induce RGC death, are commonly used models for glaucoma. In contrast to POAG both those models induce spontaneus damage at the TM or at the ONH and do not allow to observe the time course of IOP elevation or RGC death, which can be observed in a genetical glaucoma model with a slow onset of glaucoma.

In this study we measured IOP changes in $DCN^{-/-}$ and WT mice over one year. IOP was not changed in 4 week old $DCN^{-/-}$ animals compared to WT mice of the same age, but was significantly higher in all $DCN^{-/-}$ mice of older age groups. An increase of IOP with age was observed in WT and $DCN^{-/-}$ mice but the increase was 1.6 times higher over 12 month in $DCN^{-/-}$ mice than in WT mice. An increase of IOP with age has been reported previously in humans (Qureshi, 1995; Wong et al., 2009) and in mice (Cone et al., 2012).

The knockout of DCN lead to a significant loss of ON axons in mice older than 8 weeks. Intriguingly the increase of IOP over time did not, as expected, result in a decreasing number of optic nerve axons. 8 week old $DCN^{-/-}$ mice had the same number of ON nerve axons than WT littermates, but allready at an age of 12 weeks axon number was significantly reduced in $DCN^{-/-}$ mice. We could observe a difference of 21% between 12 week old WT and $DCN^{-/-}$ mice, a difference of 16.5% between 6 month old WT and $DCN^{-/-}$ mice and a difference of 14.5 % between 12 month old WT and $DCN^{-/-}$ mice. Axon numbers decreased slightly over time in WT mice but were almost stable in $DCN^{-/-}$ mice. These results might probably be due to small sample sizes and should be verified further in future experiments since loss of optic nerve axons with age has been reported multiple times in different species (Cepurna et al., 2005; Fortune et al., 2014; Jonas et al., 1992; Mikelberg et al., 1989). Stable axon numbers over age could also be due to the mixed background of $DCN^{-/-}$ and WT animals. CD1 mice, for example, have more optic nerve axons than C57/BL6 mice (Cone et al., 2010), so one can conclude that genetic background strongly influences axon numbers.

Analysis of CTGF levels in the corneo-scleral ring of $DCN^{-/-}$ again hardened the hypothesis that an imbalance of DCN and CTGF favors the onset of POAG. Expression and synthesis of CTGF and TGF-β were significantly higher in the corneo-scleral rings of 8 week old $DCN^{-/-}$ mice compared to WT mice. It was shown before that DCN can bind CTGF and is so able to inhibit its profibrotic effects and that DCN null myoblasts are more sensitive to CTGF, showing in an increased accumulation of FN (Vial et al., 2011), but there is no data on how DCN influences the expression of CTGF and vice versa.

Seeing that *in vitro* murine ON astrocytes showed negative reciprocal effects of TGF-β2, CTGF and DCN we investigated if the knockout of DCN leads to expression changes in the ON. Expression of TGF-β1, TGF-β2 and CTGF was significantly higher in the ON of

$DCN^{-/-}$ compared to WT mice, indicating that cell types in this tissue react to DCN deficiency with an upregulation of growth factor expression.

5.5 ONH astrocytes of $DCN^{-/-}$ mice show signs of reactivation

Reactivation of astrocytes in the ONH is a typical observation in POAG. In human ONH with chronically elevated IOP and moderate or advanced glaucomatous axonal damage astrocytes show thickening of processes, hypertrophy of the cell body and an increased immunoreactivity for GFAP (Hernandez and Pena, 1997; Varela and Hernandez, 1997; Wang et al., 2002).

In tangential sections of the region of the glial lamina of 12 week old $DCN^{-/-}$ mice we observed similar changes, indicating astrocyte reactivation. The same observation has already been made in other murine glaucoma models (Lye-Barthel et al., 2013; Son et al., 2010), leading to the conclusion that reactivation of astrocytes in the region of the glial lamina is a typical phenomenon in mice, too. Moreover it again shows the usability of $DCN^{-/-}$ mice as a model for POAG.

Long-term studies with a genetic model, like the DBA/2J mice, show a constantly significant increased GFAP expression in the ONH, hinting at an association of the reactive phenotype with severe axon loss. This suggestion is supported by findings that the recovery of the astrocytic organization is dependent on the grade of axon loss. Astrocytes, after a moderate axon loss, have the capability to re-establish the honeycomb arrangement in the glial lamina (Sun et al., 2013). After an optic nerve crush, astrocytes do not regain the structure of a glial lamina and lead to the formation of a glial scar (Sun et al., 2010). In this study we could not observe further axon loss over time after 12 weeks, so possibly the reactivation of astrocytes at that time point has a beneficial effect on axon survival. To prove this hypothesis, further experiments have to be carried out in which the reactivation status of astrocytes and the structure of the glial lamina have to be analyzed at older ages.

5.6 DCN deficiency reduces pAKT/AKT signaling

DCN is able to influence the activity and thereby also the expression of TGF-β and CTGF via the pAKT/AKT signaling pathway (Schonherr et al., 2005). Our *in vitro* experiments showed that DCN activates pAKT/AKT signaling in murine ON astrocytes. Vice versa the absence of DCN should lead to a decreased activity of this pathway. Activation of the named signaling pathway results in upregulation of FBN1 synthesis. FBN1 controls TGF-β activation, as it controls the assembly and stability of the latent TGF-β complex (Annes et al., 2003). Hence reduced activity of the pAKT/AKT pathway should lead to elevated activity of TGF-β.

Immunohistochemical staining against pAKT showed a lower signal in the retina and in the chamber angle of $DCN^{-/-}$ mice than in WT littermates. pAKT signal in the retina spanned from the nuclear layer to the outer plexiform layer, so probably Mueller cells are the main source of pAKT in the retina. Double staining against pAKT and GFAP or pAKT and glutamine synthetase should be carried out to clarify this.

Signal for pAKT was lower in ON cross sections of $DCN^{-/-}$ animals, too. Double staining against GFAP and pAKT in tangential sections of the glial lamina showed co-localization of both proteins, proofing that astrocytes of that region engage in pAKT/AKT signaling. It would be of great interest to investigate if a decreased pAKT/AKT signaling in astrocytes of the glial lamina leads to an increase of TGF-β and CTGF expression and synthesis. First attempts to isolate RNA and protein of mouse ONHs were successful, so these analyses will be carried out in the future.

In vitro blocking of the pAKT/AKT signaling pathway in human brain derived astrocytes does not lead to changes in viability or cell number, but leads to significant increase in GFAP synthesis (Garwood et al., 2015). Therefore the increased signal for GFAP in the glial lamina of $DCN^{-/-}$ mice might be a result of the lowered activity of the pAKT/AKT pathway. *In vivo* an adeno-associated virus transduction with a gene encoding a constitutively active form of Akt/PKB reduced apoptotic cell death in a highly destructive neurotoxin model by activating intracellular neurotrophic signaling pathways (Ries et al., 2006). This hints that a decreased activity of pAKT/AKT signaling might have negative effects on the expression and synthesis of neurotrophic factors and could thereby contribute to RGC death.

Analysis of the pAKT/AKT ratio in the anterior eye segment, the retina and the ONH has to be carried out to ensure changes in the activity of this pathway in $DCN^{-/-}$ mice. Additionally it is of interest to investigate if these changes have influence on expression and synthesis of neurotrophic factors *in vivo* and *in vitro*.

5.7 DCN deficiency leads to expression changes of pathways and genes associated with glaucoma in the corneo-scleral ring

In addition to the expression and synthesis changes in TGF-β2 and CTGF in the corneo-scleral ring we further proved an elevated expression and synthesis of FN and Col IV in the corneo-scleral rings of $DCN^{-/-}$ animals. Both ECM molecules are structural components of the healthy TM (Tamm, 2009; Tawara et al., 1989; Ueda et al., 2002), but are known to be elevated in the TM during POAG (Lutjen-Drecoll et al., 1981) and most likely contribute to an elevation of IOP by increasing outflow resistance to AH (Tamm and Fuchshofer, 2007). The increase of FN and Col IV in the corneo-scleral ring of $DCN^{-/-}$ mice is most likely due to the elevated levels of TGF-β2 and CTGF in that region since both growth factors are known to upregulate ECM expression and synthesis in human TM cells and also decrease the expression and synthesis of ECM degradation proteins (Fuchshofer and Tamm, 2009; Junglas et al., 2009).

RNA-sequencing was performed to create an overview over genes and pathways that are differentially expresses in $DCN^{-/-}$ and WT mice's corneo-scleral rings. Due to the fact that a first elevation of IOP was observed in 12 week old $DCN^{-/-}$ mice, mice of that age were used for analysis.

Results were analyzed using the DAVID software to check for significantly enriched gene ontology terms (GO terms). Among the significantly enriched GO terms were for example extracellular matrix organization and actin cytoskeleton organization. Reorganization of the ECM is a critical feature of POAG. In the TM deposition of ECM is increased and fibrous plates are formed which contribute to an increased outflow resistance (Lutjen-Drecoll et al., 1981; Tamm and Fuchshofer, 2007). In the ONH remodeling of the ECM leads to stiffening of the peripapillary sclera (Coudrillier et al., 2012), thickening of the connective tissue sheaths around the capillaries (Tektas et al., 2010) and a restructuring of the LC (Pena et al., 1998; Quigley et al., 1991b; Quigley et

al., 1983). Changes in the actin cytoskeleton in POAG show manly in stiffening of the TM (Last et al., 2011) and can contribute to reducing AH outflow by an increased contractility of TM cells induced by CTGF (Junglas et al., 2012). The Wnt receptor signaling pathway seems also to be altered in the corneo-scleral ring of DCN deficient mice. Wnt signaling is associated with glaucoma via myocillin (Myoc), which is an important modulator of this pathway (Kwon et al., 2009a). It is documented that dominant mutations in the MYOC gene may lead to juvenile- or adult onset POAG and are found in 3 to 4% of POAG patients (Fingert et al., 1999; Fingert et al., 2002). Additionally it could be shown that inhibition of Wnt signaling by secreted frizzled-related protein-1 (sFRP-1) increases IOP in *ex vivo* perfusion-cultured human eyes and that sFRP-1 is overexpressed in glaucomatous TM cells (Wang et al., 2008). TGF-β2 is also able to inhibit the Wnt pathway (Webber et al., 2016). So the crosstalk between Wnt- and TGF-β signaling very likely could contribute to an elevation of IOP in POAG.

After narrowing all genes down to genes with an expression ratio differences of either greater than 0.5 $\log_2$-fold or less than -1.0 $\log_2$-fold and a p-value of ≤ 0.05, the resulting 258 genes we carried out literature screening to identify genes that had been reported in the context of glaucoma previously. We found literature references for 21 genes related to glaucoma. This hints that the absence of DCN not only affects TGF-β and CTGF, but also other genes that could play a role in the pathogenesis of POAG, like wnt4 (Yuan et al., 2013) or tgm2 (Tovar-Vidales et al., 2008). Interactions of DCN and the other genes related to glaucoma were not investigated in this study.

Gene	Reference
branched chain amino acid transaminase 1	(Yasuda et al., 2014)
leucine rich repeat and immunoglobin-like domain-containing protein 1	(Fu et al., 2009)
versican	(Lukas et al., 2008)
fibromodulin	(Steinhart et al., 2014)
BCL2 associated X protein	(Levkovitch-Verbin et al., 2013)
ras homolog gene family member A	(Saracaloglu et al., 2016)
transporter associated with antigen 1	(Hysi et al., 2014)
uncoupling protein 2	(Yang et al., 2015)
transporter associated with antigen 2	(Hysi et al., 2014)
collagen type IV	(Tektas and Lutjen-Drecoll, 2009)
EGF receptor	(Liu et al., 2006)
transglutaminase 2	(Tovar-Vidales et al., 2008)
exportin for tRNA	(Fingert et al., 2011)
signal transducer and activator of transcription 6	(Thanos and Naskar, 2004)
small mother against decapentaplegic 7	(Fuchshofer et al., 2009)
wnt4	(Yuan et al., 2013)
C-X-C motif chemokine 10	(Freedman and Iserovich, 2013)
signal transducer and activator of transcription 1	(Yang et al., 2007)
matrix metalloproteinase-2	(Ashworth Briggs et al., 2015)
tafazzin	(Raghunathan et al., 2013)
tropomyosin	(Zhao et al., 2004)

Table 30: Genes associated with glaucoma altered in the corneo-scleral ring of DCN$^{-/-}$ mice and sources.

5. 8 Outlook

In vitro the effects of DCN on the synthesis of TGF-β2 in human TM cells, human ONH astrocytes and murine ON astrocytes should be investigated. By silencing of TGF-β2 the question if the effect of DCN on CTGF expression and synthesis is direct one could be answered. This setup was already used in our group to show that CTGF alone is able to induce ECM production in human TM cells (Junglas et al., 2009). Via silencing of TGF-β and CTGF possible direct effects of DCN on ECM production could be analyzed. Since we saw signs of reactivation of ONH astrocytes in $DCN^{-/-}$ mice it would be interesting to find out if DCN affects GFAP expression and synthesis of GFAP, morphology and migration in murine ON astrocytes, because those are signs of astrogliosis (Hernandez and Pena, 1997; Varela and Hernandez, 1997; Wang et al., 2002).

We demonstrated first proof that DCN synthesis is reduced in the outflow tissue of POAG patients. Analyzing expression and synthesis of DCN, TGF-β2 and CTGF in human TM cells of healthy and glaucomatous donors could give deeper insight in the reciprocal effects of these proteins in health and POAG. In this study an imbalance between CTGF, TGF-β2 and DCN in the region of the TM could be shown in two different mouse models that show an elevated IOP and loss of optic nerve axons. Hence we state that a shift of the balance between those factors in favor of CTGF and TGF-β2 promotes the onset and progression of POAG.

Mice with a lens-specific overexpression of CTGF are an acknowledged model for POAG. They show increased ECM production in the TM, elevated IOP and loss of ON axons (Junglas et al., 2012). This study shows that *in vitro* DCN is able to reduce expression and synthesis of CTGF and that it can contribute to reduction of ECM expression and deposition. In addition to our work it has been reported that intracameral injection of DCN reduces TGF-β2 induced IOP and RGC loss by reducing fibrotic components in the TM (Hill et al., 2015). In this study high amounts of DCN (3 x 17.5 µg) were necessary to lower IOP, so administration of DCN via a different way might be desirable. AAV-5 DCN gene therapy significantly inhibits corneal scarring (Mohan et al., 2011) due to an inhibitory effect of DCN on TGF-β in corneal fibroblasts (Mohan et al., 2010). This indicates that viral gene transfer of DCN in the eye is a usable way to reduce the profibrotic effects of TGF- β. Delivering DCN via an adeno virus to the

eyes of βB1-CTGF mice would be a good model to assess the possible use of DCN as a therapeutic against POAG. IOP, axon numbers in the ON and expression and synthesis of ECM components in the TM should be analyzed in untreated and DCN adeno virus treated eyes.

Regarding $DCN^{-/-}$ mice future studies should investigate possible structural changes in the TM on electron microscopy level that could contribute to the observed increase in IOP. Increasing n numbers of Axon number quantification would probably elucidate if axon number really do not decrease with age in WT and $DCN^{-/-}$ mice. Observing RGC death using e.g. TUNEL assay and analyzing functionality of the retina via electroretinography could help answering the question whether $DCN^{-/-}$ mice are a usable model of POAG.

This study gave first evidence that pAKT/AKT signaling is reduced in the eyes of DCN deficient mice, but it did not yet investigate changes in pAKT/AKT ratio or possible effects of decreased signaling on expression and synthesis of neurotrophic factors. Since deprivation of neurotrophic factors is a major cause of RGC death (Pease et al., 2000; Quigley et al., 2000), and AKT signaling seems to involved in regulation of neurotrophic factors (Ries et al., 2006) a reduced activity could contribute to increased RGC death.

In addition all experiments carried out in this study could be repeated in CD1 WT and CD1 $DCN^{-/-}$ animals to find out if the effects of DCN deficiency are enhanced in mice in a pure CD1 background, since it has been shown before that CD1 mice are more susceptible to glaucomatous damage than other mice strains (Cone et al., 2010; Cone et al., 2012).

6. Conclusion

Overall this is the first study to report negative reciprocal effects of DCN, TGF-β and CTGF in cell types involved in the pathogenesis of POAG. The ability of DCN to reduce TGF-β, CTGF and ECM components in TM cells and astrocytes of the ON makes it a highly interesting protein for glaucoma research. DCN could contribute to fybrolisis in the TM and in the ONH and thereby be able to slow down the progression or even prevent the onset of POAG.

In vivo we found evidence that a disturbance of the balance between DCN and CTGF favors the onset and progression of POAG. While DCN synthesis is reduced in the human glaucomatous chamber angle, DCN deficiency leads to glaucomatous changes in mice. $DCN^{-/-}$ mice have an elevated IOP and show loss of optic nerve axons while having no obvious morphological changes in the chamber angle, meaning that they fulfill the main criteria of POAG. Hence we postulate that $DCN^{-/-}$ mice are a new model for POAG.

All results of this study strongly hint that DCN is a good candidate for a new therapeutic approach to treat or prevent POAG.

7. Sources

Abbott, N.J., Ronnback, L., Hansson, E., 2006. Astrocyte-endothelial interactions at the blood-brain barrier. Nat Rev Neurosci 7, 41-53.

Acott, T.S., Kelley, M.J., 2008. Extracellular matrix in the trabecular meshwork. Exp Eye Res 86, 543-561.

Albon, J., Purslow, P.P., Karwatowski, W.S., Easty, D.L., 2000. Age related compliance of the lamina cribrosa in human eyes. Br J Ophthalmol 84, 318-323.

Allen, J.B., Davidson, M.G., Nasisse, M.P., Fleisher, L.N., McGahan, M.C., 1998. The lens influences aqueous humor levels of transforming growth factor-beta 2. Graefes Arch Clin Exp Ophthalmol 236, 305-311.

Allingham, R.R., de Kater, A.W., Ethier, C.R., 1996. Schlemm's canal and primary open angle glaucoma: correlation between Schlemm's canal dimensions and outflow facility. Exp Eye Res 62, 101-109.

Anderson, D.R., 1969. Ultrastructure of human and monkey lamina cribrosa and optic nerve head. Arch Ophthalmol 82, 800-814.

Annes, J.P., Munger, J.S., Rifkin, D.B., 2003. Making sense of latent TGFbeta activation. J Cell Sci 116, 217-224.

Ashworth Briggs, E.L., Toh, T., Eri, R., Hewitt, A.W., Cook, A.L., 2015. TIMP1, TIMP2, and TIMP4 are increased in aqueous humor from primary open angle glaucoma patients. Mol Vis 21, 1162-1172.

Baghy, K., Dezso, K., Laszlo, V., Fullar, A., Peterfia, B., Paku, S., Nagy, P., Schaff, Z., Iozzo, R.V., Kovalszky, I., 2011. Ablation of the decorin gene enhances experimental hepatic fibrosis and impairs hepatic healing in mice. Lab Invest 91, 439-451.

Baghy, K., Iozzo, R.V., Kovalszky, I., 2012. Decorin-TGFbeta axis in hepatic fibrosis and cirrhosis. J Histochem Cytochem 60, 262-268.

Bi, X., Tong, C., Dockendorff, A., Bancroft, L., Gallagher, L., Guzman, G., Iozzo, R.V., Augenlicht, L.H., Yang, W., 2008. Genetic deficiency of decorin causes intestinal tumor formation through disruption of intestinal cell maturation. Carcinogenesis 29, 1435-1440.

Bill, A., Phillips, C.I., 1971. Uveoscleral drainage of aqueous humour in human eyes. Exp Eye Res 12, 275-281.

Bollinger, K.E., Crabb, J.S., Yuan, X., Putliwala, T., Clark, A.F., Crabb, J.W., 2012. Proteomic similarities in steroid responsiveness in normal and glaucomatous trabecular meshwork cells. Mol Vis 18, 2001-2011.

Border, W.A., Noble, N.A., Yamamoto, T., Harper, J.R., Yamaguchi, Y., Pierschbacher, M.D., Ruoslahti, E., 1992. Natural inhibitor of transforming growth factor-beta protects against scarring in experimental kidney disease. Nature 360, 361-364.

Border, W.A., Okuda, S., Languino, L.R., Ruoslahti, E., 1990. Transforming growth factor-beta regulates production of proteoglycans by mesangial cells. Kidney Int 37, 689-695.

Bouzier-Sore, A.K., Pellerin, L., 2013. Unraveling the complex metabolic nature of astrocytes. Front Cell Neurosci 7, 179.

Bozoky, B., Savchenko, A., Guven, H., Ponten, F., Klein, G., Szekely, L., 2014. Decreased decorin expression in the tumor microenvironment. Cancer Med 3, 485-491.

Braakman, S.T., Read, A.T., Chan, D.W., Ethier, C.R., Overby, D.R., 2015. Colocalization of outflow segmentation and pores along the inner wall of Schlemm's canal. Exp Eye Res 130, 87-96.

Bradley, J.M., Kelley, M.J., Zhu, X., Anderssohn, A.M., Alexander, J.P., Acott, T.S., 2001. Effects of mechanical stretching on trabecular matrix metalloproteinases. Invest Ophthalmol Vis Sci 42, 1505-1513.

Bradley, J.M., Vranka, J., Colvis, C.M., Conger, D.M., Alexander, J.P., Fisk, A.S., Samples, J.R., Acott, T.S., 1998. Effect of matrix metalloproteinases activity on outflow in perfused human organ culture. Invest Ophthalmol Vis Sci 39, 2649-2658.

Brigstock, D.R., 2003. The CCN family: a new stimulus package. J Endocrinol 178, 169-175.

Browne, J.G., Ho, S.L., Kane, R., Oliver, N., Clark, A.F., O'Brien, C.J., Crean, J.K., 2011. Connective tissue growth factor is increased in pseudoexfoliation glaucoma. Invest Ophthalmol Vis Sci 52, 3660-3666.

Buller, C., Johnson, D.H., Tschumper, R.C., 1990. Human trabecular meshwork phagocytosis. Observations in an organ culture system. Invest Ophthalmol Vis Sci 31, 2156-2163.

Cepurna, W.O., Kayton, R.J., Johnson, E.C., Morrison, J.C., 2005. Age related optic nerve axonal loss in adult Brown Norway rats. Exp Eye Res 80, 877-884.

Chen, C.C., Yeh, L.K., Liu, C.Y., Kao, W.W., Samples, J.R., Lin, S.J., Hu, F.R., Wang, I.J., 2008. Morphological differences between the trabecular meshworks of zebrafish and mammals. Curr Eye Res 33, 59-72.

Chomczynski, P., Sacchi, N., 1987. Single-step method of RNA isolation by acid guanidinium thiocyanate-phenol-chloroform extraction. Anal Biochem 162, 156-159.

Chudgar, S.M., Deng, P., Maddala, R., Epstein, D.L., Rao, P.V., 2006. Regulation of connective tissue growth factor expression in the aqueous humor outflow pathway. Mol Vis 12, 1117-1126.

Collaborative-Normal-Tension-Glaucoma-Study-Group, 1998. The effectiveness of intraocular pressure reduction in the treatment of normal-tension glaucoma. Collaborative Normal-Tension Glaucoma Study Group. Am J Ophthalmol 126, 498-505.

Cone, F.E., Gelman, S.E., Son, J.L., Pease, M.E., Quigley, H.A., 2010. Differential susceptibility to experimental glaucoma among 3 mouse strains using bead and viscoelastic injection. Exp Eye Res 91, 415-424.

Cone, F.E., Steinhart, M.R., Oglesby, E.N., Kalesnykas, G., Pease, M.E., Quigley, H.A., 2012. The effects of anesthesia, mouse strain and age on intraocular pressure and an improved murine model of experimental glaucoma. Exp Eye Res 99, 27-35.

Conery, A.R., Cao, Y., Thompson, E.A., Townsend, C.M., Jr., Ko, T.C., Luo, K., 2004. Akt interacts directly with Smad3 to regulate the sensitivity to TGF-beta induced apoptosis. Nat Cell Biol 6, 366-372.

Coudrillier, B., Tian, J., Alexander, S., Myers, K.M., Quigley, H.A., Nguyen, T.D., 2012. Biomechanics of the Human Posterior Sclera: Age- and Glaucoma-Related Changes Measured Using Inflation Testing. Investigative Ophthalmology & Visual Science 53, 1714-1728.

Cousins, S.W., Trattler, W.B., Streilein, J.W., 1991. Immune privilege and suppression of immunogenic inflammation in the anterior chamber of the eye. Curr Eye Res 10, 287-297.

Danielson, K.G., Baribault, H., Holmes, D.F., Graham, H., Kadler, K.E., Iozzo, R.V., 1997. Targeted disruption of decorin leads to abnormal collagen fibril morphology and skin fragility. J Cell Biol 136, 729-743.

Derynck, R., Zhang, Y.E., 2003. Smad-dependent and Smad-independent pathways in TGF-beta family signalling. Nature 425, 577-584.

Dietz, H.C., Cutting, G.R., Pyeritz, R.E., Maslen, C.L., Sakai, L.Y., Corson, G.M., Puffenberger, E.G., Hamosh, A., Nanthakumar, E.J., Curristin, S.M., et al., 1991. Marfan syndrome caused by a recurrent de novo missense mutation in the fibrillin gene. Nature 352, 337-339.

Downs, J.C., Suh, J.K., Thomas, K.A., Bellezza, A.J., Burgoyne, C.F., Hart, R.T., 2003. Viscoelastic characterization of peripapillary sclera: material properties by quadrant in rabbit and monkey eyes. J Biomech Eng 125, 124-131.

Ethier, C.R., Kamm, R.D., Palaszewski, B.A., Johnson, M.C., Richardson, T.M., 1986. Calculations of flow resistance in the juxtacanalicular meshwork. Invest Ophthalmol Vis Sci 27, 1741-1750.

Fahmy, 2008. Role of Aqueous Humor Matrix Metalloproteinase-2 and Its Inhibitor and Connective Tissue Growth Factor in the Pathogenesis of Primary Open

Angle Glaucoma and pseudoexfoliative glaucoma. Rawal Medical Journal 2008; 33(2), 179-182.

Faivre, L., Collod-Beroud, G., Loeys, B.L., Child, A., Binquet, C., Gautier, E., Callewaert, B., Arbustini, E., Mayer, K., Arslan-Kirchner, M., Kiotsekoglou, A., Comeglio, P., Marziliano, N., Dietz, H.C., Halliday, D., Beroud, C., Bonithon-Kopp, C., Claustres, M., Muti, C., Plauchu, H., Robinson, P.N., Ades, L.C., Biggin, A., Benetts, B., Brett, M., Holman, K.J., De Backer, J., Coucke, P., Francke, U., De Paepe, A., Jondeau, G., Boileau, C., 2007. Effect of mutation type and location on clinical outcome in 1,013 probands with Marfan syndrome or related phenotypes and FBN1 mutations: an international study. Am J Hum Genet 81, 454-466.

Fingert, J.H., Heon, E., Liebmann, J.M., Yamamoto, T., Craig, J.E., Rait, J., Kawase, K., Hoh, S.T., Buys, Y.M., Dickinson, J., Hockey, R.R., Williams-Lyn, D., Trope, G., Kitazawa, Y., Ritch, R., Mackey, D.A., Alward, W.L., Sheffield, V.C., Stone, E.M., 1999. Analysis of myocilin mutations in 1703 glaucoma patients from five different populations. Hum Mol Genet 8, 899-905.

Fingert, J.H., Robin, A.L., Stone, J.L., Roos, B.R., Davis, L.K., Scheetz, T.E., Bennett, S.R., Wassink, T.H., Kwon, Y.H., Alward, W.L., Mullins, R.F., Sheffield, V.C., Stone, E.M., 2011. Copy number variations on chromosome 12q14 in patients with normal tension glaucoma. Hum Mol Genet 20, 2482-2494.

Fingert, J.H., Stone, E.M., Sheffield, V.C., Alward, W.L., 2002. Myocilin glaucoma. Surv Ophthalmol 47, 547-561.

Fleenor, D.L., Shepard, A.R., Hellberg, P.E., Jacobson, N., Pang, I.H., Clark, A.F., 2006. TGFbeta2-induced changes in human trabecular meshwork: implications for intraocular pressure. Invest Ophthalmol Vis Sci 47, 226-234.

Fortune, B., Reynaud, J., Cull, G., Burgoyne, C.F., Wang, L., 2014. The Effect of Age on Optic Nerve Axon Counts, SDOCT Scan Quality, and Peripapillary Retinal Nerve Fiber Layer Thickness Measurements in Rhesus Monkeys. Transl Vis Sci Technol 3, 2.

Freedman, J., Iserovich, P., 2013. Pro-inflammatory cytokines in glaucomatous aqueous and encysted Molteno implant blebs and their relationship to pressure. Invest Ophthalmol Vis Sci 54, 4851-4855.

Fu, Q.L., Li, X., Yip, H.K., Shao, Z., Wu, W., Mi, S., So, K.F., 2009. Combined effect of brain-derived neurotrophic factor and LINGO-1 fusion protein on long-term survival of retinal ganglion cells in chronic glaucoma. Neuroscience 162, 375-382.

Fuchshofer, R., Birke, M., Welge-Lussen, U., Kook, D., Lutjen-Drecoll, E., 2005. Transforming growth factor-beta 2 modulated extracellular matrix component expression in cultured human optic nerve head astrocytes. Invest Ophthalmol Vis Sci 46, 568-578.

Fuchshofer, R., Stephan, D.A., Russell, P., Tamm, E.R., 2009. Gene expression profiling of TGFbeta2- and/or BMP7-treated trabecular meshwork cells: Identification of Smad7 as a critical inhibitor of TGF-beta2 signaling. Exp Eye Res 88, 1020-1032.

Fuchshofer, R., Tamm, E.R., 2009. Modulation of extracellular matrix turnover in the trabecular meshwork. Exp Eye Res 88, 683-688.

Fuchshofer, R., Welge-Lussen, U., Lutjen-Drecoll, E., 2003. The effect of TGF-beta2 on human trabecular meshwork extracellular proteolytic system. Exp Eye Res 77, 757-765.

Fuchshofer, R., Welge-Lussen, U., Lutjen-Drecoll, E., Birke, M., 2006. Biochemical and morphological analysis of basement membrane component expression in corneoscleral and cribriform human trabecular meshwork cells. Invest Ophthalmol Vis Sci 47, 794-801.

Fuchshofer, R., Yu, A.H., Welge-Lussen, U., Tamm, E.R., 2007. Bone morphogenetic protein-7 is an antagonist of transforming growth factor-beta2 in human trabecular meshwork cells. Invest Ophthalmol Vis Sci 48, 715-726.

Funderburgh, J.L., Hevelone, N.D., Roth, M.R., Funderburgh, M.L., Rodrigues, M.R., Nirankari, V.S., Conrad, G.W., 1998. Decorin and biglycan of normal and pathologic human corneas. Invest Ophthalmol Vis Sci 39, 1957-1964.

Garwood, C.J., Ratcliffe, L.E., Morgan, S.V., Simpson, J.E., Owens, H., Vazquez-Villasenor, I., Heath, P.R., Romero, I.A., Ince, P.G., Wharton, S.B., 2015. Insulin and IGF1 signalling pathways in human astrocytes in vitro and in vivo; characterisation, subcellular localisation and modulation of the receptors. Mol Brain 8, 51.

Goldbaum, M.H., Jeng, S.Y., Logemann, R., Weinreb, R.N., 1989. The extracellular matrix of the human optic nerve. Arch Ophthalmol 107, 1225-1231.

Gordon, M.O., Beiser, J.A., Brandt, J.D., Heuer, D.K., Higginbotham, E.J., Johnson, C.A., Keltner, J.L., Miller, J.P., Parrish, R.K., 2nd, Wilson, M.R., Kass, M.A., 2002. The Ocular Hypertension Treatment Study: baseline factors that predict the onset of primary open-angle glaucoma. Arch Ophthalmol 120, 714-720; discussion 829-730.

Gottanka, J., Chan, D., Eichhorn, M., Lutjen-Drecoll, E., Ethier, C.R., 2004. Effects of TGF-beta2 in perfused human eyes. Invest Ophthalmol Vis Sci 45, 153-158.

Gottanka, J., Johnson, D.H., Martus, P., Lutjen-Drecoll, E., 1997. Severity of optic nerve damage in eyes with POAG is correlated with changes in the trabecular meshwork. J Glaucoma 6, 123-132.

Guo, L., Moss, S.E., Alexander, R.A., Ali, R.R., Fitzke, F.W., Cordeiro, M.F., 2005. Retinal ganglion cell apoptosis in glaucoma is related to intraocular pressure and IOP-induced effects on extracellular matrix. Invest Ophthalmol Vis Sci 46, 175-182.

Hakkinen, L., Strassburger, S., Kahari, V.M., Scott, P.G., Eichstetter, I., Lozzo, R.V., Larjava, H., 2000. A role for decorin in the structural organization of periodontal ligament. Lab Invest 80, 1869-1880.

Hann, C.R., Fautsch, M.P., 2011. The elastin fiber system between and adjacent to collector channels in the human juxtacanalicular tissue. Invest Ophthalmol Vis Sci 52, 45-50.

Helbig, H., Kittredge, K.L., Coca-Prados, M., Davis, J., Palestine, A.G., Nussenblatt, R.B., 1991. Mammalian ciliary-body epithelial cells in culture produce transforming growth factor-beta. Graefes Arch Clin Exp Ophthalmol 229, 84-87.

Hellerbrand, C., Stefanovic, B., Giordano, F., Burchardt, E.R., Brenner, D.A., 1999. The role of TGFbeta1 in initiating hepatic stellate cell activation in vivo. J Hepatol 30, 77-87.

Hernandez, M.R., 1992. Ultrastructural immunocytochemical analysis of elastin in the human lamina cribrosa. Changes in elastic fibers in primary open-angle glaucoma. Invest Ophthalmol Vis Sci 33, 2891-2903.

Hernandez, M.R., 2000. The optic nerve head in glaucoma: role of astrocytes in tissue remodeling. Prog Retin Eye Res 19, 297-321.

Hernandez, M.R., Agapova, O.A., Yang, P., Salvador-Silva, M., Ricard, C.S., Aoi, S., 2002. Differential gene expression in astrocytes from human normal and glaucomatous optic nerve head analyzed by cDNA microarray. Glia 38, 45-64.

Hernandez, M.R., Igoe, F., Neufeld, A.H., 1988. Cell culture of the human lamina cribrosa. Invest Ophthalmol Vis Sci 29, 78-89.

Hernandez, M.R., Pena, J.D., 1997. The optic nerve head in glaucomatous optic neuropathy. Arch Ophthalmol 115, 389-395.

Hernandez, M.R., Wang, N., Hanley, N.M., Neufeld, A.H., 1991. Localization of collagen types I and IV mRNAs in human optic nerve head by in situ hybridization. Invest Ophthalmol Vis Sci 32, 2169-2177.

Hernandez, M.R., Ye, H., Roy, S., 1994. Collagen type IV gene expression in human optic nerve heads with primary open angle glaucoma. Exp Eye Res 59, 41-51.

Hill, L.J., Mead, B., Blanch, R.J., Ahmed, Z., De Cogan, F., Morgan-Warren, P.J., Mohamed, S., Leadbeater, W., Scott, R.A., Berry, M., Logan, A., 2015. Decorin Reduces Intraocular Pressure and Retinal Ganglion Cell Loss in Rodents Through Fibrolysis of the Scarred Trabecular Meshwork. Invest Ophthalmol Vis Sci 56, 3743-3757.

Hocking, A.M., Shinomura, T., McQuillan, D.J., 1998. Leucine-rich repeat glycoproteins of the extracellular matrix. Matrix Biol 17, 1-19.

Hysi, P.G., Cheng, C.Y., Springelkamp, H., Macgregor, S., Bailey, J.N., Wojciechowski, R., Vitart, V., Nag, A., Hewitt, A.W., Hohn, R., Venturini, C., Mirshahi, A., Ramdas, W.D., Thorleifsson, G., Vithana, E., Khor, C.C., Stefansson, A.B., Liao, J., Haines, J.L., Amin, N., Wang, Y.X., Wild, P.S., Ozel, A.B., Li, J.Z., Fleck, B.W., Zeller, T., Staffieri, S.E., Teo, Y.Y., Cuellar-Partida, G., Luo, X., Allingham, R.R., Richards, J.E., Senft, A., Karssen, L.C., Zheng, Y., Bellenguez, C., Xu, L., Iglesias, A.I., Wilson, J.F., Kang, J.H., van Leeuwen, E.M., Jonsson, V., Thorsteinsdottir, U., Despriet, D.D., Ennis, S., Moroi, S.E., Martin, N.G., Jansonius, N.M., Yazar, S., Tai, E.S., Amouyel, P., Kirwan, J., van Koolwijk, L.M., Hauser, M.A., Jonasson, F., Leo, P., Loomis, S.J., Fogarty, R., Rivadeneira, F., Kearns, L., Lackner, K.J., de Jong, P.T., Simpson, C.L., Pennell, C.E., Oostra, B.A., Uitterlinden, A.G., Saw, S.M., Lotery, A.J., Bailey-Wilson, J.E., Hofman, A., Vingerling, J.R., Maubaret, C., Pfeiffer, N., Wolfs, R.C., Lemij, H.G., Young, T.L., Pasquale, L.R., Delcourt, C., Spector, T.D., Klaver, C.C., Small, K.S., Burdon, K.P., Stefansson, K., Wong, T.Y., Viswanathan, A., Mackey, D.A., Craig, J.E., Wiggs, J.L., van Duijn, C.M., Hammond, C.J., Aung, T., 2014. Genome-wide analysis of multi-ancestry cohorts identifies new loci influencing intraocular pressure and susceptibility to glaucoma. Nat Genet 46, 1126-1130.

Ignotz, R.A., Massague, J., 1986. Transforming growth factor-beta stimulates the expression of fibronectin and collagen and their incorporation into the extracellular matrix. J Biol Chem 261, 4337-4345.

Inatani, M., Tanihara, H., Honjo, M., Hangai, M., Kresse, H., Honda, Y., 1999. Expression of proteoglycan decorin in neural retina. Invest Ophthalmol Vis Sci 40, 1783-1791.

Inatani, M., Tanihara, H., Katsuta, H., Honjo, M., Kido, N., Honda, Y., 2001. Transforming growth factor-beta 2 levels in aqueous humor of glaucomatous eyes. Graefes Arch Clin Exp Ophthalmol 239, 109-113.

Iozzo, R.V., 1998. Matrix proteoglycans: from molecular design to cellular function. Annu Rev Biochem 67, 609-652.

Jampel, H.D., Roche, N., Stark, W.J., Roberts, A.B., 1990. Transforming growth factor-beta in human aqueous humor. Curr Eye Res 9, 963-969.

Jester, J.V., Barry-Lane, P.A., Petroll, W.M., Olsen, D.R., Cavanagh, H.D., 1997. Inhibition of corneal fibrosis by topical application of blocking antibodies to TGF beta in the rabbit. Cornea 16, 177-187.

John, S.W., Smith, R.S., Savinova, O.V., Hawes, N.L., Chang, B., Turnbull, D., Davisson, M., Roderick, T.H., Heckenlively, J.R., 1998. Essential iris atrophy, pigment dispersion, and glaucoma in DBA/2J mice. Invest Ophthalmol Vis Sci 39, 951-962.

Johnson, C.A., Keltner, J.L., Cello, K.E., Edwards, M., Kass, M.A., Gordon, M.O., Budenz, D.L., Gaasterland, D.E., Werner, E., 2002. Baseline visual field characteristics in the ocular hypertension treatment study. Ophthalmology 109, 432-437.

Johnson, M., 2006. 'What controls aqueous humour outflow resistance?'. Exp Eye Res 82, 545-557.

Johnson, M., Shapiro, A., Ethier, C.R., Kamm, R.D., 1992. Modulation of outflow resistance by the pores of the inner wall endothelium. Invest Ophthalmol Vis Sci 33, 1670-1675.

Jonas, J.B., Schmidt, A.M., Muller-Bergh, J.A., Schlotzer-Schrehardt, U.M., Naumann, G.O., 1992. Human optic nerve fiber count and optic disc size. Invest Ophthalmol Vis Sci 33, 2012-2018.

Junglas, B., Kuespert, S., Seleem, A.A., Struller, T., Ullmann, S., Bosl, M., Bosserhoff, A., Kostler, J., Wagner, R., Tamm, E.R., Fuchshofer, R., 2012. Connective tissue growth factor causes glaucoma by modifying the actin cytoskeleton of the trabecular meshwork. Am J Pathol 180, 2386-2403.

Junglas, B., Yu, A.H., Welge-Lussen, U., Tamm, E.R., Fuchshofer, R., 2009. Connective tissue growth factor induces extracellular matrix deposition in human trabecular meshwork cells. Exp Eye Res 88, 1065-1075.

Kaartinen, V., Warburton, D., 2003. Fibrillin controls TGF-beta activation. Nat Genet 33, 331-332.

Kahari, V.M., Larjava, H., Uitto, J., 1991. Differential regulation of extracellular matrix proteoglycan (PG) gene expression. Transforming growth factor-beta 1 up-regulates biglycan (PGI), and versican (large fibroblast PG) but down-regulates decorin (PGII) mRNA levels in human fibroblasts in culture. J Biol Chem 266, 10608-10615.

Kanzler, S., Lohse, A.W., Keil, A., Henninger, J., Dienes, H.P., Schirmacher, P., Rose-John, S., zum Buschenfelde, K.H., Blessing, M., 1999. TGF-beta1 in liver fibrosis: an inducible transgenic mouse model to study liver fibrogenesis. Am J Physiol 276, G1059-1068.

Karamichos, D., Guo, X.Q., Hutcheon, A.E., Zieske, J.D., 2010. Human corneal fibrosis: an in vitro model. Invest Ophthalmol Vis Sci 51, 1382-1388.

Keller, K.E., Aga, M., Bradley, J.M., Kelley, M.J., Acott, T.S., 2009. Extracellular matrix turnover and outflow resistance. Exp Eye Res 88, 676-682.

Kirwan, R.P., Leonard, M.O., Murphy, M., Clark, A.F., O'Brien, C.J., 2005. Transforming growth factor-beta-regulated gene transcription and protein expression in human GFAP-negative lamina cribrosa cells. Glia 52, 309-324.

Kirwan, R.P., Wordinger, R.J., Clark, A.F., O'Brien, C.J., 2009. Differential global and extra-cellular matrix focused gene expression patterns between normal and glaucomatous human lamina cribrosa cells. Mol Vis 15, 76-88.

Ko, M.K., Kim, E.K., Gonzalez, J.M., Jr., Tan, J.C., 2016. Dose- and time-dependent effects of actomyosin inhibition on live mouse outflow resistance and aqueous drainage tissues. Sci Rep 6, 21492.

Kobayashi, S., Vidal, I., Pena, J.D., Hernandez, M.R., 1997. Expression of neural cell adhesion molecule (NCAM) characterizes a subpopulation of type 1 astrocytes in human optic nerve head. Glia 20, 262-273.

Krusius, T., Ruoslahti, E., 1986. Primary structure of an extracellular matrix proteoglycan core protein deduced from cloned cDNA. Proc Natl Acad Sci U S A 83, 7683-7687.
Kwon, H.S., Lee, H.S., Ji, Y., Rubin, J.S., Tomarev, S.I., 2009a. Myocilin is a modulator of Wnt signaling. Mol Cell Biol 29, 2139-2154.

Kwon, Y.H., Fingert, J.H., Kuehn, M.H., Alward, W.L., 2009b. Primary open-angle glaucoma. N Engl J Med 360, 1113-1124.

Laemmli, U.K., 1970. Cleavage of structural proteins during the assembly of the head of bacteriophage T4. Nature 227, 680-685.

Last, J.A., Pan, T., Ding, Y., Reilly, C.M., Keller, K., Acott, T.S., Fautsch, M.P., Murphy, C.J., Russell, P., 2011. Elastic Modulus Determination of Normal and Glaucomatous Human Trabecular Meshwork. Investigative Ophthalmology & Visual Science 52, 2147-2152.

Leske, M.C., Heijl, A., Hussein, M., Bengtsson, B., Hyman, L., Komaroff, E., 2003. Factors for glaucoma progression and the effect of treatment: the early manifest glaucoma trial. Arch Ophthalmol 121, 48-56.

Levkovitch-Verbin, H., Makarovsky, D., Vander, S., 2013. Comparison between axonal and retinal ganglion cell gene expression in various optic nerve injuries including glaucoma. Mol Vis 19, 2526-2541.

Liang, S., Xu, J.F., Cao, W.J., Li, H.P., Hu, C.P., 2013. Human decorin regulates proliferation and migration of human lung cancer A549 cells. Chin Med J (Engl) 126, 4736-4741.

Liu, B., Chen, H., Johns, T.G., Neufeld, A.H., 2006. Epidermal growth factor receptor activation: an upstream signal for transition of quiescent astrocytes into reactive astrocytes after neural injury. J Neurosci 26, 7532-7540.

Lukas, T.J., Miao, H., Chen, L., Riordan, S.M., Li, W., Crabb, A.M., Wise, A., Du, P., Lin, S.M., Hernandez, M.R., 2008. Susceptibility to glaucoma: differential comparison of the astrocyte transcriptome from glaucomatous African American and Caucasian American donors. Genome Biol 9, R111.

Lutjen-Drecoll, E., 1999. Functional morphology of the trabecular meshwork in primate eyes. Prog Retin Eye Res 18, 91-119.

Lutjen-Drecoll, E., Futa, R., Rohen, J.W., 1981. Ultrahistochemical studies on tangential sections of the trabecular meshwork in normal and glaucomatous eyes. Invest Ophthalmol Vis Sci 21, 563-573.

Lutjen-Drecoll, E., Gabelt, B.T., Tian, B., Kaufman, P.L., 2001. Outflow of aqueous humor. J Glaucoma 10, S42-44.

Lutjen-Drecoll, E., Shimizu, T., Rohrbach, M., Rohen, J.W., 1986a. Quantitative analysis of 'plaque material' between ciliary muscle tips in normal- and glaucomatous eyes. Exp Eye Res 42, 457-465.

Lutjen-Drecoll, E., Shimizu, T., Rohrbach, M., Rohen, J.W., 1986b. Quantitative analysis of 'plaque material' in the inner- and outer wall of Schlemm's canal in normal- and glaucomatous eyes. Exp Eye Res 42, 443-455.

Lye-Barthel, M., Sun, D., Jakobs, T.C., 2013. Morphology of astrocytes in a glaucomatous optic nerve. Invest Ophthalmol Vis Sci 54, 909-917.

McEwan, P.A., Scott, P.G., Bishop, P.N., Bella, J., 2006. Structural correlations in the family of small leucine-rich repeat proteins and proteoglycans. J Struct Biol 155, 294-305.

McMenamin, P.G., Steptoe, R.J., 1991. Normal anatomy of the aqueous humour outflow system in the domestic pig eye. J Anat 178, 65-77.

Mikelberg, F.S., Drance, S.M., Schulzer, M., Yidegiligne, H.M., Weis, M.M., 1989. The normal human optic nerve. Axon count and axon diameter distribution. Ophthalmology 96, 1325-1328.

Mohan, R.R., Gupta, R., Mehan, M.K., Cowden, J.W., Sinha, S., 2010. Decorin transfection suppresses profibrogenic genes and myofibroblast formation in human corneal fibroblasts. Exp Eye Res 91, 238-245.

Mohan, R.R., Tandon, A., Sharma, A., Cowden, J.W., Tovey, J.C., 2011. Significant inhibition of corneal scarring in vivo with tissue-selective, targeted AAV5 decorin gene therapy. Invest Ophthalmol Vis Sci 52, 4833-4841.

Morrison, J.C., Jerdan, J.A., Dorman, M.E., Quigley, H.A., 1989a. Structural proteins of the neonatal and adult lamina cribrosa. Arch Ophthalmol 107, 1220-1224.

Morrison, J.C., L'Hernault, N.L., Jerdan, J.A., Quigley, H.A., 1989b. Ultrastructural location of extracellular matrix components in the optic nerve head. Arch Ophthalmol 107, 123-129.

Munger, J.S., Harpel, J.G., Gleizes, P.E., Mazzieri, R., Nunes, I., Rifkin, D.B., 1997. Latent transforming growth factor-beta: structural features and mechanisms of activation. Kidney Int 51, 1376-1382.

Munger, J.S., Huang, X., Kawakatsu, H., Griffiths, M.J., Dalton, S.L., Wu, J., Pittet, J.F., Kaminski, N., Garat, C., Matthay, M.A., Rifkin, D.B., Sheppard, D., 1999. The integrin alpha v beta 6 binds and activates latent TGF beta 1: a mechanism for regulating pulmonary inflammation and fibrosis. Cell 96, 319-328.

Murphy-Ullrich, J.E., Poczatek, M., 2000. Activation of latent TGF-beta by thrombospondin-1: mechanisms and physiology. Cytokine Growth Factor Rev 11, 59-69.

Neill, T., Schaefer, L., Iozzo, R.V., 2012. Decorin: a guardian from the matrix. Am J Pathol 181, 380-387.

Netland, P.A., Ye, H., Streeten, B.W., Hernandez, M.R., 1995. Elastosis of the lamina cribrosa in pseudoexfoliation syndrome with glaucoma. Ophthalmology 102, 878-886.

Neumann, C., Yu, A., Welge-Lussen, U., Lutjen-Drecoll, E., Birke, M., 2008. The Effect of TGF- 2 on Elastin, Type VI Collagen, and Components of the Proteolytic Degradation System in Human Optic Nerve Astrocytes. Investigative Ophthalmology & Visual Science 49, 1464-1472.

Nunes, I., Gleizes, P.E., Metz, C.N., Rifkin, D.B., 1997. Latent transforming growth factor-beta binding protein domains involved in activation and transglutaminase-dependent cross-linking of latent transforming growth factor-beta. J Cell Biol 136, 1151-1163.

Ochiai, Y., Ochiai, H., 2002. Higher concentration of transforming growth factor-beta in aqueous humor of glaucomatous eyes and diabetic eyes. Jpn J Ophthalmol 46, 249-253.

Ohta, K., Wiggert, B., Yamagami, S., Taylor, A.W., Streilein, J.W., 2000a. Analysis of immunomodulatory activities of aqueous humor from eyes of mice with experimental autoimmune uveitis. J Immunol 164, 1185-1192.

Ohta, K., Yamagami, S., Taylor, A.W., Streilein, J.W., 2000b. IL-6 antagonizes TGF-beta and abolishes immune privilege in eyes with endotoxin-induced uveitis. Invest Ophthalmol Vis Sci 41, 2591-2599.

Okka, M., Tian, B., Kaufman, P.L., 2004. Effects of latrunculin B on outflow facility, intraocular pressure, corneal thickness, and miotic and accommodative responses to pilocarpine in monkeys. Trans Am Ophthalmol Soc 102, 251-257; discussion 257-259.

Overby, D.R., Bertrand, J., Schicht, M., Paulsen, F., Stamer, W.D., Lutjen-Drecoll, E., 2014a. The structure of the trabecular meshwork, its connections to the ciliary muscle, and the effect of pilocarpine on outflow facility in mice. Invest Ophthalmol Vis Sci 55, 3727-3736.

Overby, D.R., Stamer, W.D., Johnson, M., 2009. The changing paradigm of outflow resistance generation: towards synergistic models of the JCT and inner wall endothelium. Exp Eye Res 88, 656-670.

Overby, D.R., Zhou, E.H., Vargas-Pinto, R., Pedrigi, R.M., Fuchshofer, R., Braakman, S.T., Gupta, R., Perkumas, K.M., Sherwood, J.M., Vahabikashi, A., Dang, Q., Kim, J.H., Ethier, C.R., Stamer, W.D., Fredberg, J.J., Johnson, M., 2014b. Altered mechanobiology of Schlemm's canal endothelial cells in glaucoma. Proc Natl Acad Sci U S A 111, 13876-13881.

Pasquale, L.R., Dorman-Pease, M.E., Lutty, G.A., Quigley, H.A., Jampel, H.D., 1993. Immunolocalization of TGF-beta 1, TGF-beta 2, and TGF-beta 3 in the anterior segment of the human eye. Invest Ophthalmol Vis Sci 34, 23-30.

Pease, M.E., McKinnon, S.J., Quigley, H.A., Kerrigan-Baumrind, L.A., Zack, D.J., 2000. Obstructed axonal transport of BDNF and its receptor TrkB in experimental glaucoma. Invest Ophthalmol Vis Sci 41, 764-774.

Pena, J.D., Netland, P.A., Vidal, I., Dorr, D.A., Rasky, A., Hernandez, M.R., 1998. Elastosis of the lamina cribrosa in glaucomatous optic neuropathy. Exp Eye Res 67, 517-524.

Pena, J.D., Taylor, A.W., Ricard, C.S., Vidal, I., Hernandez, M.R., 1999. Transforming growth factor beta isoforms in human optic nerve heads. Br J Ophthalmol 83, 209-218.

Picht, G., Welge-Luessen, U., Grehn, F., Lutjen-Drecoll, E., 2001. Transforming growth factor beta 2 levels in the aqueous humor in different types of glaucoma and the relation to filtering bleb development. Graefes Arch Clin Exp Ophthalmol 239, 199-207.

Quigley, H.A., 2011. Glaucoma. Lancet 377, 1367-1377.

Quigley, H.A., Brown, A., Dorman-Pease, M.E., 1991a. Alterations in elastin of the optic nerve head in human and experimental glaucoma. Br J Ophthalmol 75, 552-557.

Quigley, H.A., Dorman-Pease, M.E., Brown, A.E., 1991b. Quantitative study of collagen and elastin of the optic nerve head and sclera in human and experimental monkey glaucoma. Curr Eye Res 10, 877-888.

Quigley, H.A., Hohman, R.M., Addicks, E.M., Massof, R.W., Green, W.R., 1983. Morphologic changes in the lamina cribrosa correlated with neural loss in open-angle glaucoma. Am J Ophthalmol 95, 673-691.

Quigley, H.A., McKinnon, S.J., Zack, D.J., Pease, M.E., Kerrigan-Baumrind, L.A., Kerrigan, D.F., Mitchell, R.S., 2000. Retrograde axonal transport of BDNF in retinal ganglion cells is blocked by acute IOP elevation in rats. Invest Ophthalmol Vis Sci 41, 3460-3466.

Qureshi, I.A., 1995. Age and intraocular pressure: how are they correlated? J Pak Med Assoc 45, 150-152.

Raghunathan, V.K., Morgan, J.T., Dreier, B., Reilly, C.M., Thomasy, S.M., Wood, J.A., Ly, I., Tuyen, B.C., Hughbanks, M., Murphy, C.J., Russell, P., 2013. Role of substratum

stiffness in modulating genes associated with extracellular matrix and mechanotransducers YAP and TAZ. Invest Ophthalmol Vis Sci 54, 378-386.

Raghunathan, V.K., Morgan, J.T., Park, S.A., Weber, D., Phinney, B.S., Murphy, C.J., Russell, P., 2015. Dexamethasone Stiffens Trabecular Meshwork, Trabecular Meshwork Cells, and Matrix. Invest Ophthalmol Vis Sci 56, 4447-4459.

Ransom, B., Behar, T., Nedergaard, M., 2003. New roles for astrocytes (stars at last). Trends Neurosci 26, 520-522.

Rasmussen, C.A., Kaufman, P.L., Ritch, R., Haque, R., Brazzell, R.K., Vittitow, J.L., 2014. Latrunculin B Reduces Intraocular Pressure in Human Ocular Hypertension and Primary Open-Angle Glaucoma. Transl Vis Sci Technol 3, 1.

Ries, V., Henchcliffe, C., Kareva, T., Rzhetskaya, M., Bland, R., During, M.J., Kholodilov, N., Burke, R.E., 2006. Oncoprotein Akt/PKB induces trophic effects in murine models of Parkinson's disease. Proc Natl Acad Sci U S A 103, 18757-18762.

Rodahl, E., Van Ginderdeuren, R., Knappskog, P.M., Bredrup, C., Boman, H., 2006. A second decorin frame shift mutation in a family with congenital stromal corneal dystrophy. Am J Ophthalmol 142, 520-521.

Rohen, J.W., Futa, R., Lutjen-Drecoll, E., 1981. The fine structure of the cribriform meshwork in normal and glaucomatous eyes as seen in tangential sections. Invest Ophthalmol Vis Sci 21, 574-585.

Rohen, J.W., Schachtschabel, D.O., Berghoff, K., 1984. Histoautoradiographic and biochemical studies on human and monkey trabecular meshwork and ciliary body in short-term explant culture. Graefes Arch Clin Exp Ophthalmol 221, 199-206.

Rohen, J.W., van der Zypen, E., 1968. The phagocytic activity of the trabecularmeshwork endothelium. An electron-microscopic study of the vervet (Cercopithecus aethiops). Albrecht Von Graefes Arch Klin Exp Ophthalmol 175, 143-160.

Roughley, P.J., Melching, L.I., Recklies, A.D., 1994. Changes in the expression of decorin and biglycan in human articular cartilage with age and regulation by TGF-beta. Matrix Biol 14, 51-59.

Sambrook, J., Fristch, E. F., Maniatis, T. (1989). "Molecular Cloning: A Laboratory Manual."

Sappington, R.M., Carlson, B.J., Crish, S.D., Calkins, D.J., 2010. The microbead occlusion model: a paradigm for induced ocular hypertension in rats and mice. Invest Ophthalmol Vis Sci 51, 207-216.

Saracaloglu, A., Demiryurek, S., Okumus, S., Oztuzcu, S., Bozgeyik, I., Coskun, E., Aksoy, U., Kaydu, E., Erbagci, I., Gurler, B., Alasehirli, B., Demiryurek, A.T., 2016. Toward Novel Diagnostics for Primary Open-Angle Glaucoma? An Association Study of Polymorphic Variation in Ras Homolog Family Member (A, B, C, D) Genes RHOA, RHOB, RHOC, and RHOD. OMICS 20, 290-295.

Sato, Y., Rifkin, D.B., 1989. Inhibition of endothelial cell movement by pericytes and smooth muscle cells: activation of a latent transforming growth factor-beta 1-like molecule by plasmin during co-culture. J Cell Biol 109, 309-315.

Savinova, O.V., Sugiyama, F., Martin, J.E., Tomarev, S.I., Paigen, B.J., Smith, R.S., John, S.W., 2001. Intraocular pressure in genetically distinct mice: an update and strain survey. BMC Genet 2, 12.

Schaefer, L., 2011. Small leucine-rich proteoglycans in kidney disease. J Am Soc Nephrol 22, 1200-1207.

Schaefer, L., Iozzo, R.V., 2008. Biological functions of the small leucine-rich proteoglycans: from genetics to signal transduction. J Biol Chem 283, 21305-21309.

Schaefer, L., Tsalastra, W., Babelova, A., Baliova, M., Minnerup, J., Sorokin, L., Grone, H.J., Reinhardt, D.P., Pfeilschifter, J., Iozzo, R.V., Schaefer, R.M., 2007. Decorin-mediated regulation of fibrillin-1 in the kidney involves the insulin-like growth factor-I receptor and Mammalian target of rapamycin. Am J Pathol 170, 301-315.

Schlotzer-Schrehardt, U., Dorfler, S., 1993. Immunolocalization of growth factors in the human ciliary body epithelium. Curr Eye Res 12, 893-905.

Schmittgen, T.D., Livak, K.J., 2008. Analyzing real-time PCR data by the comparative C(T) method. Nat Protoc 3, 1101-1108.

Schonherr, E., Sunderkotter, C., Iozzo, R.V., Schaefer, L., 2005. Decorin, a novel player in the insulin-like growth factor system. J Biol Chem 280, 15767-15772.

Scott, J.E., 1996. Proteodermatan and proteokeratan sulfate (decorin, lumican/fibromodulin) proteins are horseshoe shaped. Implications for their interactions with collagen. Biochemistry 35, 8795-8799.

Sharma, K., Ziyadeh, F.N., 1994. Renal hypertrophy is associated with upregulation of TGF-beta 1 gene expression in diabetic BB rat and NOD mouse. Am J Physiol 267, F1094-1001.

Shepard, A.R., Millar, J.C., Pang, I.H., Jacobson, N., Wang, W.H., Clark, A.F., 2010. Adenoviral gene transfer of active human transforming growth factor-{beta}2 elevates intraocular pressure and reduces outflow facility in rodent eyes. Invest Ophthalmol Vis Sci 51, 2067-2076.

Sherwood, M.E., Richardson, T.M., 1988. Phagocytosis by trabecular meshwork cells: sequence of events in cats and monkeys. Exp Eye Res 46, 881-895.

Son, J.L., Soto, I., Oglesby, E., Lopez-Roca, T., Pease, M.E., Quigley, H.A., Marsh-Armstrong, N., 2010. Glaucomatous optic nerve injury involves early astrocyte reactivity and late oligodendrocyte loss. Glia 58, 780-789.

Speakman, J., 1959. Aqueous outflow channels in the trabecular meshwork in man. Br J Ophthalmol 43, 129-138.

Steinhart, M.R., Cone-Kimball, E., Nguyen, C., Nguyen, T.D., Pease, M.E., Chakravarti, S., Oglesby, E.N., Quigley, H.A., 2014. Susceptibility to glaucoma damage related to age and connective tissue mutations in mice. Exp Eye Res 119, 54-60.

Streilein, J.W., 1999a. Immunologic privilege of the eye. Springer Semin Immunopathol 21, 95-111.

Streilein, J.W., 1999b. Immunoregulatory mechanisms of the eye. Prog Retin Eye Res 18, 357-370.

Sun, D., Lye-Barthel, M., Masland, R.H., Jakobs, T.C., 2009. The morphology and spatial arrangement of astrocytes in the optic nerve head of the mouse. The Journal of Comparative Neurology 516, 1-19.

Takeuchi, Y., Matsumoto, T., Ogata, E., Shishiba, Y., 1993. Effects of transforming growth factor beta 1 and L-ascorbate on synthesis and distribution of proteoglycans in murine osteoblast-like cells. J Bone Miner Res 8, 823-830.

Tamm, E.R., 2009. The trabecular meshwork outflow pathways: structural and functional aspects. Exp Eye Res 88, 648-655.

Tamm, E.R., Fuchshofer, R., 2007. What increases outflow resistance in primary open-angle glaucoma? Surv Ophthalmol 52 Suppl 2, S101-104.

Tanihara, H., Ohira, A., Takahashi, M., Honda, Y., Suzuki, S., 1995. Localization and possible gene expression of proteoglycan decorin in the trabecular meshwork. Curr Eye Res 14, 727-730.

Tawara, A., Varner, H.H., Hollyfield, J.G., 1989. Distribution and characterization of sulfated proteoglycans in the human trabecular tissue. Invest Ophthalmol Vis Sci 30, 2215-2231.

Taylor, A.W., Alard, P., Yee, D.G., Streilein, J.W., 1997. Aqueous humor induces transforming growth factor-beta (TGF-beta)-producing regulatory T-cells. Curr Eye Res 16, 900-908.

Tektas, O.Y., Lutjen-Drecoll, E., 2009. Structural changes of the trabecular meshwork in different kinds of glaucoma. Exp Eye Res 88, 769-775.

Tektas, O.Y., Lutjen-Drecoll, E., Scholz, M., 2010. Qualitative and quantitative morphologic changes in the vasculature and extracellular matrix of the prelaminar optic nerve head in eyes with POAG. Invest Ophthalmol Vis Sci 51, 5083-5091.

Tham, Y.C., Li, X., Wong, T.Y., Quigley, H.A., Aung, T., Cheng, C.Y., 2014. Global prevalence of glaucoma and projections of glaucoma burden through 2040: a systematic review and meta-analysis. Ophthalmology 121, 2081-2090.

Thanos, S., Naskar, R., 2004. Correlation between retinal ganglion cell death and chronically developing inherited glaucoma in a new rat mutant. Exp Eye Res 79, 119-129.

Thomson, B.R., Heinen, S., Jeansson, M., Ghosh, A.K., Fatima, A., Sung, H.K., Onay, T., Chen, H., Yamaguchi, S., Economides, A.N., Flenniken, A., Gale, N.W., Hong, Y.K., Fawzi, A., Liu, X., Kume, T., Quaggin, S.E., 2014. A lymphatic defect causes ocular hypertension and glaucoma in mice. J Clin Invest 124, 4320-4324.

Tian, B., Geiger, B., Epstein, D.L., Kaufman, P.L., 2000. Cytoskeletal involvement in the regulation of aqueous humor outflow. Invest Ophthalmol Vis Sci 41, 619-623.

Tomarev, S.I., Wistow, G., Raymond, V., Dubois, S., Malyukova, I., 2003. Gene expression profile of the human trabecular meshwork: NEIBank sequence tag analysis. Invest Ophthalmol Vis Sci 44, 2588-2596.

Tovar-Vidales, T., Roque, R., Clark, A.F., Wordinger, R.J., 2008. Tissue transglutaminase expression and activity in normal and glaucomatous human trabecular meshwork cells and tissues. Invest Ophthalmol Vis Sci 49, 622-628.

Tripathi, R.C., 1971. Mechanism of the aqueous outflow across the trabecular wall of Schlemm's canal. Exp Eye Res 11, 116-121.

Tripathi, R.C., Chan, W.F., Li, J., Tripathi, B.J., 1994a. Trabecular cells express the TGF-beta 2 gene and secrete the cytokine. Exp Eye Res 58, 523-528.

Tripathi, R.C., Li, J., Chan, W.F., Tripathi, B.J., 1994b. Aqueous humor in glaucomatous eyes contains an increased level of TGF-beta 2. Exp Eye Res 59, 723-727.

Ueberham, E., Low, R., Ueberham, U., Schonig, K., Bujard, H., Gebhardt, R., 2003. Conditional tetracycline-regulated expression of TGF-beta1 in liver of transgenic mice leads to reversible intermediary fibrosis. Hepatology 37, 1067-1078.

Ueda, J., Wentz-Hunter, K., Yue, B.Y., 2002. Distribution of myocilin and extracellular matrix components in the juxtacanalicular tissue of human eyes. Invest Ophthalmol Vis Sci 43, 1068-1076.

Varela, H.J., Hernandez, M.R., 1997. Astrocyte responses in human optic nerve head with primary open-angle glaucoma. J Glaucoma 6, 303-313.

Varga, J., Rosenbloom, J., Jimenez, S.A., 1987. Transforming growth factor beta (TGF beta) causes a persistent increase in steady-state amounts of type I and type III collagen and fibronectin mRNAs in normal human dermal fibroblasts. Biochem J 247, 597-604.

Vial, C., Gutierrez, J., Santander, C., Cabrera, D., Brandan, E., 2011. Decorin interacts with connective tissue growth factor (CTGF)/CCN2 by LRR12 inhibiting its biological activity. J Biol Chem 286, 24242-24252.

Wang, L., Cioffi, G.A., Cull, G., Dong, J., Fortune, B., 2002. Immunohistologic evidence for retinal glial cell changes in human glaucoma. Invest Ophthalmol Vis Sci 43, 1088-1094.

Wang, W.H., McNatt, L.G., Pang, I.H., Millar, J.C., Hellberg, P.E., Hellberg, M.H., Steely, H.T., Rubin, J.S., Fingert, J.H., Sheffield, V.C., Stone, E.M., Clark, A.F., 2008. Increased expression of the WNT antagonist sFRP-1 in glaucoma elevates intraocular pressure. J Clin Invest 118, 1056-1064.

Webber, H.C., Bermudez, J.Y., Sethi, A., Clark, A.F., Mao, W., 2016. Crosstalk between TGFbeta and Wnt signaling pathways in the human trabecular meshwork. Exp Eye Res 148, 97-102.

Weber, A.J., Zelenak, D., 2001. Experimental glaucoma in the primate induced by latex microspheres. J Neurosci Methods 111, 39-48.

Weber, I.T., Harrison, R.W., Iozzo, R.V., 1996. Model structure of decorin and implications for collagen fibrillogenesis. J Biol Chem 271, 31767-31770.

Wiederholt, M., Thieme, H., Stumpff, F., 2000. The regulation of trabecular meshwork and ciliary muscle contractility. Prog Retin Eye Res 19, 271-295.

Wong, M.L., Medrano, J.F., 2005. Real-time PCR for mRNA quantitation. Biotechniques 39, 75-85.

Wong, T.T., Wong, T.Y., Foster, P.J., Crowston, J.G., Fong, C.W., Aung, T., 2009. The relationship of intraocular pressure with age, systolic blood pressure, and central corneal thickness in an asian population. Invest Ophthalmol Vis Sci 50, 4097-4102.

Wu, Z., Horgan, C.E., Carr, O., Owens, R.T., Iozzo, R.V., Lechner, B.E., 2014. Biglycan and decorin differentially regulate signaling in the fetal membranes. Matrix Biol 35, 266-275.

Yamaguchi, Y., Mann, D.M., Ruoslahti, E., 1990. Negative regulation of transforming growth factor-beta by the proteoglycan decorin. Nature 346, 281-284.

Yamaguchi, Y., Ruoslahti, E., 1988. Expression of human proteoglycan in Chinese hamster ovary cells inhibits cell proliferation. Nature 336, 244-246.

Yamamoto, N., Itonaga, K., Marunouchi, T., Majima, K., 2005. Concentration of transforming growth factor beta2 in aqueous humor. Ophthalmic Res 37, 29-33.

Yamamoto, T., Nakamura, T., Noble, N.A., Ruoslahti, E., Border, W.A., 1993. Expression of transforming growth factor beta is elevated in human and experimental diabetic nephropathy. Proc Natl Acad Sci U S A 90, 1814-1818.

Yang, J.G., Zhou, C.J., Li, X.Y., Sun, P.R., Li, S.P., Ren, B.C., 2015. Alteration of UCP2 and ZO-1 expression in trabecular meshwork of neovascular glaucoma patients. J Glaucoma 24, 291-296.

Yang, Z., Quigley, H.A., Pease, M.E., Yang, Y., Qian, J., Valenta, D., Zack, D.J., 2007. Changes in gene expression in experimental glaucoma and optic nerve transection: the equilibrium between protective and detrimental mechanisms. Invest Ophthalmol Vis Sci 48, 5539-5548.

Yasuda, M., Tanaka, Y., Nishiguchi, K.M., Ryu, M., Tsuda, S., Maruyama, K., Nakazawa, T., 2014. Retinal transcriptome profiling at transcription start sites: a cap analysis of gene expression early after axonal injury. BMC Genomics 15, 982.

Ye, H., Hernandez, M.R., 1995. Heterogeneity of astrocytes in human optic nerve head. J Comp Neurol 362, 441-452.

Yu, Q., Stamenkovic, I., 2000. Cell surface-localized matrix metalloproteinase-9 proteolytically activates TGF-beta and promotes tumor invasion and angiogenesis. Genes Dev 14, 163-176.

Yuan, Y., Yeh, L.K., Liu, H., Yamanaka, O., Hardie, W.D., Kao, W.W., Liu, C.Y., 2013. Targeted overexpression of TGF-alpha in the corneal epithelium of adult transgenic mice induces changes in anterior segment morphology and activates noncanonical Wnt signaling. Invest Ophthalmol Vis Sci 54, 1829-1837.

Zhao, X., Ramsey, K.E., Stephan, D.A., Russell, P., 2004. Gene and protein expression changes in human trabecular meshwork cells treated with transforming growth factor-beta. Invest Ophthalmol Vis Sci 45, 4023-4034.

Ziyadeh, F.N., 1994. Role of transforming growth factor beta in diabetic nephropathy. Exp Nephrol 2, 137.

Zode, G.S., Sethi, A., Brun-Zinkernagel, A.M., Chang, I.F., Clark, A.F., Wordinger, R.J., 2011. Transforming growth factor-beta2 increases extracellular matrix proteins in optic nerve head cells via activation of the Smad signaling pathway. Mol Vis 17, 1745-1758.

8. Tables

9. Figures

10. Abbreviations

µg	microgram
µl	microliter
µm	micrometer
AAV-5	adeno associated virus 5
AC	anterior chamber
AGS	astrocyte growth supplement
AH	aqueous humor
AKT	AKT serine/threonine kinase
AP	alkaline phosphatase
APS	ammonium persulfate
bp	base pairs
BSA	bovine serum albumin
CB	ciliary body
cDNA	complementary deoxyribonucleic acid
CM	ciliary muscle
Co	cornea
Col	collagen
Ct	cycle threshold
CTGF	connective tissue growth factor
CTM	corneoscleral trabecular meshwork
DAPI	4′,6-Diamidin-2-phenylindol
DCN	decorin
DMEM	Dulbecco's Modified Eagle's Medium
DMSO	dimethylsulfoxide
DNA	deoxyribonucleic acid
dNTPs	deoxynucleotide
DTT	dithiothreitol
ECM	extracellular matrix
EDTA	ethylenediaminetetraacetic acid
EL	elastin
EM	electron microscopy
EtBr	ethidium bromide
ETOH	ethanol
FCS	fetal calve serum
FBN1	fibrillin 1
FN	fibronectin
g	gram
GAG	glycosaminoglycan
GCL	ganglion cell layer

GFAP	glial fibrillary acid protein
GNB2L	guanine nucleotide binding protein
GO	gene ontology
H_2O	water
h	hour
HCl	hydrochloric acid
Hg	mercury
HRP	horseradish peroxidase
IFN	interferon
IgG	immune globulin G
IL	interleukin
INL	inner nuclear layer
IOP	intraocular pressure
JCT	juxtacanalicular meshwork
kg	kilogram
l	iris
LAP	latency Associated Peptide
LC	lamina cribrosa
LRR	leucine rich repeat
LTBP	latent TGF-β-binding protein
M	molar
mA	milliampere
min	minute
ml	millilitre
mm	millimeter
mM	millimolar
MMP	matrix metallo proteinase
mRNA	messenger ribonucleic acid
mTOR	mammalian target of rapamycin
Neo	neomycin
ng	nanogram
OD	optical density
ON	optic nerve
ONH	optic nerve head
ONL	outer nuclear layer
PAI-1	plasminogen activator inhibitor 1
PBS	phosphate-buffered saline
PCR	polymerase chain reaction
PFA	paraformaldehyde
Pgk	phosphoglycerate kinase
Php	phosphate
POAG	primary open angle glaucoma

PVDF	polyvinylidene difluoride
Re	retina
RGC	retinal ganglion cell
RIPA	radioimmunoprecipitation assay
RNA	ribonucleic acid
RPE	retinal pigment epithelium
RPL32	ribosomal protein L32
rpm	rounds per minute
RT	room temperature
SC	Schlemm’s canal
SDS	sodium dodecyl sulfate
SLRP	Small leucine rich proteoglycan
SMAD	small mothers against decapentaplegic
SS	scleral spur
TBE	tris-borat-EDTA
TBS	tris-buffered saline
TBST	tris-buffered saline tween 20
TEMED	tetramethylethylendiamin
TG	transgenic
TGF-β	transforming growth factor β
TGF-β R	transforming growth factor β receptor
TM	trabecular meshwork
UTM	uveal trabecular meshwork
UV	ultra violet
V	volt
WT	wildtype
α-SMA	α-smooth muscle actin

11. Acknowledgement / Danksagung

Mein Dank gilt Prof. Dr. E. Tamm der es mir ermöglich hat meine Arbeit der letzten Jahre in seinem Labor auszuführen. Zudem bedanke ich mich herzlich für die Übernahme des Vorsitzes der Verteidigung.

Des Weiteren danke ich Prof. Dr. S. Schneuwly für die Übernahme des Zweitgutachtens für diese Arbeit, sowie Prof. Dr. C. Wagner und Prof Dr. V. Egger für die Bereitschaft das Amt des Dritt- bzw. Ersatzprüfers zu übernehmen.
P.D. Dr. A. Ohlmann danke ich herzlich für die Übernahme des Mentorats für meine Dissertation. Many thanks also go to PD Dr P. Russell for good advice on my thesis and for enabling me to work in his laboratory!

Bei Prof. Dr. R. Iozzo und Prof. Dr. L. Schaefer bedanke ich mich für die Erlaubnis mit den DCN knockout Mäusen zu arbeiten.

Ganz besonders möchte ich mich bei Prof. Dr. R. Fuchshofer bedanken, der mich in den letzten Jahren erstklassig betreut hat und das Erstgutachten für diese Arbeit übernommen hat. Ich habe sehr viel von ihm gelernt, nicht nur über die Forschung sondern auch über das Leben! Für viele lehrreiche aber auch unterhaltsame Stunden bin ich sehr dankbar!

Zudem bedanke ich mich bei allen ehemaligen und aktuellen Mitgliedern der AG Fuchshofer, im Besonderen bei Dr. Sabrina Küspert, Gregor Weber und Andrea Dillinger, die mich durch fast die gesamte Zeit am Lehrstuhl begleitet haben und mir bei vielen Problemen und Problemchen mit Rat und Tat zur Seite standen. Hervorheben möchte ich auch Mutasem-Bellah Saman, Tamara Löffler und Franziska Scherl die im Rahmen ihrer Masterarbeiten wichtige Erkenntnisse zu meiner Arbeit beigetragen haben.

Bei unseren guten Seelen des Labors, Sylvia Babl, Angelika Pach, Margit Schimmel und Elke Stauber möchte ich mich von ganzem Herzen für die gute Zusammenarbeit und die Unterstützung im Bereich Zellkultur und Histologie bedanken.
In den letzten Jahren habe ich viele schöne Stunden im aber auch außerhalb des Labors mit den Mädels aus dem Büro verbracht, Danke dafür! Danke an Anja Schlecht für ruhige Stunden im Wald beim Bogenschießen und an Nikola Fath fürs gemeinsame auspowern in diversen Boulderhallen! Allen meinen Freunden die mir während der letzten Jahre in allen Situationen beigestanden und manchmal auch meine Launen ertragen haben danke ich von ganzem Herzen!

Mein ganz spezieller Dank gilt Martin Wild, der meinen Weg die letzten Jahre in allen Höhen und Tiefen begleitet hat, mich immer wieder motiviert und aufgebaut hat und mir, egal wie und womit, immer geholfen hat.

Aus tiefstem Herzen danke ich meinen Eltern Ilse und Wolfgang Schneider. Sie haben mir mein Studium ermöglicht und alle mein Entscheidungen stets unterstützt. Ohne Sie wäre ich nie so weit gekommen! Auch meinen Schwestern Anna und Franziska möchte ich herzlich für Unterstützung in allen Lebenslagen danken!

12. Erklärung

Hiermit erkläre ich, dass ich die vorliegende Dissertation selbstständig und ohne unerlaubte Hilfsmittel angefertigt habe.

Regensburg, den

Magdalena Schneider